WAVELET COHERENCE: ANALYSIS OF TIME SERIES AND EXPLORATION TOWARDS FAULT DETECTION

by

Ali İsmail Duman

B.S., Chemical Engineering, Boğaziçi University, 2017

Submitted to the Institute for Graduate Studies in
Science and Engineering in partial fulfillment of
the requirements for the degree of
Master of Science

Graduate Program in Chemical Engineering
Boğaziçi University

2020

ACKNOWLEDGEMENTS

I would first like to thank my thesis advisor Prof. Dr. Uğur Akman, an academician from edge of the extinction .who walked me through the journey of master’s thesis. The door to Prof. Akman’s office was always open whenever I ran into a trouble spot or had a question about my thesis. He consistently revealed my academic appetency and encouraged me to embrace my master thesis. Moreover, I would like to thank Prof. Dr. Nesrin Okay for providing invaluable guidance throughout this thesis.

I am incapable of giving enough gratitude to my sister, Miray Deniz Duman, whose understanding and patience has made me more determined and perseverant in my research. In addition to my sister, I would like to give special thanks to my family.

I am extremely grateful to my dear friends R. Canan Tuğberk, Burak Kocamış, Şafak Kılıç and Şahin Sarrafi for their unlimited support during the course of my thesis. Their presence led me to move forward with each step and I could not have completed the project without their support.

ABSTRACT

WAVELET COHERENCE: ANALYSIS OF TIME SERIES AND EXPLORATION TOWARDS FAULT DETECTION

Wavelet Coherence Analysis (WCA) is a tool for depicting degree of coherency and phase differences between binary time series. The advantages of WCA are the capability to cope with non-stationary time series and to monitor the time- and frequency-domain information collectively. In this thesis, commonly used WCA software toolboxes were comparatively evaluated and a hybrid MATLAB code was developed. WCA was used to elucidate possible coherency and lead-lag relationships between binary time series. Data pertaining to engineering and economics were used. Studies with CAB (Chemical Activity Barometer) and IPI (US Industrial Production Index) disclosed the power of WCA in explicating and interpreting the coherency and lead-lag relationships hidden between these series and confirmed the claims made by ACC (American Chemistry Council) that the CAB leads IPI. Additionally, it was shown that at US Business Cycle periods (0.5 to two years), the troughs (ends of economic recessions) observed with WCA of CAB and IPI lead the troughs claimed by ACC. WCA supports that CAB is a leading indicator of the US economy, especially during economic recessions between 1945 and 2007. Comparative studies demonstrated that working with detrended series increased resolution of WCA while working with moving-averaged series distorted WCA due to introduction of artificial lags in averaging. WCA application to yearly CAB and Chemical Engineering Plant Cost Index (CEPCI) and yearly IPI and CEPCI pairs exhibited that it was not possible to decide whether CEPCI is a leading indicator for the US economy or not. Furthermore, for the first time in literature, WCA was used as a tool for Fault Detection (FD). Fault containing synthetic time series along with unfaulty one were used to evaluate the potential of WCA in FD. It was shown that WCA can detect faults quickly and is a viable tool for FD, change point identification, and template matching tasks.

ÖZET

DALGACIK UYUMLULUĞU: ZAMAN SERİLERİ ANALİZİ VE HATA TESPİTİ

Dalgacık Uyumluluk Analizi (DUA), ikili zaman serileri arasındaki uyumluluk derecesini ve faz farklılıklarını gösteren bir araçtır. DUA'nın avantajları, durağan olmayan zaman serileri ile baş edebilme ve zaman-frekans bilgilerini birlikte izleyebilmedir. Bu tezde, yaygın olarak kullanılan DUA yazılım paketleri karşılaştırılmıştır ve hibrid bir MATLAB kodu geliştirilmiştir. DUA, ikili zaman serileri arasındaki uyumluluk ve öncüllük-artçıllık ilişkilerini açıklamak için kullanılmıştır. Kimya mühendisliği ve ekonomi ile ilgili veriler araştırma için seçilmiştir. KAB (Kimyasal Aktivite Barometresi) ve EÜE (ABD Endüstriyel Üretim Endeksi) ile yapılan çalışmalar, DUA'nın bu seriler arasında gizli uyumluluk ve faz ilişkilerini açıklamadaki gücünü göstermiştir. ACC (American Chemistry Council) tarafından öne sürülen KAB'nin EÜE'ye öncülük ettiği iddiası doğrulanmıştır. Buna ek olarak, ABD İş Döngülerinde (0,5 ila iki yıllık dönemler), aylık KAB ve EÜE'nin DUA'sının, ACC tarafından öne sürülen ekonominin dip yaptığı dönemlere öncülük ettiği gösterilmiştir. KAB'ın özellikle 1945 ve 2007 arasındaki durgunluk dönemlerinde, ABD ekonomisinin öncü göstergesi gibi davrandığı DUA tarafından da kanıtlanmıştır. Karşılaştırmalı çalışmalar, hareketli ortalama serileri kullanımının yapay gecikmeler nedeniyle DUA'yı bozduğunu fakat eğimden arındırılmış serilerle çalışmanın DUA çözünürlüğünü artırdığını göstermiştir. Yıllık KAB ve Kimya Mühendisliği Tesisi Maliyet Endeksi (KMTME) çiftiyle yıllık EÜE ve KMTME çiftine DUA yapıldığında, KMTME'nin ABD ekonomisin öncü bir göstergesi olup olmadığına karar vermenin mümkün olmadığı sonucuna varılmıştır. Ayrıca, literatürde ilk kez DUA, Hata Tespitinde (HT) kullanılmıştır. Hatalı ve hatasız sentetik seriler, DUA'nın HT potansiyelini değerlendirmek için kullanılmış olup, DUA'nın hataları hızlı bir şekilde algılayabildiği ve HT, değişim noktası tanıma ve şablon eşleştirme görevleri için uygun bir araç olabileceği gösterilmiştir.

TABLE OF CONTENT

ACKNOWLEDGEMENTS iii
ABSTRACT iv
LIST OF FIGURES viii
LIST OF TABLE xi
LIST OF SYMBOLS xii
LIST OF ACRONYMS/ABBREVATIONS xiv
1. INTRODUCTION 1
2. TECHNICAL BACKGROUND FOR WAVELET COHERENCE ANALYSIS AND THE TOOLBOX USED 15
2.1.Wavelets and the Morlet Wavelet 15
2.2. Continuous Wavelet Transform 17
2.3. Wavelet Power Spectrum 18
2.4. Cross Wavelet Transform and Wavelet Coherence Analysis 18
2.5. Phase Difference 19
2.6. Wavelet Coherency Analysis Software Toolboxes 20
2.7. Major Calculation Steps of MATLAB's Default WCA Function 20
2.8. Major Calculation Steps of the ASToolbox 21
2.9. Major Calculation Steps of the AGToolbox 23
3. MOTIVATING EXAMPLE 25
3.1. Definition and Properties of the Synthetic Time Series 25
3.2. Windowed Cross Correlation Analysis of the Synthetic Time Series 27
3.3. Univariate Analysis of the Synthetic Time Series 29
3.4. Wavelet Coherence Analysis of the Synthetic Time Series 31
4. WAVELET COHERENCE ANALYSIS OF THE CHEMICAL ACTIVITY BAROMETER AND U.S. INDUSTRIAL PRODUCTION INDEX 40
4.1. Description and Economical Importance of the CAB and the IPI 40

4.2. Data Description and Preliminary Result 44

4.3. Univariate Wavelet-Based Analysis of the Original Trending CAB and IPI Series 46

4.4. Wavelet Coherence Analysis of the Original Trending CAB and IPI Series 48

4.5. Univariate Wavelet-Based Analysis of the Detrended CAB and IPI Series 64

4.6. Wavelet Coherence Analysis of the Detrended CAB and IPI Series 66

4.7. Univariate Wavelet-Based Analysis of the Moving-Average-Smoothed First-Order Differenced CAB and IPI Series 81

4.8. Wavelet Coherence Analysis of the Moving-Average-Smoothed First-Order Differenced CAB and IPI Series 82

4.9. Summary of the Effects of Detrending and Three-Month MA Smoothing 87

5. WAVELET COHERENCE ANALYSES FOR THE YEARLY CEPCI, CAB, AND IPI DATA 89

5.1. Description of Cost Indices and the CEPCI 89

5.2. Description of the Yearly Data 91

5.3. WCA of the Detrended Yearly CAB and IPI Series 94

5.4. WCA of the Detrended Yearly CAB and CEPCI Series 100

5.5. WCA of the Detrended Yearly IPI and CEPCI Series 107

5.6. Summary on the Performance of CEPCI as a Leading Indicator for the US Economy 114

6. APLICATION OF WCA TO FAULT DETECTION 115

6.1. Definition of the Synthetic Time Series 118

6.2. Application of WCA to Fault Detection 121

7. CONCLUSIONS AND RECOMENDATIONS 130

REFERENCES 135

APPENDIX A: MATLAB CODE USED 145

LIST OF FIGURES

Figure 3.1. Individual and Superimposed Plots of the Synthetic Time Series. 26

Figure 3.2. Moving Centered-Window Correlations of the Synthetic Time Series for Different Window Lengths. 28

Figure 3.3. Windowed and Lagged Correlation between the Synthetic Time Series. 29

Figure 3.4. Wavelet Power Spectrums and Power Spectral Densities of the Synthetic Time Series. 30

Figure 3.5. Lead-Lag and Phase-State Relationships in Wavelet Coherence Analysis. 31

Figure 3.6. Wavelet Coherence Analysis and Phase-Difference Plots of the Synthetic Time Series. 33

Figure 3.7. Distribution of Phase Angles between the Synthetic Time Series. 37

Figure 3.8. Mean Coherence and Mean Phase-Difference between the Synthetic Time Series across Time and Frequency Domains. 39

Figure 4.1. Original Trending, Detrended, and Three-Month Moving-Average-Smoothed Yearly-Differenced CAB and IPI Series………………………………………45

Figure 4.2. Wavelet Power Spectra and Power Spectral Densities of the Original Trending CAB and IPI Series. 47

Figure 4.3. Wavelet Coherence Analysis and Phase-Difference Plots of the Original Trending CAB and IPI Series. 49

Figure 4.4. Mean Coherence and Mean Phase-Difference between the Original Trending CAB and IPI Series across Time and Frequency Domains. 50

Figure 4.5. Quantized Distribution of Phase Angles between the Original Trending CAB and IPI Series. 63

Figure 4.6. Wavelet Power Spectra and Power Spectral Densities of the Detrended CAB and IPI Series. 65

Figure 4.7. Wavelet Coherence Analysis and Phase-Difference Plots of the Detrended CAB and IPI Series. 67

Figure 4.8. Mean Coherence and Mean Phase-Difference between the Detrended CAB and IPI Series across Time and Frequency Domains. 68

Figure 4.9. Quantized Distribution of Phase Angles between the Detrended CAB and IPI Series. 80

Figure 4.10. Wavelet Power Spectra and Power Spectral Densities of the Year-to-Year Change of Three-Month MA of the CAB and IPI Series. 82

Figure 4.11. Wavelet Coherence Analysis of the Year-to-Year Change of the Three-Month MA of the CAB and IPI Series. 84

Figure 4.12. Mean Coherence and Mean Phase-Difference between the Year-to-Year Change of the Three-Month MA of the CAB and IPI Series across Time and Frequency Domains. 85

Figure 4.13. Quantized Distribution of Phase Angles between the Year-to-Year Change of the Three-Month MA of the CAB and IPI Series. 86

Figure 5.1 Original Trending and Detrended Yearly CEPCI, CAB and IPI Series……….93

Figure 5.2. Wavelet Coherence Analysis and Phase-Difference Plots of the Detrended Yearly CAB and IPI Series. 95

Figure 5.3. Mean Coherence and Mean Phase-Difference between the Detrended Yearly CAB and IPI Series across Time and Frequency Domains. 96

Figure 5.4. Quantized Distribution of Phase Angles between the Detrended Yearly CAB and IPI Series. 99

Figure 5.5. Wavelet Coherence Analysis and Phase-Difference Plots of the Detrended Yearly CAB and CEPCI Series..101

Figure 5.6. Mean Coherence and Mean Phase-Difference between the Detrended Yearly CAB and CEPCI Series across Time and Frequency Domains. 103

Figure 5.7. Quantized Distribution of Phase Angles between the Detrended Yearly CAB and CEPCI Series..106

Figure 5.8. Wavelet Coherence Analysis and Phase-Difference Plots of the Detrended Yearly IPI and CEPCI Series. 108

Figure 5.9. Mean Coherence and Mean Phase-Difference between the Detrended Yearly IPI and CEPCI Series across Time and Frequency Domains. 110

Figure 5.10. Quantized Distribution of Phase Angles between the Detrended Yearly IPI and CEPCI Series..113

Figure 6.1. Normal and Fault-Added Synthetic Time Series……………………………120

Figure 6.2. WCA of Series $x2t$ (no fault) and $x2f2t$ (no fault)…………………………122

Figure 6.3. WCA of Series $x1t$ (no fault) and $x1f1t$ (fault-1)…………………………..124

Figure 6.4. WCA of Series $x2t$ (no fault) and $x2f1t$ (fault-1)…………………………..126

Figure 6.5. WCA of Series $x1t$ (no fault) and $x1f2t$ (fault-2)…………………………..128

LIST OF TABLES

Table 3.1. Values of Some Important Parameters used in the WCA Computations. 32

Table 4.1. Values of Some Important Parameters used in the WCA Computations………48

Table 4.2. Dates of the CAB Turning Points and Phase Difference between the Peaks Claimed by ACC (CAB) and NBER. 52

Table 4.3. Performance Summary of WCA on the Original Trending CAB and IPI Data. 61

Table 4.4. Values of Some Important Parameters used in the WCA Computations. 66

Table 4.5. Performance Summary of WCA on the Detrended CAB and IPI Data. 77

Table 5.1. Values of Some Important Parameters used in the WCA Computations………94

Table 5.2. Values of Some Important Parameters used in the WCA Computations. 100

Table 5.3. Values of Some Important Parameters used in the WCA Computations. 107

Table 6.1. Values of Some Important Parameters used in the WCA Computations……..121

Table 6.2. Summary of the Potential of the WCA for Applications in FDD (+: Definitely Positive, ?: Requires Further Investigation)...129

LIST OF SYMBOLS

α	Scale parameter of signal to noise ratio
B	Buildings index
C_ψ	Admissibility constant
CL	Construction labor index
d	Fault vector
E	Equipment index
ES	Engineering and supervision index
I	Imaginary operator
I	Index
L^2	Function spaces
N	Normal distribution
P	The order of the autoregressive polynomial
Q	The order of the moving average polynomial
R	Real operator
R^2	Coherency Strength
s	Scale parameter
S	Smoothing operator
t	Time
U	Uniform numbers
W_x	Continuous wavelet transform of $x(t)$
$\overline{W_y}$	Complex conjugate of Continuous wavelet transform of $y(t)$
$x(t)$	Time series $x(t)$
$x_1(t)$	Time series $x_1(t)$
$x_{1_{f1}}(t)$	Time series $x_1(t)$ with fault $f1$
$x_{1_{f2}}(t)$	Time series $x_1(t)$ with fault $f2$
$x_2(t)$	Time series $x_2(t)$
$x_{2_{f1}}(t)$	Time series $x_2(t)$ with fault $f1$
$x_{2_{f2}}(t)$	Time series $x_2(t)$ with fault $f2$
$y(t)$	Time series $y(t)$

$\in(i)$	Disturbance
$\in_t$	Noise
μ_f	Center of frequency
Σ	Summation symbol
τ	Location parameter
φ_{xy}	Phase difference between $x(t)$ and $y(t)$
$\psi(t)$	Mother wavelet
$\psi^M(t)$	Morlet wavelet
$\overline{\psi}$	Complex conjugate of a wavelet
$\Psi(\omega)$	Fourier Transform of wavelet
ω_0	Central frequency

LIST OF ABBREVATIONS

ACC	American Chemistry Council
ASEAN	Association of Southeast Asian Nations
BC	Business Cycle
BRICS	Brazil, Russia, India, China and South Africa
CAB	Chemical Activity Barometer
CEPCI	Chemical Engineering Plant Cost Index
COI	Cone of Influence
CPI	Chemical Processing Industries
CWT	Continuous Wavelet Transform
DUA	Dalgacık Uyumluluk Analizi
EIOZWA	Equatorial Indian Ocean Zonal Wind Anomalies
ENSO	El Nino-Southern Oscillation
EU ETS	European Union Emission Trading Scheme
EÜE	ABD Endüstriyel Üretim Endeksi
FD	Fault Detection
FDD	Process Fault Detection and Diagnosis
FT	Fourier Transformation
GDP	Gross Domestic Product
GNP	Gross National Product
HT	Hata Tespiti
IOD	Indian Ocean Dipole
IODMI	Indian Ocean Dipole Mode Index
IPI	US Industrial Production Index
KAB	Kimyasal Aktivite Barometresi
MA	Moving Average
MENA	Middle East and North Africa

MMA	Monthly Moving Average
NBER	National Bureau of Economic Research
OECD	The Organization for Economic Co-operation and Development
PFD	Process Fault Detection
PIIGS	Portugal, Ireland, Italy, Greece, and Spain
PM	Process Monitoring
PMI	Purchasing Managers' Index
PPI	Producer Price Indices
PSD	Power Spectral Density
PWC	Partial Wavelet Coherence
WC	Wavelet Coherence
WCA	Wavelet Coherence Analysis
WPS	Wavelet Power Spectrum
WT	Wavelet Transform
WTA	Wavelet Transform Analysis
XWPS	Cross Wavelet Power Spectrum

1. INTRODUCTION

In many time-series related studies, frequency-domain analyses such as the Fourier Transformation (FT) are preferred over time-domain analyses to discover the cyclic natures at different frequencies that are hidden otherwise. However, there are two problems about the FT. (Tiwari, 2013). First, temporal locations are disregarded (overlooked) because the time-domain data are lost while doing the transformation. Second, the FT is argued to be applicable only to the stationary time-series data which consist superposition of linear, independent, and non-evolving periodicities (Labat, 2005). But most of data series in which we are interested, such as macroeconomic- or engineering-related data, data are often noisy and non-stationary, thus not convenient for FT-related applications. One attempt to solve those problems is the short-time FT developed by Gabor (1946). In this method, windows are shifted over the time-series and the FT are applied to resulting sub-samples. Nonetheless, this is also not as efficient as desired because such windowed samples are not instantaneously adaptive.

On the other hand, the Wavelet Transformation (WT) as both a frequency- and time- domain method is a promising solution to all of the aforementioned problems. It is a natural local analysis of time-series since the length of wavelets varies endogenously by stretching into a long wavelet function to measure the low-frequency movements and by compressing into a short wavelet function to measure the high-frequency movements (Aguiar-Conraria and Soares, 2011). In this way, local analysis of non-stationary time-series data can be performed and transient changes can be well captured. Moreover, the WT preserves the temporal locations of time-series data as a function of time and hence allows us to simultaneously observe time- and frequency- domain information.

Use of Wavelet Transform Analysis (WTA) has become increasingly popular in geophysics since 1990s. Although early adopters of the WTA were using colorful images to provide results, they were not sufficient to depict quantitative findings. This is partly because the WTA (i.e. transformation from only-time to time-frequency domain) needs to pass the statistical significance test to be valid. According to Torrence and Compo (1998), former analyses were not reliable due to the lack of statistical significance. Subsequently, Torrence and Compo (1998) introduced statistically significant WTA toolbox. Their work makes the WTA comprehensible to researches by providing detailed and unique examples. They use the El Nino-Southern Oscillation (ENSO) data for their analysis and cover the choice of wavelet function, finite nature of time-series, and transformation from wavelet scale to Fourier frequency.

Later on, Grinsted et al. (2004) presented a new MATLAB toolbox for the WTA which is also known as AGToolbox. This a user-friendly package that covers Continuous Wavelet Transform (CWT), cross wavelet transform (XWT), Wavelet Coherence Analysis (WCA), and phase angle relationship between time series. The article uses geophysical data (the Arctic Oscillation index and the Baltic maximum sea ice extent record) to systematically demonstrate the prospects of the WA user. Additionally, the statistical significance test is performed by using Monte Carlo method in this article/toolbox.

More recently in 2011, Soares and Aguiar-Conraria (2011) developed a new MATLAB toolbox which is called ASToolbox. They aim to improve the toolbox that belongs to Torrence and Compo (1998) and bring all the necessary functions together in a single package. In addition to former toolboxes, it also performs partial and multiple WCA. Moreover, bootstrapping, Monte Carlo, and ARMA processes can be chosen in order to conduct the significant test. Competences of ASToolbox are shown in their work by applying to synthetic time series. Additionally, CWT is exemplified by using the data of Gross National Product (GNP) growth rate in the US, WCA is demonstrated by using the data of stock markets in the UK, the US, and Germany, and Partial Wavelet Coherence (PWC) by using the US stock market data and oil prices.

Additionally, MATLAB has adapted WCA and included a basic function since MATLAB version R2016a.

In the literature, WCA has become increasingly more preferable over stationary methods. The WCA has been extensively used in macroeconomics, finance, stock markets, energy markets, medical studies, and meteorology etc. Scholars focus on finding a coherent relationship or interaction between different variables in the form of cyclical co-movements. I first review the studies on economics and financial markets. In those fields, macroeconomics- or finance-related indicators such as economic growth, inflation, market pricing, or real wages have been investigated in the literature. Specifically, the studies on the co-movements of different stock markets are very common in the literature. Following this, I review several more papers on the co-movements of different commodity prices. Lastly, I look at limited number of papers from medical and biological studies and meteorology, which utilize WCA as well.

First of all, many studies examine market cycles as the subject of WCA. Mayes et al. (2011) compare the Gross Domestic Product (GDP) growth cycles in three major Eurozone economies: France, Germany, and Italy. They find that there is coherence at the conventional business-cycle frequencies of those three countries to a large degree whereas, in high frequencies, the coherency is low. In addition, the phase relation between Italy and France is not significant. Tiwari et al. (2013) look for the co-movements of the inflation rates among G7 countries and find significant continuous coherencies for longer time scales of four to 10 years and over 16 years. Moreover, the findings suggest that the inflation coherencies among G7 countries exist during the recent subprime crisis in varying time scales.

Marczak and Gómez (2015) examine the lag-lead patterns over time between consumer and producer real wages and business cycles in the US and Germany. The findings suggest that the US and Germany are different in that sense. In the US, the business cycle is led by both real wages whereas the business cycle is leading the consumer real wages in Germany. Bilgili (2015) uses WCA to probe the coherency relation between renewable-energy consumption and industrial production, and finds that renewables have a positive impact at all frequencies and more so at higher ones.

Yang et al. (2016) examine returns of some exchange rates against US dollar (EUR/USD, GBP/USD, and JPY/USD) by WCA. Their goal is to inform policymakers and investors by observing volatility fluctuations, effects of global financial crises, and European debt crisis. WCA indicate that the euro and the pound are strongly coherent while the yen and the pound are coherent in long periods. Conversely, the yen and the pound are not coherent at long-term periods. They presume that for long-term rate exchange assessment of euro-pound and euro-yen, interest rate parity is a successful leading indicator.

The WCA is a useful tool to analyze not only the conventional markets. Kristoufek (2015) wants to understand the reason behind tremendous increase in popularity of Bitcoin and Chinese market contribution. Kristoufek (2015) performs WCA for Bitcoin prices. Several possible contributing factors seem to exist as both speculative and technical ones for the Chinese market. The evidences depict that contrary to common thoughts, technical drivers (e.g. money supply, price level, and usage in trade) are also related with Bitcoin price in the long-term. Additionally, the number of coin miners increases with the Bitcoin price. Nonetheless, the price effect on miners fades away with time. Although the US Dollar and Chinese Yen are tightly connected, Kristoufek (2015) finds no clear evidence that the Chinese market influences the US market. He argues that such an outcome is due to the structure and frequencies of the data analyzed. Bitcoin seems to be a unique form of asset having the properties of both a standard financial instrument and a speculative one.

Aguiar-Conraria et al. (2008) uses cross wavelet coherency and cross wavelet power to probe the impact of interest rate price changes on macroeconomic variables such as industrial production, inflation, and monetary aggregates M1 and M2. This paper contributes to the literature by showing that “great moderation” is not a phenomenon that occurred in 1980s but actually happened in 1950s.

Two studies explore the interrelation between carbon emission and macroeconomic parameters such as economic growth and trade openness in France. Mutascu (2018) explores the interrelation between emissions and economic growth in France by using various wavelet tools including WCA. It is hypothesized that the environmental pollution is supposed to increase as the economy grows. In other words, it reaches a peak with growing economy then falls afterward. However, the findings indicate that such a co-movement does not exist for France in medium-term meaning that carbon emissions do not go along with the growing economy. However, this is more likely the result of environmentalist policies in France before 2002. Mutascu (2018) investigates the co-movements between carbon emissions and trade openness. This paper’s findings show no coherency between carbon emissions and trade openness at high frequencies but at medium and low frequencies, because the insufficient environmental regulations may drive exports based on pollutants at medium term whereas the business cycle drives the interaction between trade and emissions at long term (low frequency).

The use of macroeconomic variables such as economic growth in WCA is not limited to the studies on carbon emissions. Ferrer et al. (2018) examine the interactions between the financial-stress variables and real economic activity in the US. The results show that the coherence between financial stress and real economy in the US varies over time. According to the findings, the most significant coherence between financial stress and real economic activities exists following the subprime-mortgage crisis, meaning that the coherent interaction between the stress and the real economy is the strongest during periods of financial crises. Aguiar-Conraria et al. (2012) investigate the relation between the yield curve and the macroeconomic variables in the US and found varying deterministic relations between the level, slope, and curvature of the yield curve and fundamental macroeconomic parameters, such as real activities, unemployment, inflation, and Federal Reserve Bank (FED) funds rate.

Several papers utilized the WCA to investigate the co-movement relations between stock markets in the same or different countries. Graham et al. (2013) finds that there is a modest degree of coherency in stock returns between S&P 500 and MENA region stock markets as well as within the MENA region stock markets (particularly Egypt, Kuwait, and Saudi Arabia) themselves. Most significantly, Egypt market correlates with the US market the most. The authors explain this by the relative openness of the Egyptian stock markets to foreign participation. The WCA of Barunik et al. (2011) finds the strongest interdependency (particularly during the period of the subprime-mortgage crisis) among Czech (PX) and Polish (WIG) stock markets in a sample of several Central- and Western-European stock markets as well as the US. The findings suggest that the wavelet coherencies are different between Central-European, Western-European and the US stock markets. Moreover, another significant evidence is that British (FTSE) and German (DAX) stock markets are highly correlated on a daily basis between 2004 and 2009.

Tiwari et al. (2016) scrutinize relationship of stock markets of PIIGS countries with the stock markets of UK and Germany. WCAs between stock markets of PIIGS countries and UK reveal that they move “in phase” along the entire time span. The stock markets are mostly coherent in medium- and long-term periods (64 days to 512 days). For long-term coherency, they postulate that the stock markets of PIIGS countries with the exception of Italy lead the stock market of UK between 2008 and 2011. Conversely, the stock market of UK leads the stock market of PIIGS for medium-term period after the collapse of Lehman Brothers. Similarly, WCAs between stock markets of PIIGS countries and Germany are roughly analogous to WCAs of PIIGS and UK. During the subprime crisis, German stock market leads that of Ireland, Greece and Portugal in very short periods and coherency level between PIIGS and German stock market is higher.

Jiang et al. (2017) work with six stock markets of Association of Southeast Asian Nations (ASEAN) countries (Indonesia, Thailand, Philippines, Malaysia, Singapore and Vietnam) to monitor the co-evolution of markets and the effect of causal events on volatility. WCAs point out that stock markets in ASEAN countries have a stronger tendency to move together, especially during financial turbulence. In contrast to the claims of different studies utilizing other methods, such as Azman-Saini et al. (2002), Singapore is found to be the least dependent market. They say that the stock market of Vietnam does not move coherently with the rest of stock markets of ASEAN countries. Specifically, Indonesia is coherent with Thailand and the Philippines at high frequencies, whereas, it is coherent with Malaysia at low frequencies. The authors thus conclude that a portfolio, which includes only ASEAN stock markets, is likely to fail decreasing the risks.

Saâdaoui et al. (2017) study the co-movement relationships between conventional and Islamic stock markets via cross wavelet analyses. The subject indexes include Dow Jones (DJ) index and their Islamic counterparts such as DJ Islamic Market World Index (DJWI), DJ Islamic Market Developed Markets Index (DJDI), and DJ Islamic Market Emerging Markets Index (DJEI). Islamic countries’ lifestyle and Islamic-based fiscal affairs attract attention of policymakers, market participants and investors to Islamic stock markets as an alternative option to conventional markets in the matters of portfolio diversification and risk reduction during financial depressions since this situation encourages risk sharing. Covariation figures of conventional stock markets vs. Islamic stock markets show that they are coherent at long-term periods. On the other hand, covariations show differences in shorter periods. During slumps, conventional stock markets move mostly coherent in all periods whereas co-movement of Islamic stock markets is not as strong as among conventional markets. Therefore, Islamic is a considerable option for portfolio diversification.

Academicians and economist have become more motivated to understand interrelation between stock markets especially after big financial turmoil. Marfatia (2017) investigates the integration of risks in international stock markets by examining 22 leading stock markets of the world via wavelet analyses. The author uses XWT to assess coherency of these stock markets to guide policy makers and portfolio managers. Evidences display that US market and Eurozone markets are coherent in long-term periods; however, they are not significantly coherent in short-term periods. Hence, risks are possible to be observed in the long run. Additionally, comparisons of WCAs depict that level of co-movement between a stock market and another stock market in the same region is higher than co-movement level between the stock market and the US stock market. The study also reveals that despite the common belief about the contagion effect of financial crisis from one country to others, the spillover of risks was mostly limited at lower frequencies.

Furthermore, economics-related applications of WCA include several studies on the interactions between commodity, real estate, or equity prices such as oil or housing and other related market movements. McCarthy and Orlov (2012) work on the links between volatility of the futures price of crude oil and S&P500. They additionally study volume of crude oil futures and US stock market futures contracts. Unlike Awerbuch and Sauter (2006) and Jones and Kaul (1996), they claim that oil prices and the US stock market have positive relationship. Akoum et al. (2012) inspect relationship among six GCC countries' (Bahrain, Kuwait, Oman, Qatar, Saudi Arabia, and the United Arab Emirates) stock markets and crude oil prices. They also work on stock markets of Egypt and Jordan, which are also located in the same region yet not producing oil, to enlarge the scope of the study. They conclude that evidence of WCA discloses that stock markets and oil price co-move in the long term (more than six months), more strongly after 2007. Also, the relationship between stock-market and oil prices is stronger for Jordan compared to Egypt. Subsequently, they draw a conclusion that linking function between stock-market and oil prices varies from country to country.

Aguiar-Conraria et al. (2014) perform WCA to industrial production indexes of Euroland countries and oil price to uncover the outcomes of Euro adoption for macroeconomics in the context of oil prices. The findings show that zones of coherence are located around 6-year period between 1985 and 1995. Nevertheless, coherency zones move to shorter periods in the last decade. Moreover, after Euro adoption, industrial production of most of the Euroland countries react synchronized to oil shocks. However, among 11 countries, Ireland, Belgium and Portugal do not have similar economical response to sudden changes in oil price.

Vacha et al. (2013) probe biofuels (ethanol and Biodiesel) and several commodities (gasoline, diesel, crude oil, corn, wheat, soybeans, sugarcane and rapeseed oil) via WCA to observe the relationship between them in time and frequency domains. Among analyzed, biofuel and commodity pairs, the pairs of ethanol and corn, and German diesel and biodiesel are the prominent ones. All of these pairs are coherent around 6-month period but the coherency shows discrepancy during periods of food crisis. In that period, the coherency becomes important only in short periods and phase differences between biofuels and commodities prevail to be more important. In food crisis, corn leads ethanol whereas German diesel leads biodiesel.

Aloui and Hkiri (2014) examine GCC countries' (Bahrain, Kuwait, Oman, Qatar, Saudi Arabia, and the United Arab Emirates) stock market co-movement behaviors using WCA. They assert that stock markets are highly affected from economic crises and they start to move together more strongly together after 2007 at short-term periods. Madaleno and Pinho (2014) apply WCA to oil price and world general stock market index and its 10 subgroups (basic materials, consumer goods, consumer services, financials, health care, industrials, oil and gas, technology, telecommunications, utilities) to elaborate their former study. Results show that oil price, and world and sectoral stock markets have high coherency in long periods (0.7 years to 5.6 years). However, coherency is not stable over years. Before and after crises, the co-movement of oil price and stock indexes becomes more significant. Specially, in 2008 (during the global financial crisis), the series are coherent in short, medium and long periods. Furthermore, stock markets lead in all periods in which the global financial crisis was taking place.

Vacha and Barunik (2012) try to reveal the interconnection between energy commodities such as gasoline, heating oil, natural gas, and crude oil. Results indicate that gasoline, heating oil and crude oil are highly correlated to each other and relations between commodities are highly dependent on investment horizon. Additionally, the fear of recession results in a tendency to move in unison for commodities but heating oil and crude oil is highly coherent in 64- to 128-day period band, even exterior of recession.

Li et al. (2015) analyze the evolution of co-movement between US housing and stock markets. They claim that the US housing and stock markets are coherent over 1890 to 2012, except for the period from 1998 to 2002. In this period, they move "in phase". On the other hand, the coherency is observed the most in long-term periods throughout the time span. Between 1905 and 1910 and between 1998 and 2002, the US housing and stock markets have coherency in the short-term period.

Mudakkar and Zaman (2013) perform WCA to indicate the effects of oil price on stock exchange of Pakistan (KSE 100) and India (NIFTY 50). They conclude that co-movements between oil price and stock exchanges are significant during financial shocks. The effects of financial shocks before 2007 are observed in short term whereas, after 2007, the shocks influence stock exchanges in medium term. In Huang et al. (2016), Shanghai Composite index (SH), Brent oil prices and London gold fixing price data are analyzed using WCA to uncover hidden information caused by nonlinear relationship between prices. Results of WCAs exhibit that SH and Brent oil are coherent in short, medium and long periods. At short-term periods (2 to 16 days band), coherent zones are discrete but unstable. In medium term periods (16 to 256 days band), there are more coherent zones than that of long-term periods (256 to 512 days band), and in long-term periods SH and Brent oil is coherent between 2003 and 2012. Similarly, SH and gold price WCA depicts close results for short and medium periods, however the coherent region is comparatively smaller and it is located between 2004 and 2010.

Graham et al. (2013) apply WCA to the stock market (S&P500) and commodities (S&P Goldman Sachs Commodity Index), energy, light-energy, non-energy, reduced energy, agriculture, livestock, petroleum, industrial metal, precious metals and softs commodities (corn, wheat, sugar etc.) in order to discover possible connections between these markets. They aim at giving evidence of cross-market relations for investors preparing portfolios. They deduce the results that there is generally no significant coherency between the stock market and commodities. Therefore, they claim that commodities are still good options to sustain diversification. Additionally, taking term differences into account shows that short-term investment is a good option for diversification whereas, after 2007, long-term investment is a little bit doubtful during a financial crisis period.

Sousa et al. (2014) aim to give insight about the noteworthy variables for the co-movement among CO_2 prices, energy prices (gas, coal and electricity), and economic activity for carbon-market actors of The European Union Emission Trading Scheme (EU ETS) using WCA. Their results display that CO_2 and energy prices are coherent over 8 to 20 months and energy price is lagging behind CO_2 price. They associate the results with the CO_2 emissions suppression success of the EU ETS. They also add that Kyoto Protocol generates an uncertain atmosphere that results in an increase in volatility. Moreover, CO_2 price and economic activity analysis shows that the economic trends lead the carbon markets.

Papaioannou et al. (2015) focus on dynamics of the interrelation between Greek and Italian electricity markets. They believe that the outcomes attained by the application of WCA will bring light to authorities for preparing national markets according to the European model during coupling process of the two markets. Results reveal that two markets are highly coherent between 2005 and 2013. Furthermore, regulations and failures create higher coherency in short periods. Reboredo et al. (2017) want to observe dynamic relationship between fossil fuel and renewable energy to see the results of developments. They conduct WCA to oil price, renewable energy stock prices, and three renewable-energy sectoral indices (wind, solar, smart technology). Results display that although sectoral indices have differences, level of co-movement between oil and renewable energy is low for short-term periods and it is getting higher over longer-term periods, especially between 2008 and 2012. They suggest that volatility reduction of portfolios can be accomplished for short-term investors by investing in oil as an alternative to renewable energy.

Pal and Mitra (2017) study crude oil prices, world food price indices, and sub-indices (dairy, cereals, vegetable oil, sugar) for policymakers and farmers to determine beneficial crop choices. Results show that crude oil and food prices are coherent between 2001 and 2012. Coherencies are mostly observed in long-term periods. WCAs also catch that food crisis happened between 2006 and 2008 and financial turbulence occurred between 2007 and 2009. During periods of crisis, oil prices lead food prices in short time periods and the authors suggest policy makers to move accordingly.

Aloui et al. (2016) attempt to investigate the co-movement between investors' sentiment and equity returns in Islamic and conventional market indexes. Their empirical findings show that the co-movement is shifting over time and frequencies and the Islamic equity returns do not behave differently from their conventional counterparts in the context of investor sentiments. Yang et al. (2017) examine association between crude oil price and exchange rate market of markets with the power of WCA. Unlike previous studies, they group stock markets as markets of oil-importing countries (EU, India, Japan, and South Korea) and markets of oil-exporting countries (Brazil, Canada, Mexico and Russia) for better understanding. The evidence show that around 2008, both oil importing and oil-exporting countries have strong coherency, but coherency for oil-importing countries start from 2005. The study make it clear for policy makers that crude oil price is a more important factor for oil-importing countries for determining the exchange rate comparing to oil-exporting countries. Moreover, with respect to investors, the stability of interaction between crude oil and exchange rate is low in short-term.

Mensi et al. (2018) conduct WCA for BRICS countries' stock markets and two macro economically important commodities to reveal international connections of those countries. WCA results reveal that stock markets are coherent with crude oil price at long-term periods and global financial crises reflect on WCA as highly coherent zones. Conversely, there is no finding of co-movement between stock markets and gold price. Therefore, it is suggested that BRICS stock markets and gold price are alternative assets of each other during financial turmoil.

Abid and Kaffel (2018) examine the relationship between four asset prices (stock, gold, oil, Forex) and their volatility index to demonstrate behavior differences under different economic conditions, strength levels between prices, and volatility in a period in which they are significant and worthiness for portfolio managers. Wavelet Power Spectrums (WPS) show that during some financial stresses, assets are affected in medium periods while risk indexes are affected almost in all periods. WCAs show that the assets and their volatility indexes do not have stable coherency during the entire period and phase differences between them changes from period to period. On the other hand, S&P 500 and its volatility index are coherent in short, medium and long periods and they are "out of phase". Finally, they conclude that putting an assets and its risk index in the same portfolio is disadvantageous, because they are correlated.

Global economy and business are highly affected from financial crises and from stresses on crude-oil prices resulting from geopolitical indecisions. Uddin et al. (2018) use WCA to clarify co-evaluation between crude-oil price and possible roots of fluctuations of crude-oil price such as financial speculation, uncertainty in financial markets and macro economy, and market sentiment. WCAs show that oil price and indecisions are coherent at short-term periods and at business-cycle periods. The phase relation between them range between $-\pi/2$ and $+\pi/2$ $-\pi/2$ and $+\pi/2$. For higher periods, oil price lags behind the uncertainties indexes. On the other hand, crude-oil price and speculation index are highly coherent at 4.5- and 8-year period bands. However, they are "out of phase" according to the WCA.

Meteorology is another field in which WCA is taken advantage of. Torrence and Webster (1999) apply WCA to El Nino-Southern Oscillation (ENSO) and Indian monsoon data over 125 years to investigate the relationship between coherency and variance. They argue that the coherency between ENSO and Indian monsoon is high in 2- to 8-year bands over 1875-1920 and 1960-1990. Additionally, if only decadal parts of data are analyzed, coherency and variance shows parallelism (i.e., higher the coherency, higher the variance).

Likewise, Ashok et al. (2003) study meteorological indicators to enhance the knowledge about Indian Ocean Dipole (IOD), which is a physical entity. WCA of the Equatorial Indian Ocean zonal wind anomalies (EIOZWA) and Indian Ocean Dipole Mode Index (IODMI) significantly shows that coherent zones on the years with IOD have a dominant effect. Additionally, El Nino/Southern Oscillation (ENSO) and EIOZWA are also found coherent. On the other hand, ENSO and IODMI do not have coherency at the periods in which ENSO and EIOZWA are coherent. Thus, the study reveals that the IOD events may be a result of regional air-sea interactions rather than an external forcing.

Lastly, WCAs are found in medical and biological studies. Garg et al. (2013) work with WCA to test the capability of distinguishing connections between cardiovascular- and postural-control system. They report that WCA over blood pressure and calf-muscle electromyography is successful to recognize co-activity between them. Hassan et al. (2010) use the data collected from uterine of three pregnant women for WCA to characterize electrical activity of uterine. Hypothesis about the uterine electrical activity claims that electromyogram signal of pregnant abdomen is classified as Fast Wave Low, which is interpreted as propagation, and Fast Wave High which is interpreted as excitability of the uterus (Devedeux et al., 1993).

The main purpose of this thesis is to investigate capabilities of CWT, WPS, and WCA; additionally, to discover hidden associations between US chemical-industry-related/-based time series (CAB and CEPCI) and US Industrial Production Index (IPI), and to clarify phase relations between them.

In Chapter 2, the fundamentals of wavelets and theoretical background on CWT, WPS, WPS, XWT, WCA, and phase difference are briefly reviewed. Moreover, definitions of FT, cone of influence (COI), padding, smoothing, phase relations between two time series are also included. Additionally, algorithmic structures of MATLAB's default WCA function, the ASToolbox, and AGToolbox are explained systematically.

In Chapter 3, analysis of a motivating example is presented with the Pearson correlation method, windowed cross correlation, windowed and lagged correlation, WPS and WCA. Subsequently, results come from conventional methods and wavelet based methods are compared in terms of coherency and phase difference extend.

In Chapter 4, the American Chemistry Council's (ACC) Chemical Activity Barometer (CAB) and business cycle phenomena are defined. Monthly data of CAB and Industrial Production Index (IPI) of US are deeply investigated by WPS and WCA to test whether CAB is a leading indicator of IPI and is able to detect business cycles in US economy. Outcomes are compared with already determined business cycles taken from ACC. Additionally, overall phase difference relation images between the CAB and IPI is generated.

In Chapter 5, WCA is applied to binary pairs of CAB-Chemical Engineering Plant Cost Index (CEPCI) data and IPI-CEPCI data in order to assess the potential of CEPCI as a leading indicator of the US economy. However, since only the yearly CEPCI data are available, firstly the effects of data collection frequency on WCA of CAB and IPI are re-examined with the yearly versions of the CAB and IPI data. The results of the yearly WCA of CAB and IPI are compared with the results of Chapter 4, where monthly CAB and IPI data are used. However, the main purpose of this chapter is on the CEPCI data and its WCA with CAB and IPI pairs.

In Chapter 6, as groundwork, WCA is applied to Process Fault Detection and Diagnosis (FDD) field to assess the viability WCA as a new FDD tool, for the first time in literature. For this purpose, first, the synthetic time series already used in Chapter 3 are reviewed within the framework of FDD and WCA is concluded to be a successful tool for fault and change point detection tasks. Moreover, two new synthetic time series are generated and several faults are added to these time series and fault detection ability of WCA under permanent and temporal faults is demonstrated.

2. TECHNICAL BACKGROUND FOR WAVELET COHERENCE ANALYSIS AND THE TOOLBOX USED

2.1.Wavelets and the Morlet Wavelet

Wavelets are small dynamic waves which have characteristic oscillation. Amplitudes of waves begin from zero, then increases, and then returns to zero. Wavelets are generated by positioning and scaling a wavelet function $\psi(t)$ (i.e., mother wavelet) which is defined as:

$$\psi_{s,\tau}(t) = \frac{1}{\sqrt{s}}\psi\left(\frac{t-\tau}{s}\right) \tag{2.1}$$

where, $1/\sqrt{s}$ is the normalization factor, τ is the location parameter, and s is the scale parameter (Akoum et al., 2012). While τ determines position of the wavelet, s shows how the wavelet is stretched or dilated. In order to compress the wavelet, s parameter must be decreased which will make it possible to investigate higher frequencies (minor oscillations), or vice versa (Benhmad, 2013).

Wavelet function $\psi(t)$ is assumed to be a square integrable function ($\psi = L^2 \in R$) and it has to satisfy several theoretical conditions (Aguiar-Conraria et al., 2008). In order to ensure back transform from frequency domain to time domain, wavelet function must be successfully localized in time and frequency domain. To do so, a wavelet has to rapidly decay in both (left and right) directions which is also the reason behind success of wavelet analysis with dealing nonstationary series and discontinuities (jumps) (Auth, 2013). In other words, a wavelet has to fulfill admissibility condition, which will be explained in detail in the following section, to be used as an orthogonal function for Continuous Wavelet Transform (CWT)). The admissibility condition is given as:

$$C_{\psi} = 2\pi \int_{-\infty}^{\infty} \frac{|\Psi(\omega)|^2}{|\omega|} d\omega < \infty \tag{2.2}$$

where, C_{ψ} is the admissibility constant and $\Psi(\omega)$ is the Fourier Transform (FT) of wavelet $\psi(t)$. Gençay et al. (2002) show that admissibility condition holds when mean of a wavelet is zero:

$$\int_{-\infty}^{\infty} \psi(t) dt = 0 \tag{2.3}$$

and

$$\int_{-\infty}^{\infty} \psi^2(t) dt = 1. \tag{2.4}$$

In other words, total area under positive parts of a wavelet has to be equal to total area under negative parts of the wavelet and the wavelet has to have values other than zero.

There are different types of wavelets such as the Haar, Daubechies, Biorthogonal, Coiflets, Symlets, Morlet, Mexician Hat, Meyer etc. (Misiti et al., 2010). Among wavelets, the Morlet wavelet is successfully localized in frequency domain (Tiwari et al., 2013) and it is widely used in economics (Aguiar-Conraria et al., 2008, 2013; Crowley, 2007; Madaleno and Pinho, 2014; Percival and Walden, 2000; Rua and Nunes, 2009). In this study, following the path of literature, we use the Morlet wavelet which is defined as:

$$\psi^M(t) = \pi^{-\frac{1}{4}}(e^{i\omega_0 t} - e^{-\frac{\omega_0^2}{2}})e^{-\frac{t^2}{2}} \tag{2.5}$$

where, ω_0 denotes central frequency of the wavelet and $e^{-\frac{\omega_0^2}{2}}$ is added to ensure that the admissibility condition holds. Fortunately, in almost all cases, ω_0 is chosen bigger than 5 and thus $e^{-\frac{\omega_0^2}{2}}$ becomes negligible (Aguiar-Conraria et al., 2008). Hence, the Morlet wavelet reduces to:

$$\psi^M(t) = \pi^{-\frac{1}{4}} e^{i\omega_0 t} e^{-\frac{t^2}{2}}. \qquad (2.6)$$

Aguiar-Conraria and Soares (2007) shows that the center of wavelet is located on the point $(0, \frac{\omega_0}{2\pi})$ in time-frequency plane and in most cases $\omega_0 = 6$ is chosen. Thus:

$$\mu_f = \frac{\omega_0}{2\pi} \approx 1 \qquad (2.7)$$

where μ_f is center of frequency and hence the relationship between scale and frequency becomes:

$$f = \frac{\mu_f}{s} \approx \frac{1}{s}. \qquad (2.8)$$

2.2. Continuous Wavelet Transform

Projecting the specific wavelet onto the time series studied, $x(t)$, gives the Continuous Wavelet Transform (CWT), W_x, of the series as:

$$W_x(s,\tau) = \int_{-\infty}^{\infty} x(t) \frac{1}{\sqrt{s}} \overline{\psi}(\frac{t-\tau}{s})\, dt \qquad (2.9)$$

where, $\overline{\psi}$ is the complex conjugate of ψ. The time series can be reconstructed from this continuous wavelet transform as (Barunik et al., 2011):

$$x(t) = \frac{1}{C_\psi} \int_0^{\infty} [\int_{-\infty}^{\infty} W_x(s,\tau) \psi_{s,\tau}(t) d\tau] \frac{ds}{s^2}, \qquad s > 0 \qquad (2.10)$$

where, C_ψ is admissibility constant (see (Akansu and Haddad, 2001) for its derivation) . Another useful inference is that the energy of $x(t)$, that is $||x||^2$, is preserved after back transformation (Aguiar-Conraria and Soares, 2007):

$$||x||^2 = \frac{1}{C_\psi}\int_{-\infty}^{\infty}[\int_{-\infty}^{\infty}|W_x(s,\tau)|^2\,d\tau]\frac{ds}{s^2}. \tag{2.11}$$

2.3. Wavelet Power Spectrum

Wavelet Power Spectrum (WPS) is a univariate analysis tool. It allows observing local variance of a time series for different scales and time localizations. WPS differs from FT-based power spectrum (Torrence and Compo, 1998). Significance testing for WPS is also possible (Grinsted et al., 2004; Torrence and Compo, 1998).WPS is defined as the square of the absolute value of the CWT and is given by:

$$WPS_x(s,\tau) = |W_x(s,\tau)|^2. \tag{2.12}$$

2.4. Cross Wavelet Transform and Wavelet Coherence Analysis

WCA is a bivariate analysis which is used to observe interaction between two time series. In WCA, both the Cross Wavelet Transform (XWT) and the cross wavelet power of two series ($x(t)$, $y(t)$) must be computed.

$$W_{xy}(s,\tau) = W_x(s,\tau)\overline{W_y}(s,\tau) \tag{2.13}$$

where, $W_{xy}(s,\tau)$ denotes XWT of $x(t)$ and $y(t)$, $W_x(s,\tau)$ denotes CWT of $x(t)$, and $\overline{W_y}(s,\tau)$ denotes complex conjugate of CWT of $y(t)$. Cross wavelet power, $|W_{xy}(s,\tau)|$, is the absolute value of XWT.

The Wavelet Cohrence (WC) is defined as:

$$R^2(s,\tau) = \frac{\left|S\left(s^{-1}W_{xy}(s,\tau)\right)\right|^2}{S(s^{-1}\,|W_x(s,\tau)|^2)S\left(s^{-1}\,|W_y(s,\tau)|^2\right)} \tag{2.14}$$

where, S is a smoothing operator and $0 \leq R^2 \leq 1$ shows the coherency strength. When R^2 is close to 1, the coherence between time series is high and when R^2 is close to 0, the coherence between time series is low.

Unfortunately, there is no consensus on how the smoothing should be implemented. In other words, it is not clear that what type of smoothing is appropriate and also it is not clear that on which domain smoothing should be performed (time domain, frequency domain or both) (Torrence and Compo, 1998).

2.5. Phase Difference

WCA also shows the phase differences between two time series of different frequencies. WC phase difference is defined as:

$$\varphi_{xy}(s,\tau) = tan^{-1}\left(\frac{I\left(S\left(s^{-1}W_{xy}(s,\tau)\right)\right)}{R\left(S\left(s^{-1}W_{xy}(s,\tau)\right)\right)}\right) \tag{2.15}$$

where, I represents the imaginary operator and R represents the real operator. Phase differences calculated by Eq. 2.15 are shown in WCA figures with arrows. Right-directed arrows show that the two time series are “in phase” while left-directed arrows shows that the two time series are “in anti-phase” (i.e., “out of phase”). Additionally, upward arrows mean that the second time series, $y(t)$, leads the first time series, $x(t)$, by 90°, and downward arrows mean that the first time series, $x(t)$, leads the second time series, $y(t)$, by 90°.

2.6. Wavelet Coherency Analysis Software Toolboxes

There are mainly three MATLAB software toolboxes commonly used in the literature, namely AGToolbox, ASToolbox and MATLAB's default WCA function, "wcoherence". Most parts of those toolboxes are similar to each other. Generally, calculation of XWT and the smoothing sections of these software show minor differences. Subsequently, WCA shows minor differences. Some important sections of these toolboxes are highlighted in the following sections (2.7 - 2.9).

2.7. Major Calculation Steps of MATLAB's Default WCA Function

In MATLAB's default WCA function, "wcoherence" there are eight major computational sections.

1. Two time series are individually sent to "cwtft" function subroutine for CWT calculation. Each time series follow the next steps in "cwtft":

   i. The time series is sent to "ftt" function for discrete Fourier transform.

   ii. All family members of the mother wavelet are sent to "waveft" function for wavelet Fourier transformation.

   iii. Transformed time series are projected onto the transformed wavelet family to obtain CWTs of the series (Eq. 2.9).

2. XWT is formed by multiplying CWTs of the two time series (Eq. 2.13).

3. Smoothing operations are performed only on frequency domain for both CWTs and XWT.

4. Cross Wavelet Power Spectrum (XWPS) is obtained by dividing the smoothed XWT by the square roots of the smoothed CWTs of the two time series (Eq. 2.16).

$$XWPS = \frac{S(XWT)}{\left(S\big(W_x(s,\tau)\big)^{\frac{1}{2}} * S\left(W_y(s,\tau)\right)^{\frac{1}{2}}\right)} \tag{2.16}$$

5. WC is obtained by dividing the square of absolute value of smoothed XWT by the smoothed CWTs of the two time series (Eq. 2.14).

6. Phase difference between the two series is obtained by taking the inverse tangent of division of imaginary part of the cross wavelet power spectrum to real part of the cross wavelet power spectrum (Eq.2.15).

7. Cone of Influence (COI) is calculated.

8. WCA image figure is generated by including WC, COI, and phase-difference arrows.

2.8. Major Calculation Steps of the ASToolbox

In the ASToolbox, there are collections of function subroutines with intricate dependence structure. This functional dependence of the toolbox may be outlined with three major computational sections.

1. Two time series are individually sent to “AWT” subroutine for calculation of CWT, WPS, and COI separately. Each time series then follow the next steps:

   i. The time series is sent to “fft” function for their discrete Fourier transform.

ii. All family members of the mother wavelet are transformed to Fourier domain by using definition of Fourier transformation.

iii. Transformed time series is projected onto the transformed wavelet family to find CWTs of the series (Eq. 2.9).

iv. WPS is obtained as the square of absolute value of CWT (Eq. 2.12).

v. COI is calculated.

vi. Optionally, statistical p-values for WPS are calculating based on ARMA model with bootstrapping or ARMA model with Gauss model.

2. Two time series are sent together to "AWCO" subroutine for calculation of WC. "AWCO" contains an extra "AWT" function and the following steps shows working principals of "AWCO" function.

i. XWT is obtained through CWTs of the two series (Eq. 2.13).

ii. WPS of each time series are obtained by taking the square of absolute values of CWT of the two series separately (Eq. 2.12).

iii. WPSs and XWT of the two series are smoothed in both time and scale directions.

iv. WC of the two series is obtained by the division of smoothed XWT of the two series with the square root of production of WPSs of the two series (Eq. 2.14).

3. Output of "AWCO" subroutine is feed to "AWCOOutput" function for calculation of cross wavelet power spectrum, phase difference spectrum and time lag. Steps are as follows:

i. XWPS is obtained by absolute value of XWT (Eq. 2.13).

ii. Phase difference between the two series is obtained by taking the inverse tangent of the division of the XWT imaginary part to the XWT real part (Eq. 2.15).

iii. Time lag is calculated by division of product of phase difference and mean period to 2π (Eq. 2.17).

$$Time\ lag = \frac{\varphi_{xy}(s,\tau) * mean(period)}{2\pi}. \qquad (2.17)$$

Note that ASTbx does not have a default plotting section.

2.9. Major Calculation Steps of the AGToolbox

In the AGToolbox, there are fewer collection of function subroutines with less intricate dependence structure compared to the ASToolbox. The functional dependence of the ASToolbox toolbox may be outlined with seven computational sections.

Two time series are together sent to "wtc" subroutine for WC calculation including the following intermediate steps.

1. Two time series are individually sent to "wavelet" function in which CWT of the two series are calculated (Eq. 2.9). During calculation "wave_bases" function is used for wavelet Fourier transformation and "fft" function is used for discrete Fourier transform of the time series.
2. Two CWTs of the time series are individually sent to "smoothwavelet" function for smoothing.

3. COI of the both series are calculated and the smaller one is chosen.

4. XWT is calculated via unsmoothed CWTs of the two time series (Eq. 2.13).

5. XWT is sent to “smoothwavelet” function for smoothing.

6. WC is obtained by the division of square of absolute value of smoothed XWT with the smoothed CWTs of the two time series (Eq. 2.14).

7. Phase difference between the two series is obtained by taking the inverse tangent of division of the XWT imaginary part by the XWT real part (Eq. 2.15).

In this thesis work, basically, a modified version of the original AGToolbox is used, because it is the most commonly used toolbox in the literature for WCA, such as (Andries et al., 2014; Barunik et al., 2011; Cui et al., 2012; Grinsted et al., 2004; Ng and Chan, 2012; Vacha and Barunik, 2012). Modifications made are mostly around the plotting sections and with the purpose of making the toolbox more user friendly. For example, the original AGToolbox gives only the WCA image figure overlayed with phase-difference arrows, but no phase-angle information and phase-angle plots whereas the original ASToolbox gives the WCA image figure but without phase-difference and phase-angle information (which can be obtained and plotted separately if desired). The modified AGToolbox developed in this thesis work, combines the best parts of the AGToolbox and ASToolbox, and thus gives the WCA image subplot with phase-difference arrows overlay, together with the phase-angle subplots. Therefore, a complete WCA is obtained and presented in a single figure composed of several subplots in a single run of the code.

3. MOTIVATING EXAMPLE

Wavelet Coherence Analysis (WCA) differs from the conventional time-domain and frequency-domain time-series analysis techniques. While those methods work only in one domain, namely, time domain or frequency domain, the WCA covers both the time and frequency domains (Pal and Mitra, 2019). Before investigating real time series via WCA, its demonstrative application to a synthetic time series is much more beneficial for the exhibition of its capabilities.

3.1. Definition and Properties of the Synthetic Time Series

In order to maintain reproducibility and comparability, the following synthetic data-generating process, used in Aguiar-Conraria and Soares (2011), was adopted to demonstrate the WCA and its capabilities.

$$x(t) = \sin\left(\frac{2\pi}{3}t\right) + 3\sin\left(\frac{2\pi}{6}t\right) + \in_{t} \qquad , t = \frac{1}{12}, \frac{2}{12}, \ldots, \frac{600}{12} \qquad (3.1)$$

$$y(t) = \begin{cases} 4\sin\left(\frac{2\pi}{3}\left(t + \frac{5}{12}\right)\right) - 3\sin\left(\frac{2\pi}{6}\left(t - \frac{10}{12}\right)\right) + \in_{t} & , t = \frac{1}{12}, \frac{2}{12}, \ldots, \frac{300}{12} \\ 4\sin\left(\frac{2\pi}{3}\left(t - \frac{5}{12}\right)\right) - 3\sin\left(\frac{2\pi}{6}\left(t + \frac{10}{12}\right)\right) + \in_{t} & , t = \frac{301}{12}, \frac{302}{12}, \ldots, \frac{600}{12} \end{cases} \qquad (3.2)$$

These time series are highly formalized and simple time series. Thus, they make the WCA very transparent and provide ease of comparison with the theoretical treatment presented in Chapter 2. Additionally, white noises are added to both series in order to understand effect of noise on WCA results. White noises, i.i.d. (independently and identically distributed), are generated from normal distributions with zero mean and unit variance, $\in_{t} \sim \alpha N(0,1)\ \forall t$, where α is the scale parameter that adjusts the signal to noise ratio. An added noise is called white noise if its expected value is zero, independent of time. In other words, its signal power is distributed independently over time or among frequencies. In this example, the scale parameter α is set to one.

Cyclic behaviors of the two time series are easy to observe. From Eq. 3.1 and Eq. 3.2, one can easily deduce that $x(t)$ and $y(t)$ are constructed by merging 3-year and 6-year cycles (assuming that the time unit is one year). However, the behavior of $x(t)$ is unchanged over time, whereas the behavior of $y(t)$ exhibits transient change after 25 years. In Figure 3.1a and Figure 3.1b, $x(t)$ and $y(t)$ are plotted. Their aforementioned behaviors may be deduced from Figure 3.1. Nevertheless, although we know that these two synthetic time series share similar sub-cycles, it is not possible to observe common features of these time series just by looking at their superposition; as seen in Figure 3.1c.

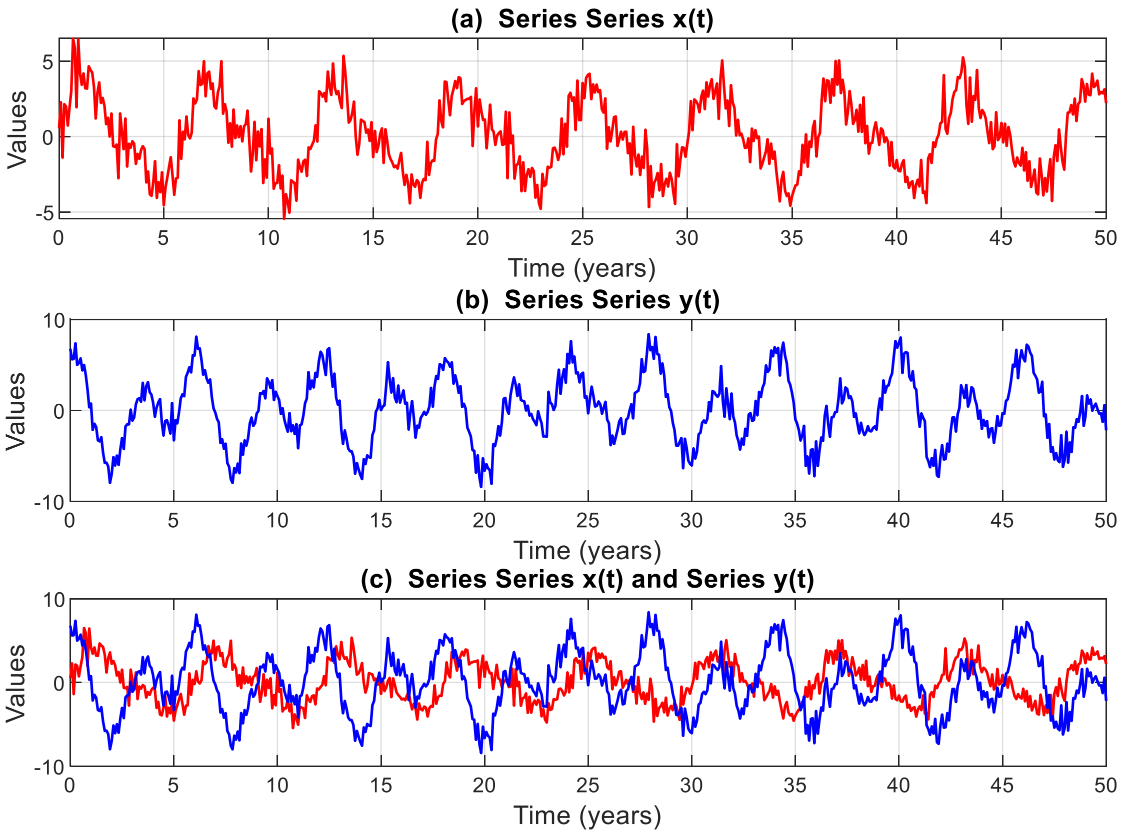

Figure 3.1. Individual and Superimposed Plots of the Synthetic Time Series.

3.2. Windowed Cross Correlation Analysis of the Synthetic Time Series

In order to reveal the hidden relationships between these two series, increasingly complex methods will be applied. Firstly, the overall Pearson linear correlation coefficient of the two series is -0.172. The Pearson correlation coefficient takes values between -1 and 1, with 1 meaning perfect positive correlation and -1 meaning perfect negative correlation between the two series. On the other hand, 0 indicates that there is no correlation between these series. Therefore, for these synthetic time series, it can be seen that the correlation is low; just based on the overall correlation coefficient. The Pearson linear correlation coefficient does not take any lags between the time series into consideration, however, windowed cross correlation can account for lags by using sliding-window approach.

To choose the best correlation-window size (window length), correlation coefficient was calculated for different window sizes. In Figure 3.2, calculated correlation coefficients were plotted. The colors represent the correlation coefficient between the time series as given by the colorbar on the right-hand side of the figure. Figure 3.2 clearly shows that windows which have window length longer than six years basically contains all sub-cycles and it is similarly colored at almost everywhere on the figure excluding the edges. Moving-average windowed correlation analysis is a low-resolution analysis and short-term transitional changes are disregarded for window lengths longer than 6 years. Additionally, when the window length is large (e.g., greater than 15 years), edge effects prevail. On the other hand, when the window length is too small, the windows start to lose their representative features. Moreover, it is known that the two time series have a common 6-year cycle from Eq. 3.1 and Eq. 3.2. Consequently, it is expected that setting the window size to three years (36 months) will have enough high representative power for these time series.

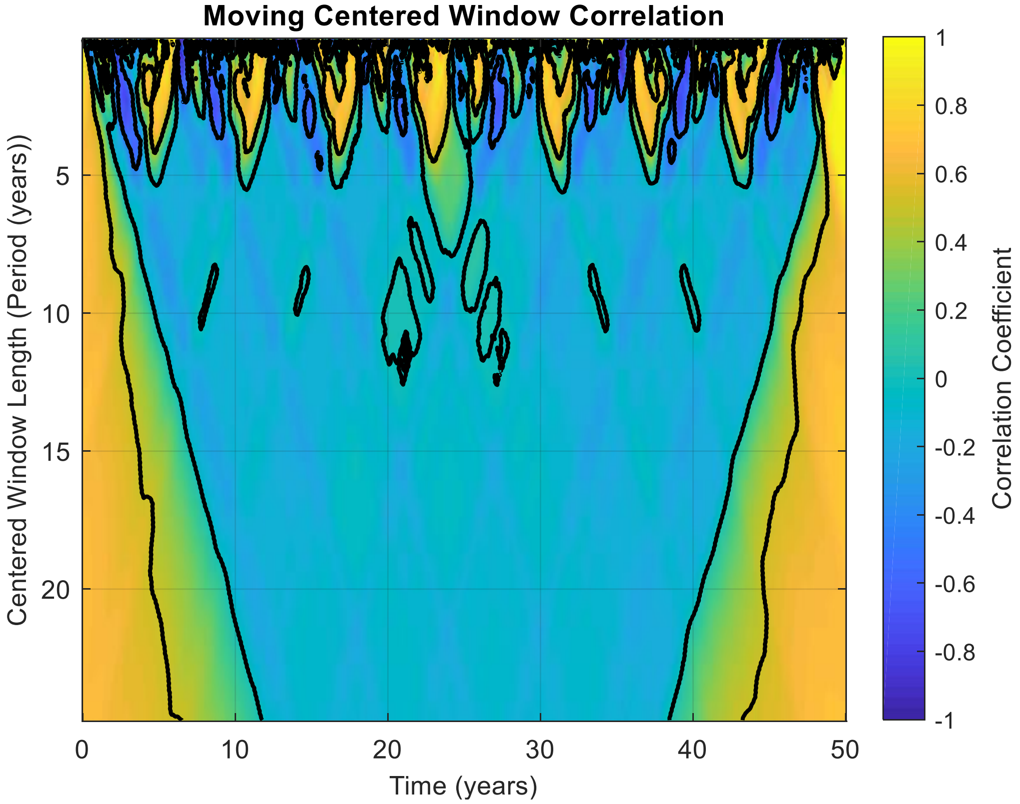

Figure 3.2. Moving Centered-Window Correlations of the Synthetic Time Series for Different Window Lengths.

In Figure 3.3a, windowed and lagged correlation of the synthetic time series was plotted by setting window length to six years (72 months). The colors represent the correlation coefficient between the time series. While bright yellow indicates positive perfect correlation (i.e., correlation coefficient is 1), dark blue indicates negative perfect correlation (i.e., correlation coefficient is -1).

The advantage of using windowed and lagged correlation is in its success to investigate correlation between the time series even if there is a phase difference between them. Figure 3.3a depicts that on the 3-year lag (y-axis) horizon and -3-year lag (or, 3-year lead) horizon, there are two broad dark yellow (high correlation) regions. Hence, it is presumed that the time series are positively correlated (color code shows that it is positive in the range 0.20 to 0.45, approximately) at ±3-year lags. Regrettably, these inferences are not enough to comment about the cyclic nature and transient change of the time series. Subplot b of Figure 3.3 shows the correlation coefficient as line plot at the zero-lag level of Figure 3.3.

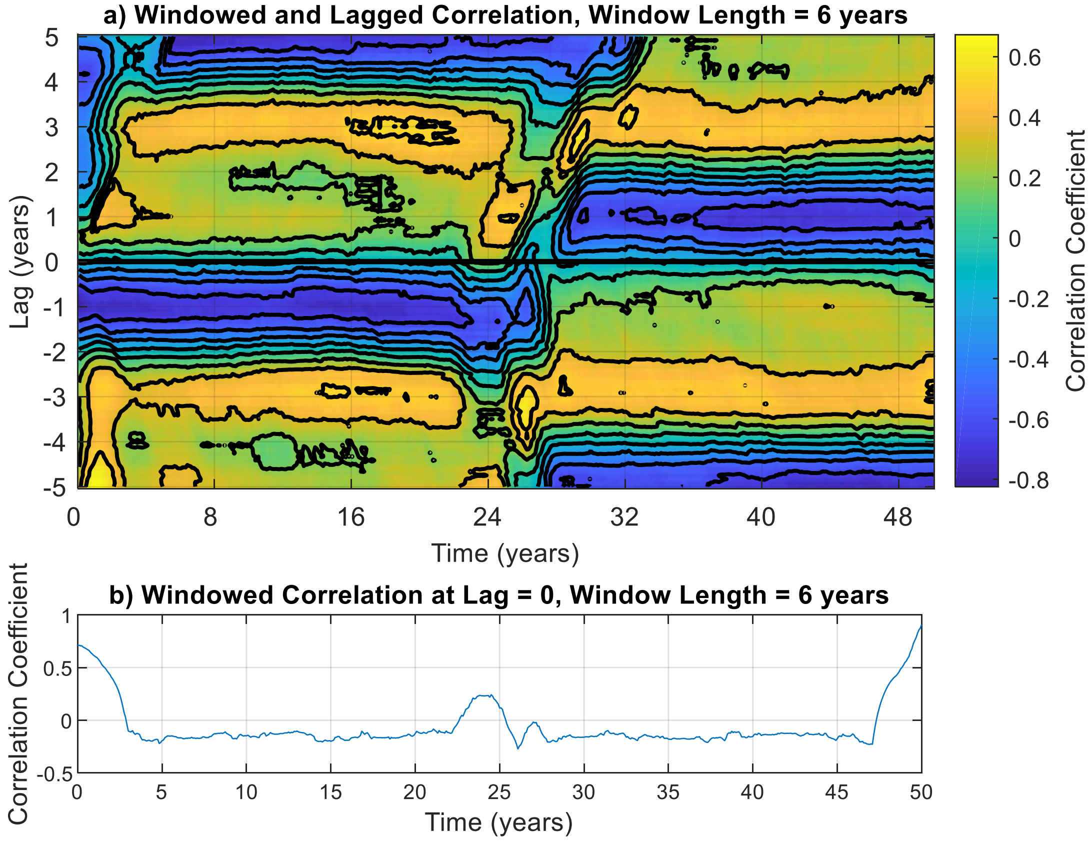

Figure 3.3. Windowed and Lagged Correlation between the Synthetic Time Series.

3.3. Univariate Analysis of the Synthetic Time Series

In order to reveal periodic components of the time series, the Wavelet Power Spectra (WPS) of the series were constructed. Continuous Wavelet Transform (CWT) was used to calculate WPS. Unlike Fourier Transformation (FT), CWT has an adaptive window size. Therefore CWT is successful at dealing with non-stationary time series (Mudakkar and Zaman, 2013). WPSs of the synthetic time series are shown in Figure 3.4. From the WPS of $y(t)$ series, one can easily distinguish the two hot-colored regions on the 3-year and 6-year period bands. This is not a coincidence, because as seen in Eq. 3.2, the $y(t)$ is constructed by the addition of two sine cycles, one with period of 3 years and the other of 6 years. Additionally, transitional changes in the time series are caught by WPS around 25 years. In contrast to WPS, the Power Spectral Density (PSD) does not show temporal changes in the time series, since it uses FT to analyze frequency domain. FT discards time-localized information (Li et al., 2015). The WPS of the $x(t)$ series contains two broad hot-colored regions located on the 3-year and 6-year period bands as well. However, the one located on the 3-year period band is not conspicuous because the magnitude of coefficient of 3-year cycle in Eq. 3.1 is smaller. Since there is no transient change in series $x(t)$, the hot-colored regions are continuous. Moreover, the coefficient of 6-year cycle in Eq. 1 is three times that of the 3-year cycle in Eq. 1 which can be observed in the PSD of series $x(t)$. In Figure 3.4, while the peak at 6 years is large, the peak at 3 years is relatively small. Although WPS and PSD explain the nature of two the time series, unfortunately they do not give any information about the association between them.

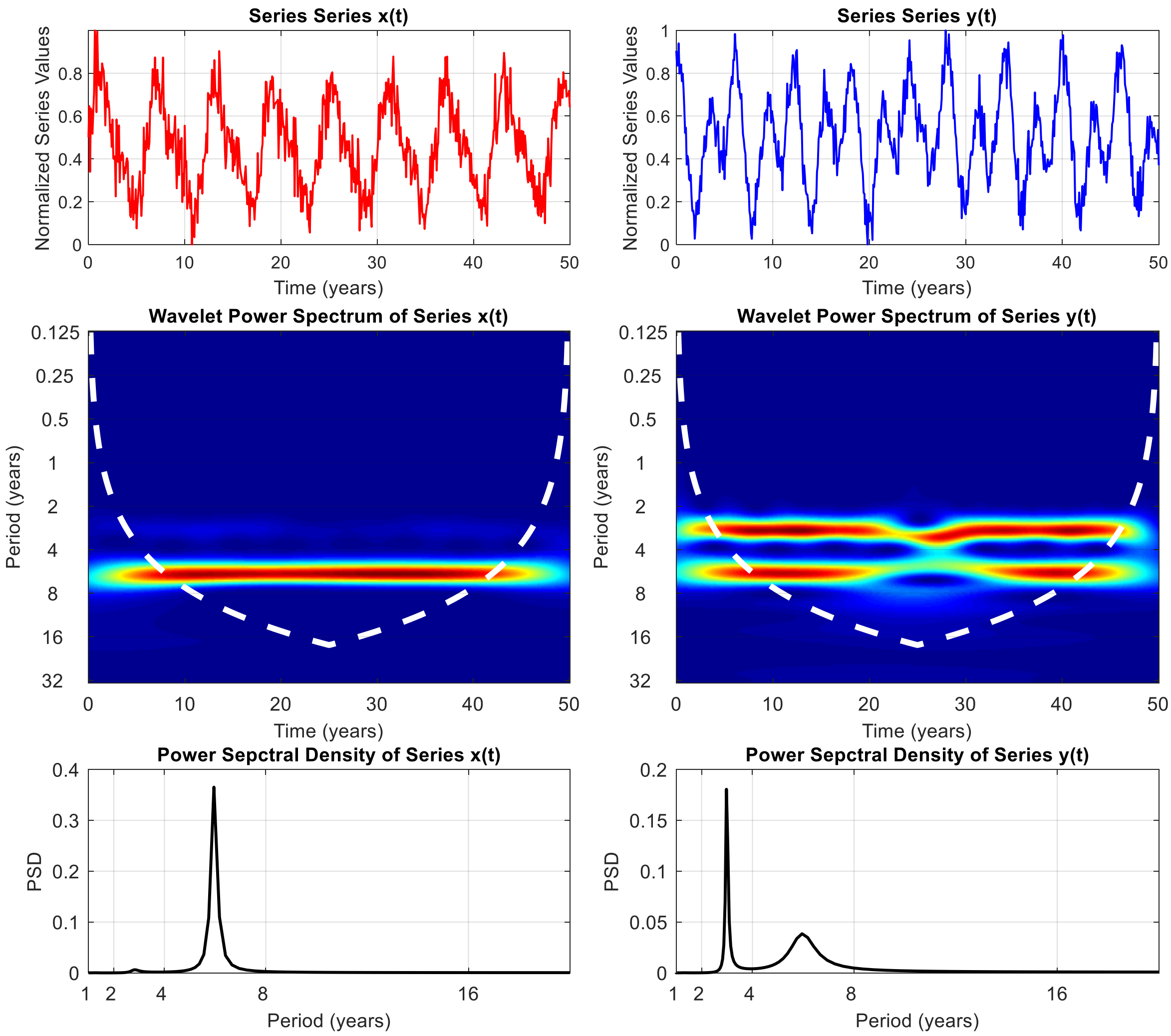

Figure 3.4. Wavelet Power Spectrums and Power Spectral Densities of the Synthetic Time Series.

3.4. Wavelet Coherence Analysis of the Synthetic Time Series

To be able to explore connections between the time series, Wavelet Coherence Analysis (WCA) should be executed. WCA is a bivariate framework; it can accommodate only two series. However it may be considered as a three-dimensional examination method; time and frequency components and power of correlation between two time series can be analyzed simultaneously (Sun and Xu, 2018). WCA can be explained as the proportion of cross-spectrum that can be obtained via multiplication of spectrum of each series individually (Aguiar-Conraria and Soares, 2007) and it enables one to visualize the degree of co-movement of two time series regarding both the time and frequency components. Unlike correlation, the range of coherency is between 0 and 1. While 1 specifies that two series are coherent, 0 indicates that there is no coherency between the two time series. Furthermore, high coherency is represented by yellow shades whereas low coherency is represented by blue shades in the WCA-related figures of this thesis work. Moreover, WCA provides phase-difference information between time series.

The lead-lag and phase-state (i.e., “in phase” or “out of phase”) relationships in WCA can be summarized handsomely by Figure 3.5, as Funashima (2017) argued.

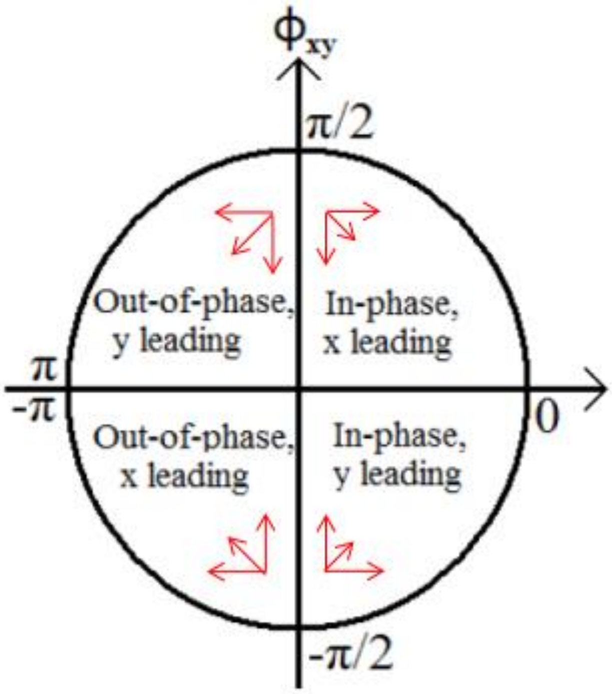

Figure 3.5. Lead-Lag and Phase-State Relationships in Wavelet Coherence Analysis.

Table 3.1 lists the values of some of the important parameters used in the WCA computations of this chapter's example. The handling of these parameters can be found in the MATLAB code of this example presented in Appendix section of this thesis.

Table 3.1. Values of Some Important Parameters used in the WCA Computations.

Parameter	**Explanation**	**Value**
dt	sampling interval	1/12 years
DJ	number of octaves per scale	1/32
LPer	lower level of period	0.15 years
UPer	upper level of period	32 years
LPhaseDif	lower levels of phase-difference bands	[2.5, 3.5, 5.0] years
UPhaseDif	upper levels of phase-difference bands	[3.5, 5.0, 7.0] years
MinScale	minimum scale	0.12 years
MaxScale	maximum scale	32 years
Mother	mother wavelet	Morlet
MonteCarloCount	number of surrogate sets	10
ArrowDensity	densitiy of arrow on WCA figure	[30 30]

Figure 3.6 is the general layout adopted in this thesis work for the compact presentation of the WCA results by means of "image of coherence" as well as phase-difference plots.

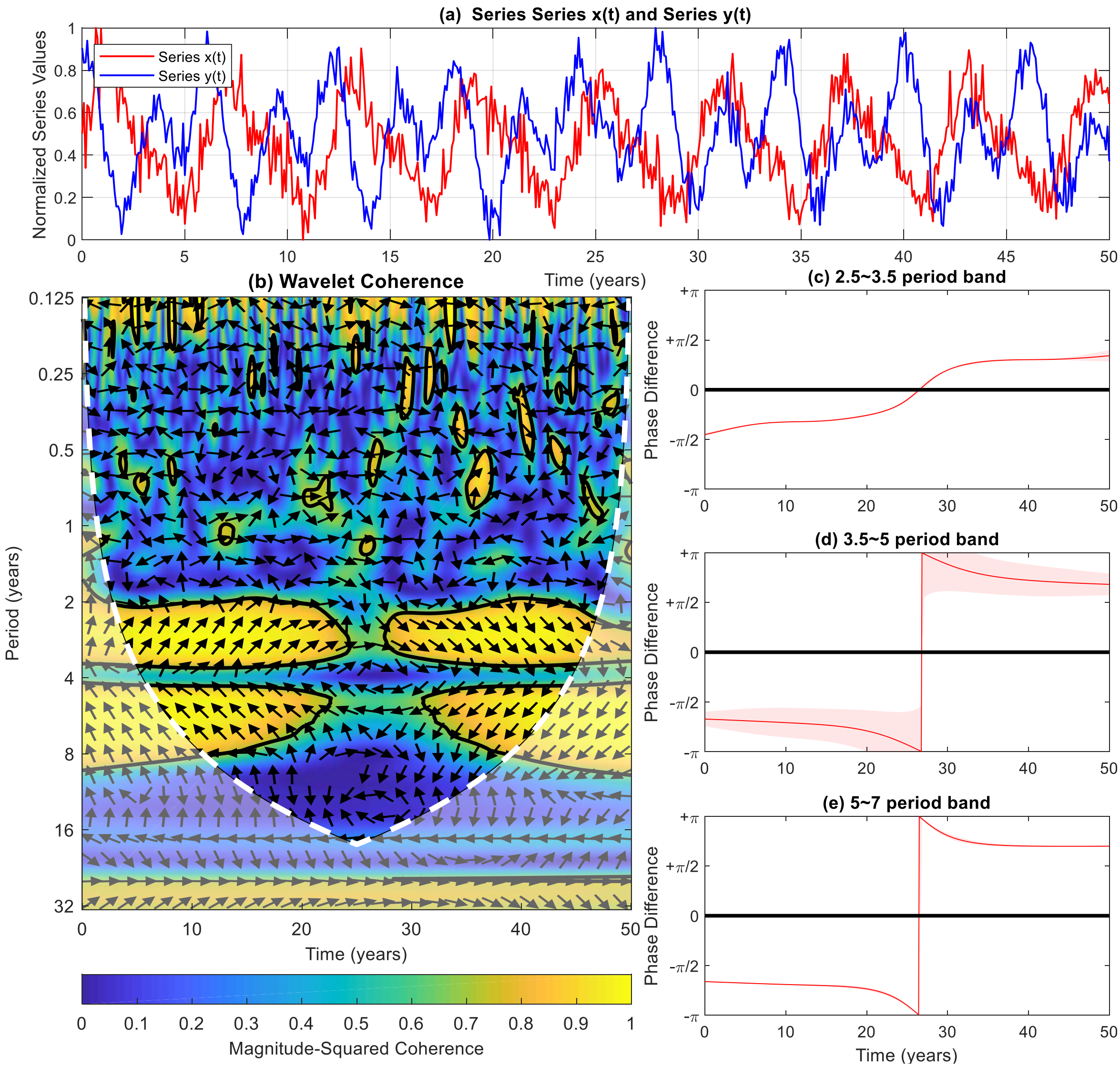

Figure 3.6. Wavelet Coherence Analysis and Phase-Difference Plots of the Synthetic Time Series.

First of all, the arrows and Figure 3.6b (as superimposed on the image of coherence) display phase differences between the time series. If the angle between arrows and the x axis is $\varphi_{x,y} \in (-\pi/2\,,0) \cup (\pi/2\,,\pi)$ then $x(t)$ leads $y(t)$, whereas if $\varphi_{x,y} \in (0,\pi/2) \cup (-\pi,-\pi/2)$ then $y(t)$ leads $x(t)$. Additionally, arrows directed right indicate that the series are "in phase" while arrows directed left indicate that the series are "out of phase" (Madaleno and Pinho, 2014). Unfortunately, the explanation of this phase-difference relationship is disputed in the literature. Funashima (2017) compared alternative interpretations of phase-difference and found that if the phase difference between two series is $\varphi_{x,y} \in (0,\pi/2) \cup (-\pi,-\pi/2)$ then $x(t)$ leads $y(t)$, whereas if $\varphi_{x,y} \in$

$(-\pi/2\,,0) \cup (\pi/2\,,\pi)$ then $y(t)$ leads $x(t)$. Additionally, Funashima reported that if $\varphi_{x,y} \in (-\pi/2\,,\pi/2)$ then $x(t)$ and $y(t)$ move "in phase" whereas if $\varphi_{x,y} \in (\pi/2\,,\pi) \cup (-\pi,-\pi/2)$then $x(t)$ and $y(t)$ move "out of phase" (Funashima, 2017).

The WCA (image of coherence) seen in Figure 3.6b and the phase differences in various period bands seen in Figure 3.6 c-d-e reveal that both interpretations are valid but while the former is based on WCA, the latter is derived from period bands' phase-difference plots. A Monte Carlo simulation is used to construct %5 significance levels (Grinsted et al., 2004) that were shown as black contour lines. WCA treats time series as cyclic series of infinite length and since time series have finite length, errors occur towards both edges of the time series. To overcome these errors, WCA pads the edge of the series with zeros. Therefore, significance of the WCA outcomes decreases towards the endpoints (Torrence and Compo, 1998). A Cone of Influence (COI) is introduced to show %95 significance level of WCA and has been indicated with a dashed white line on Figure 3.6b. In Figure 3.6b, the horizontal axis displays time domain and the vertical axis displays frequency domain. However, in order to make interpretation easier, the frequency is converted to period by taking the reciprocal of the frequency values.

Fıgure 3.6 depicts the overlay plots of the synthetic time series, WCA of the time series, and phase differences averaged over some particular period bands (2.5-3.5, 3.5-5, 5-7 year period bands). From the shape of the WCA of the two time series, periods can be classified as short term and long term. As a short-term analysis, significant strong coherency is observed in the 2-3.5 year period band between 3 and 20 years. This "island of high coherency" is caused by the common nature of the two time series around 3-year period. In addition to coherence, the arrows over this "island" have up-and-rightward orientation, meaning that series $y(t)$ leads series $x(t)$ by approximately $\pi/4$ (see also the arrows on Figure 3.5). Correspondingly, in Eq. 3.2, the 3-year cycle of series $y(t)$ has a 5-month lead. There are 36 months in 3 years and $5/36 = 0.139$. The angle between arrow representation of 5-month lag/lead in the 3-year period band becomes $2\pi \times 0.139 \approx \pi/4$, since central angle of a circle equals to 2π. Crosschecking WCA findings with Eq. 3.1 and Eq. 3.2 shows the success of WCA in capturing phase differences. Similarly, there is strong coherence in the 2-3.5 year period band between 30 and 47 years. In contrast to the region between 3 and 20 years, this region has down-and-rightward directed arrows indicating series $x(t)$ leads series $y(t)$ by approximately $\pi/4$ (see also the arrows on Figure 3.5). Again crosschecking this finding with Eq. 3.1 and Eq. 3.2 reveals that WCA consistently captures the phase differences, because in Eq. 3.2 the 3-year cycle of series $y(t)$ has a 5-month lag after $t = 25$. Additionally, since arrows in both "islands of high coherence" have rightward orientation, the two time series are "in phase" in the short term (see also the arrows on Figure 3.5). Moreover, between 20 and 30 years, WCA does not indicate coherency, as expected, because of the transient change in series $y(t)$.

As a long-term analysis, there is strong coherency in the 4.5-8 year period band between 10 and 20 years, and between 30 and 40 years. Similar to the short term analysis, Eq. 3.1, Eq. 3.2, and WCA results all confirm each other for the long term as well. The two series share a 6-year cycle and these correspond to "high-coherence islands" located at 4.5-8 year periods in the WCA of Figure 3.6b.Yet, arrows over the coherent islands are directed left and therefore the series are "out of phase" (see also the arrows on Figure 3.5). In other words, when series are "out of phase", unlike the situation in which the series are in phase, phase differences are measured by looking at the consecutive peaks of the first series and the valleys of the second series. Hence, arrows located on the left hand side island are oriented up-and-leftward (see also the arrows on Figure 3.5), which means the peaks of the series $x(t)$ lead the valleys of the series $y(t)$ by approximately $\pi/4$, whereas arrows located on the right hand side island are oriented down-and-leftward (see also the arrows on Figure 3.5) which means the peaks of the series $y(t)$ lead the valleys of the series $x(t)$ by approximately $\pi/4$. From Eq. 3.1 and Eq. 3.2, it can be seen that the series $y(t)$ has 10 months of lag for the first half and a 10-month lead for the second half with respect to series $x(t)$. There are 72 months in 6 years and $10/72 = 0.139$. The angle between arrow representation of 5-month lag/lead in the 3-year period band becomes $2\pi \times 0.139 \approx \pi/4$, since central angle of a circle equals to 2π. Additionally, sign on the 6-year cycle of series $y(t)$ is negative which also generates a phase difference of π (or.$-\pi$, according to perspective). Therefore, for the first half period, the phase difference is $\pi/4 + \pi = 5\pi/4$. For the sake of easy interpretation instead of saying that the $x(t)$ leads the $y(t)$ by $5\pi/4$, it is preferable to say that the series are "out of phase" and $x(t)$ leads $y(t)$ by $\pi/4$ (this is found by subtracting a half period from the phase difference). Similarly, for the second half period, the phase difference is $-\pi/4 - \pi = -5\pi/4$ which means $x(t)$ lags by $-5\pi/4$ (or $y(t)$ leads by $5\pi/4$). Once again to make interpretation easier it is favored to say that the series are "out of phase" and $y(t)$ leads $x(t)$ by $\pi/4$.

Phase relations may also be investigated by looking at subplots c, d and e of Figure 3.5. In subplot c, the mean phase difference for the 2.5-3.5 year period band is around $-\pi/4$ in the first half and $\pi/4$ in the second half. By taking (Funashima, 2017) interpretation into account, the series are "in phase" and $y(t)$ leads $x(t)$ in the first half, whereas $x(t)$ leads $y(t)$ in the second half. In subplot b, the mean phase difference for the 3.5-5 year period band is around $-5\pi/8$ in the first half and $5\pi/8$ in the second half. Thus, the series are "out of phase" and $x(t)$ leads $y(t)$ by $\pi/8$ in the first half, whereas $y(t)$ leads $x(t)$ $\pi/8$ in the second half. Nevertheless, a corresponding significantly coherent zone does not appear in WCA in Figure 3.5b for the 3.5-5 year period band, therefore, this phase relation is not meaningful. In subplot c, the mean phase difference for 5-7 year period band is around $-3\pi/4$ in the first half and $3\pi/4$ in the second half. Thus, the series are "out of phase" and $x(t)$ leads $y(t)$ by $\pi/4$ in the first half whereas $y(t)$ leads $x(t)$ by $\pi/4$ in the second half.

In some cases, investigation of the distribution of phase differences may be more important. For instance, comparison of phase differences of stock indexes taking different time scales (e.g., short term vs. long term) into account may create opportunities for investors. Figure 3.7 shows such a distribution of phase differences, for the first time in known literature. Phase difference between the series $x(t)$ and the series $y(t)$ is examined in 4 different (quantized) categories which are displayed in the 4-level color bar. In Figure 3.7, light-blue areas $(0 < \varphi_{x,y} < -\pi/2)$ and yellow areas $(0 < \varphi_{x,y} < \pi/2)$ belong to the "in phase region". While the yellow area indicates that the series $x(t)$ leads the series $y(t)$, the light-blue area indicates that the series $y(t)$ leads the series $x(t)$. Blue areas $(-\pi/2 < \varphi_{x,y} < -\pi)$ and red areas $(\pi/2 < \varphi_{x,y} < \pi)$ belong to the "out of phase" region. While the blue area indicates that the series $x(t)$ leads the series $y(t)$, the red area indicates that the series $y(t)$ leads the series $x(t)$. Although Figure 3.7 is a rough (quantized) representation of phase differences, it enables one to visualize the phase difference association between the two series with more simplicity and crispness.

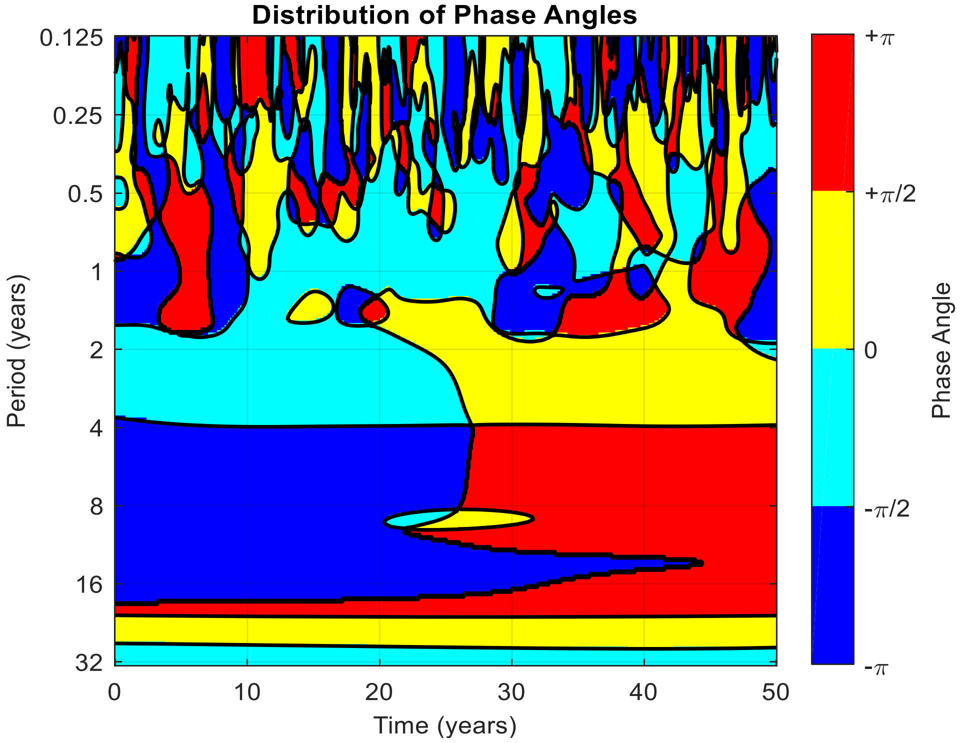

Figure 3.7. Distribution of Phase Angles between the Synthetic Time Series.

Figure 3.8 consists of four different subplots. Figure 3.8a shows the frequency-wise means (means at each x-axis value and along the y-axis of WCA image in Figure 3.6b) of coherency between the two series over time. Although there is a slight decrease in mean coherency around 25 years, general overview of the Figure 3.8a says the two time series are coherent along the time with a magnitude roughly equal to 0.5. Figure 3.8b shows the frequency-wise mean of the phase-difference between the two series over time. It can be seen that the two time series are "in phase" and the series $y(t)$ leads the series $x(t)$ in the first half, whereas the series $x(t)$ leads the series $y(t)$ in the second half. Figure 3.8c shows the time-wise mean (means at each y-axis value and along the x-axis of WCA image in Figure 3.6b) of coherency between the two series over the periods. This plot facilitates to pin down the short-, medium-, and long-term behaviors and can be used to classify such durations. There are five peaks located around 0, 3, 6, and 17 years and beyond 25 years, not all necessarily meaningful. While the first peak is discarded because of the noise which affects the lowest periods the most, the last two peaks are discarded because they are outside of the significant region (COI in WCA image of Figure 3.6b). Subsequently, only peaks located at 3 years and 6 years are used to assign terms as short-term and long-term. This figure makes it easier to conclude that the series have high coherency at 3-, 6-, and

17-year periods. Figure 3.8d shows the time-wise mean of phase difference between the two series over period. This figure makes it easier to conclude about the phase-difference between the two time series for different period bands. Around 13-20 years band they are on the average “out phase”, indicating that peak of $y(t)$ leads valley of $x(t)$ by $\pi/4$, and around 13-20 years they are on the average “in phase”, indicating that $x(t)$ leads $y(t)$ by $\pi/4$.

In all of the subplots (Figure 3.6c-d-e and Figure 3.8a-b-c-d) the light-colored shadow bands around the solid curves (which are the mean values) are the standard-error bands computed over the data points used in calculating the mean values. The regions of x-axis corresponding to more spreaded (wide) standard-error bands localize the time zones in which the variation in the subplot quantity (coherence or mean phase difference) is high and thus one should be less sure about the mean (curve) value. Vice versa, the regions of x-axis corresponding to less spreaded (narrow) standard-error bands localize the time zones in which the variation in the subplot quantity (coherence or mean phase difference) is low and thus one can be more sure about the mean (curve) value. For instance, for this example, the standard-error bands in Figure 3.8c increases significantly as period increases beyond 21 years; indicating that the mean coherence across time (solid line) represents the coherences across time, for times greater than 21 years, with high certainty. This observation can be verified from the WCA image in Figure 3.6b. A similar argument is valid for the mean phase-differences across time in Figure 3.8d for periods beyond 20 years, which can also be verified from the arrows on the WCA image in Figure 3.6b as well.

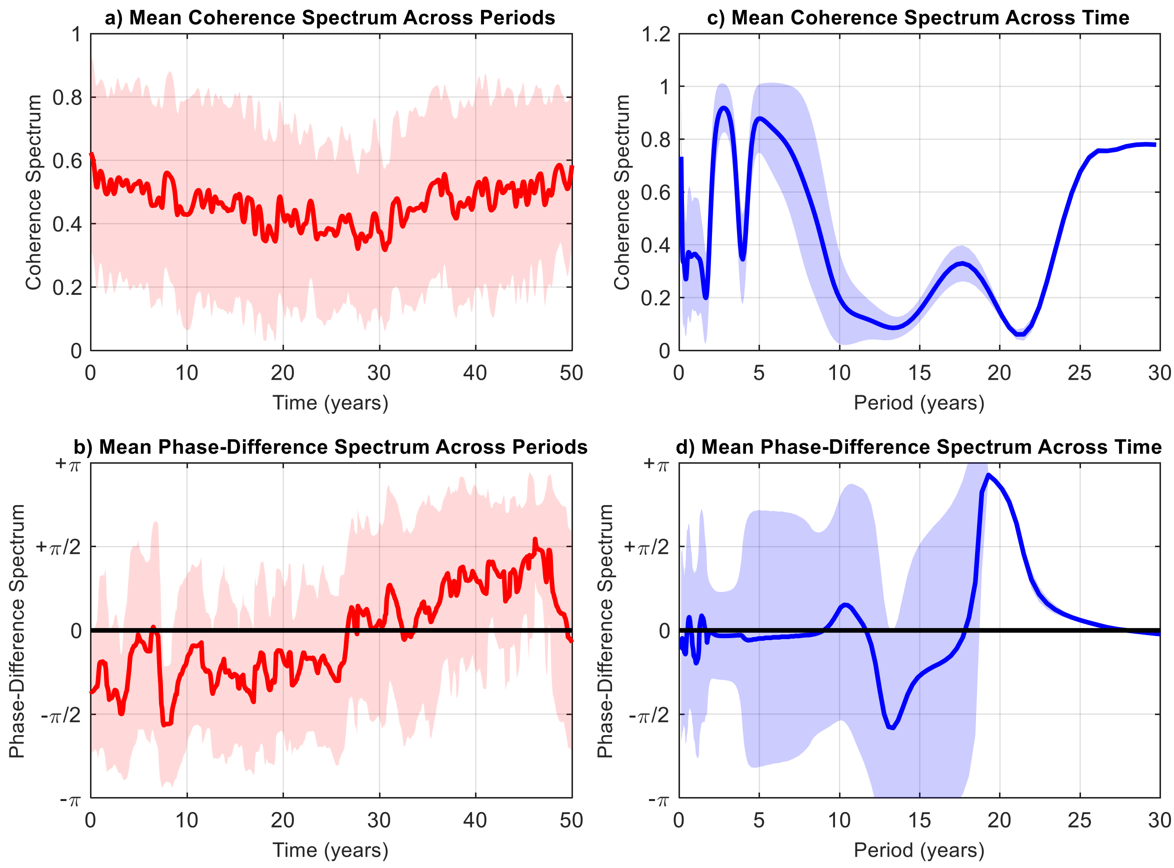

Figure 3.8. Mean Coherence and Mean Phase-Difference between the Synthetic Time Series across Time and Frequency Domains.

4. WAVELET COHERENCE ANALYSIS OF THE CHEMICAL ACTIVITY BAROMETER AND U.S. INDUSTRIAL PRODUCTION INDEX

This core chapter is on the Wavelet Coherence Analysis (WCA) of two economic time series, the Chemical Activity Barometer (CAB) and the US Industrial Production Index (IPI), and exhibits the power and features of the WCA. The aim of this chapter is to elucidate the coherency and the phase differences (lead-lag relationship) hidden in two real time series, the CAB and IPI. First, the description and economic importance of the CAB and IPI will be presented. Then, the CAB and IPI time series will be analyzed under three major sections as: *i)* analysis of the original trending series, *ii)* analysis of the detrended series, and *iii)* analysis of their moving-average-smoothed first-order differenced transformations.

4.1. Description and Economical Importance of the CAB and the IPI

The CAB is a composite index of chemical industry activity that produces a leading indicator of broader economy-wide activity. To better understand shifts in the Business Cycle (BC) it is important to distinguish between leading, coincident, and lagging indicators of the BC, which essentially reflect the timing of their movements. Leading indicators (average weekly hours, new orders, consumer expectations, building permits, stock prices, etc.) are those that consistently turn before the economy does. Coincident indicators (employment, industrial production, personal income, business sales, etc.) turn in step with the economy and track the progress of the BC. Lagging indicators (inventory-to-sales ratios, change in unit labor costs, commercial and industrial loans outstanding, etc.) turn after the economy turns, thus playing a confirming role. These three types of indicators are important in their own right although most attention is played to the role of leading indicators because they tend to shift direction in advance of BC. Leading indicators have a “look-ahead” quality and measure anticipations and new commitments. They lead the economy, and turn before the economy does. Their lead with respect to BC helps policy makers monitor the changes in the economy. Economists have been working for a long time to determine economic indicators which lead the economy. For instance, National Bureau of Economic Research (NBER) is an US organization which was founded in 1920 and provides dates of recessions in US industry. The leading indicators enable to reveal BCs and it gives signals to policy makers to anticipate prospective movements of the economy to some extent. Although, the economists have been working for almost a century, there is no concrete tool which works perfectly throughout the historical data and this is still an attractive subject for researchers.

As one of the largest industries in the US, the chemical industry pervades nearly every facet of the economy, and its products stand at the beginning of the supply chain. Found to lead the US BCs, it provides an excellent vantage point from which to observe the global economy. Not only does the chemical industry, a $760 billion enterprise, provide inputs to numerous sectors, but it also generates millions of jobs. The business of chemistry supports nearly 25% of the US Gross Domestic Product (GDP) and accounts for 12% of US exports. In 2011, e.g., $56 billion is spent for R&D in chemical industry. Also, every one of the five patents in US belongs to chemical industry. Given its principal and growing role in the US, tracking the chemical industry is a key factor to anticipate where the economy is heading (Dooley, 2012).

Chemistry’s essential role in the US economy and its early position in the supply chain give the American Chemistry Council (*ACC*) the ability to identify emerging trends in the US economy and specific sectors outside of, but closely linked to, the business of chemistry. The CAB, the ACC’s first-of-its kind, leading macroeconomic indicator will highlight the peaks and troughs in the overall US economy and illuminate potential trends in market sectors outside of chemistry. It is the chemical industry’s vital importance that makes the CAB a leading economic indicator. The barometer is a critical tool for evaluating the direction of the US economy. The CAB index provides a longer lead (performs better) than the NBER declarations. The ACC claims that the CAB leads the NBER signals by two to fourteen months, with an average lead of eight months (Swift, 2015).

The CAB is a composite index which comprises indicators drawn from a range of chemicals and sectors, including chlorine and other alkalies, pigments, plastic resins and other selected basic industrial chemicals. It first originated through a study of the relationship between the BCs in the production of selected chemicals and cycles in the larger economy during the period from 1947 to date. Other specific indicators used in the calculation of the CAB include hours worked in chemicals, chemical company stock data, publicly sourced chemical price information, end-use (or customer) industry sales-to-inventories, and several broader leading economic measures (building permits and Purchasing Managers' Index (PMI) for new orders). The CAB is constructed using a five-step procedure similar to that used by the US Conference Board to calculate composite indexes: *i)* Calculation of month-to-month changes in the component indices, *ii)* Adjusting month-to-month changes by multiplying them by the component's weighting, *iii)* Summing the adjusted month-to-month changes (across the components for each month), *iv)* Computing preliminary levels of the composite index, and *v)* Rebasing the composite index to reflect the average lead (in months) of an average 100 in the base year (the year 2007 is used) of a reference time series (the Federal Reserve's Industrial Production index is used). To update the CAB from month to month, steps *i)* through *iv)* are followed to incorporate the most recent six months of data. The revisions to the base year in step *v)* are made when the Federal Reserve changes its base year for the IPI. The CAB does not use company-specific price information as input data and data is aggregated such that company-specific and product-specific data cannot be determined (Swift, 2015).

CAB provides earlier forecasting, determines turning points and likely future trends of the wider US economy, identifies shifts in other industries within the US economy, and highlights the industry's role in driving economic growth. CAB is not a leading index of chemical industry activity. Rather, it is a leading index (barometer) based on chemical industry data that leads overall industrial production and the overall BC. The ACC claims that the relationship between CAB and IPI is such that there is a positive correlation over 0.9 between IPI and CAB, eight months prior(Swift, 2015).

CAB is supposed to lead the IPI which is the reference series chosen as a proxy for US economic activity. The industrial production has the advantage to be available on a monthly basis and to have displayed strong co-movements with GDP historically. The

ACC state that not only does the CAB identify the peaks, troughs, trends and shifts in the US economy, but it can also be used as a critical tool for forecasting.

According to McDermott and Scott (2000) there are two methodologies for BC identification. The first one, which is proposed by Burns and Mitchell (1946), is classical cycle and the second one is growth cycle which is proposed by scientists who study real BC. The main difference between them is that the measurements are performed based on trend-cycle data in classical cycle approach whereas the measurements are performed based on detrended data in growth cycle approach (Mazzi and Scocco, 2002). On the other hand, when Hughes Hallett and Richter (2006) explain the pros of time-frequency approach in their study, they say that time-frequency technique is not affected by detrending. Moreover, (Mayes and Crowley, 2009) say that wavelet analysis doesn't rely on any particular detrending method by using definition of Hughes Hallett and Richter (2006). In this chapter, we study both the original data and detrended data to observe if there is a difference.

Before diving into the analysis, it is helpful to explain briefly how NBER determine turning points for the US economy. After Burns and Mitchell (1946) scrutinize the BCs, Bry and Boschan (1971) simplify their method and generated an algorithm. Consequently, NBER committee uses these methods and more (e.g., expert views and judgements) to determine the official US peaks and troughs (Boldin, 1994). Decision rules of Bry and Boschan (1971) are as follows:

1. Peaks and troughs have to be separated

2. Duration between peak to trough or trough to peak must be at least 6 months.

3. Duration between two consecutive peaks or two consecutive troughs must be at least 15 months.

4. In the six months after the beginning of the time series and the six months before the end of the time series, peaks and troughs are not counted as turning points.

4.2. Data Description and Preliminary Result

WCA allows the characterization of the behavior of two co-varying indices, (such as the price indices of two commodities) in both the time and frequency domains. Such method is invaluable considering the cyclical behavior of the CAB and the US economy. In this thesis, co-varying behavior of the CAB and IPI is analyzed by the WCA, for the first time in the literature.

In this thesis work, 1209 monthly data of CAB and IPI covering 1919M1 to 2019M9 were used. All the data were obtained from the ACC. The ACC's claim is that the CAB holds some primacy in the behavior of other industries due to interactions in production chains in the US, and thus, CAB is a leading indicator of IPI and hence the US economy.

Values of the CAB and IPI data are depicted in Figure 4.1a. As the ACC claimed, it can be observed that the CAB and IPI move correlated over time. It is also observed that the time series have downfalls on particular years. The two time series are detrended (linear trend removal) and plotted in Figure 4.1b. The values above the linear trend become positive and the values below the trend become negative. This detrended figure better shows the years when the two times series move together. For instance, in 1946 and 1947, there is an obvious fall or in 2019 there is a dramatic fall. On the other hand, in Figure 4.1c year-on-year smoothed change of the time series are plotted, which actually is the three-month simple moving average smoothing of the yearly differenced series. This is how the ACC plots and analyzes the CAB and IPI in their monthly newsletters. Recessions between 2001 and 2002, and in 2009, as well as the leading of IPI by CAB, can easily be detected by this plot. Nevertheless, these plots in the Figure 4.1 are not enough to say interrelationship between two time series. To reveal hidden relationships between CAB and IPI, all of these series (original trending, detrended, and smoothed-difference series) are investigated via univariate Wavelet Power Spectrum (WPS) and the WCA in the following sections of this chapter.

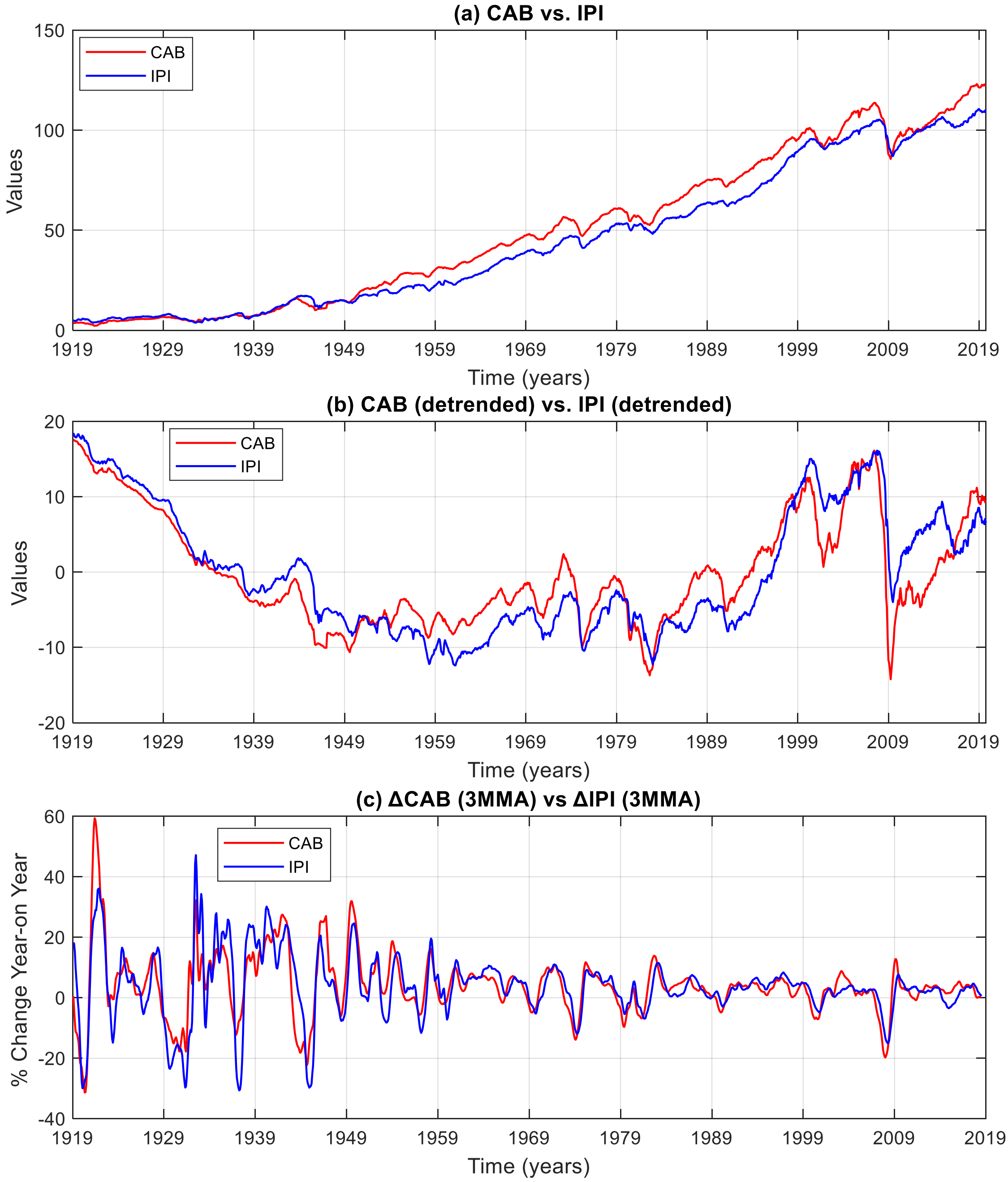

Figure 4.1. Original Trending, Detrended, and Three-Month Moving-Average-Smoothed Yearly-Differenced CAB and IPI Series.

4.3. Univariate Wavelet-Based Analysis of the Original Trending CAB and IPI Series

In literature, there are studies in which univariate WPS is individually used to define major cycles in a particular economy. For instance, Mayes and Crowley (2009) use WPS to analyze BCs of core members of Euro zone and Aguiar-Conraria and Soares (2011) use WPS to analyze BCs of the EU-15 and EU-12 countries. Although WPS shows evolution of major cycles along time, it is not possible to identify “business cycle” in the classical sense. In other words, one can not identify economic peaks and troughs by using WPS.

In this section, the original trending CAB and IPI series, as shown in Figure 4.1a, will be used. Firstly, the cyclic natures of the time series were explored by using two separate univariate analyses, WPS and Fourier Power Spectral Density (PSD). While WPSs of the time series are computed using Continuous Wavelet Transforms (CWT) of the series, the PSDs of the time series are computed by adjusting an ARMA(P,Q) model to the series (Aguiar-Conraria et al., 2008). “Q” parameter is set to zero as it is suggest in the paper (Aguiar-Conraria et al., 2008) whereas a suitable “P” parameter is experimentally found to be 200 by comparing the WPS and PSD methods and to obtain smooth and well-defined spectrum peaks.

In Figure 4.2, there are horizontal red bands at 10-year period of the WPSs of the CAB and IPI along the time span which means that both time series consist of common sub-cycles with 10-year periods. Moreover, the same conclusion can be drawn for the horizontal red bands in both WPSs located at around 20-year period, however the red line becomes indistinct between 1950 and 1975 for IPI, which means that both time series consist of common sub-cycles with 20-year periods but the sub-cycle is less dominant in between 1950 and 1975 for IPI. There are clear red lines located at 30-year period and they are also sub-cycles. Similarly, horizontal red bands located between 32-year period and 64-year period along the time span in WPSs elucidate that both time series consist of common sub-cycles with roughly 48-year period, but it must be kept in mind that these sub-cycles are slightly outside of the significant region (COI) and thus they are questionable. Additionally, at the period larger than 64 year, there are solid intense red lines. It is hard to tell that they are also sub-cycles, because they are far from the significant region outlined by the COI.

On the other hand, peaks located at 30-year period are remarkable on the PSDs of the both time series whereas peak located at 22-year period is remarkable only on the PSDs of.CAB Additionally, PSD peaks around 10-period is noteworthy as well. Moreover, when one goes to larger periods, PSD shows higher power, as in WPS figures. However, since the time data is lost in FT-based PSD analysis, it is not possible to say something about time localization of the peaks. Thus, although WPSs and PSDs give some limited information on the nature of the time series, unfortunately they do not give any information about probable associations between them.

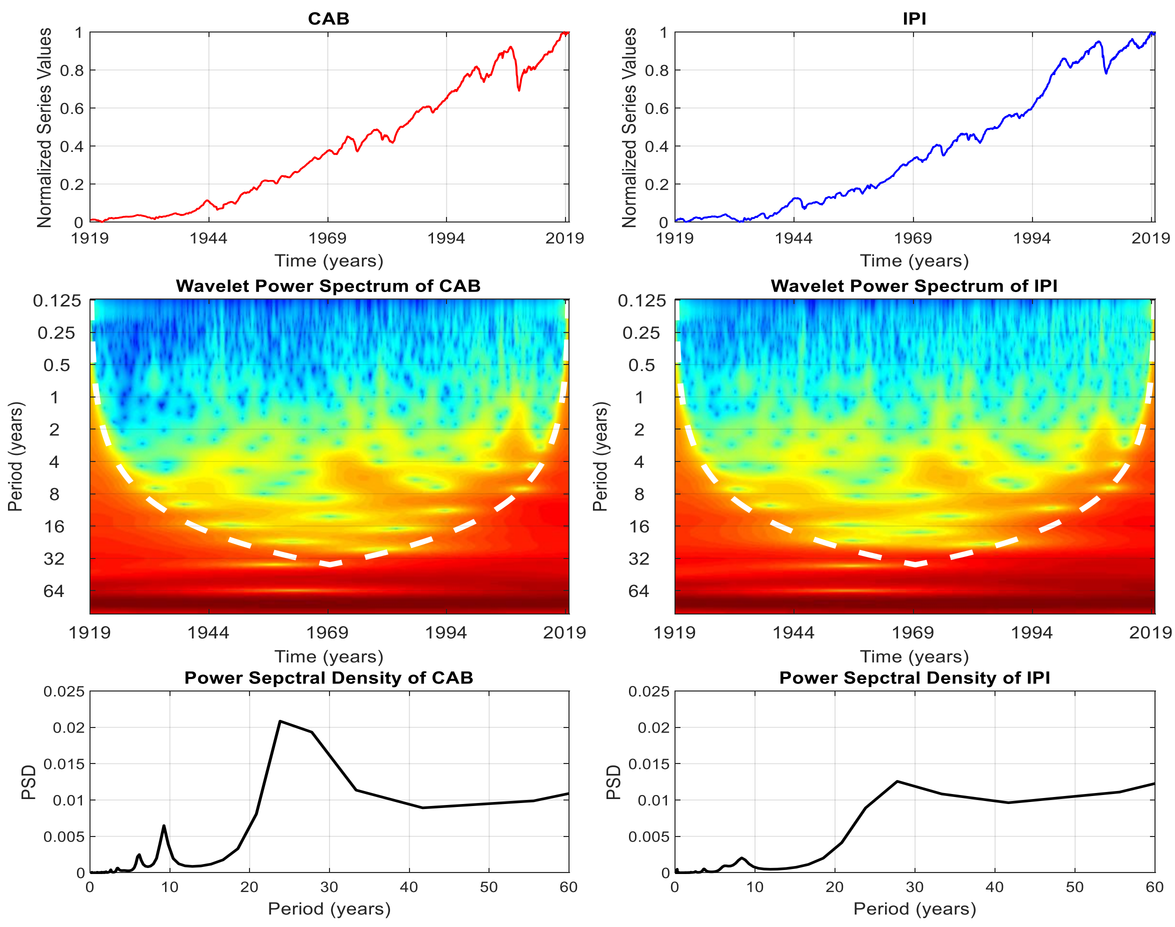

Figure 4.2. Wavelet Power Spectra and Power Spectral Densities of the Original Trending CAB and IPI Series.

4.4. Wavelet Coherence Analysis of the Original Trending CAB and IPI Series

In literature, there are studies in which WCA is used to reveal BC synchronization among two different economies. For instance, Rua (2010) uses WCA to analyze BC synchronization among European economies and Hanus and Vacha (2015) use WCA to analyze BC synchronization among Visegrad Four. However, in this thesis, WCA will be used to reveal synchronization of two economic indicator of the same economy, namely CAB and IPI. Subsequently, results of WCA will be compared to NBER’s BC turning points to decide whether WCA of the CAB and IPI is a leading indicator or not and whether the CAB leads IPI as claimed by the ACC.

Table 4.1 lists the values of some of the important parameters used in the WCA computations of this chapter’s example.

Table 4.1. Values of Some Important Parameters used in the WCA Computations.

Parameter	**Explanation**	**Value**
dt	sampling interval	1/12 years
DJ	number of octaves per scale	1/32
LPer	lower level of period	1/12 years
UPer	upper level of period	100.42 years
LPhaseDif	lower levels of phase-difference bands	[0.5, 1.0, 3.0] years
UPhaseDif	upper levels of phase-difference bands	[1.0, 2.0, 12] years
MinScale	minimum scale	0.12 years
MaxScale	maximum scale	100.42 years
Mother	mother wavelet	Morlet
MonteCarloCount	number of surrogate sets	10
ArrowDensity	densitiy of arrow on WCA figure	[60 60]

Fıgure 4.3 contains plots of normalized values of the original trending CAB and IPI series, their WCA image, and average phase difference between two series over the three particular period bands (0.5-1, 1-2, and 3-12 year period bands). WCA comprises much valuable information on the interrelation of the two series. In order to advance without

missing a point and to be companionable with real-life analysis habits of the economists, the WCA figure will be studied under the short-, medium-, and long-term perspectives.

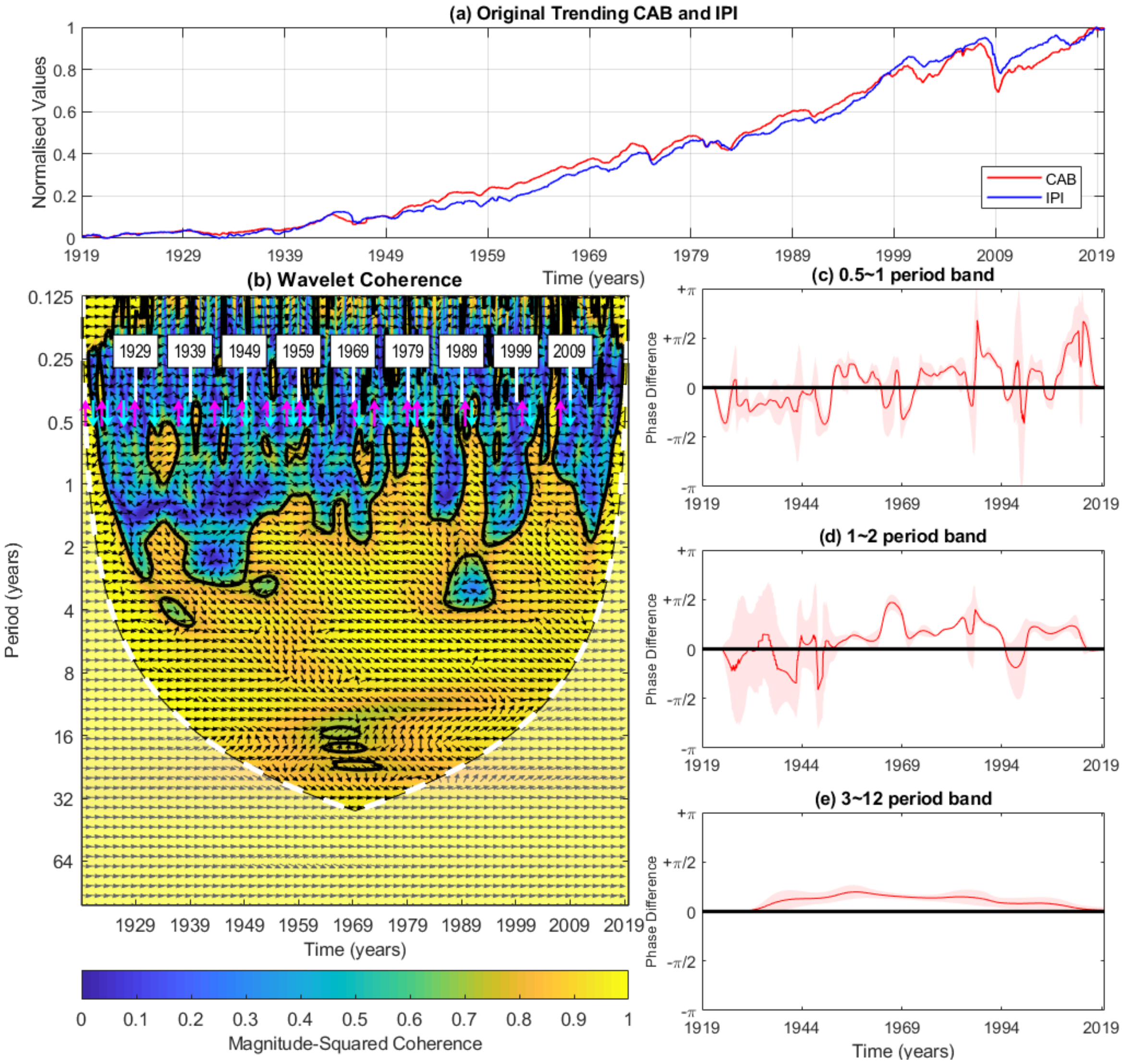

Figure 4.3. Wavelet Coherence Analysis and Phase-Difference Plots of the Original Trending CAB and IPI Series.

Figure 4.4 was generated to identify more crisply the range of these short, medium, and long terms and to behold overall time-wise and frequency-wise mean of phase difference and coherency of the CAB and IPI series. From Figure 4.4a, it can be deduced that average coherency between two series is approximately 0.7 along the timeline, which means they are highly coherent. On the other hand, Figure 4.4b contains critical information for WCA. The peaks in this sub-figure can be used for designation of short-, medium-, and long-term behavior. In this context, the peaks located at 1 and 6 years are attributed to short and medium while periods are longer than 24 years can be attributed to long terms. It is hard to deduce something from Figure 4.4c whereas Figure 4.4d roughly shows that in (business) cycles between 2- and 12-year period band and between 19-and 34-year period band, the CAB leads IPI by approximately $\pi/8$ phase angle, but at the rest of the timeline the two series are in-phase. Nevertheless, just by looking at the mean coherency spectrum and phase difference spectrum across time plots can be deceptive because two dimensional coherency plots disregard the degree of coherency. Importance of the true (un-averaged) WCA analysis and the WCA image in Figure 4.3 arises in this situation.

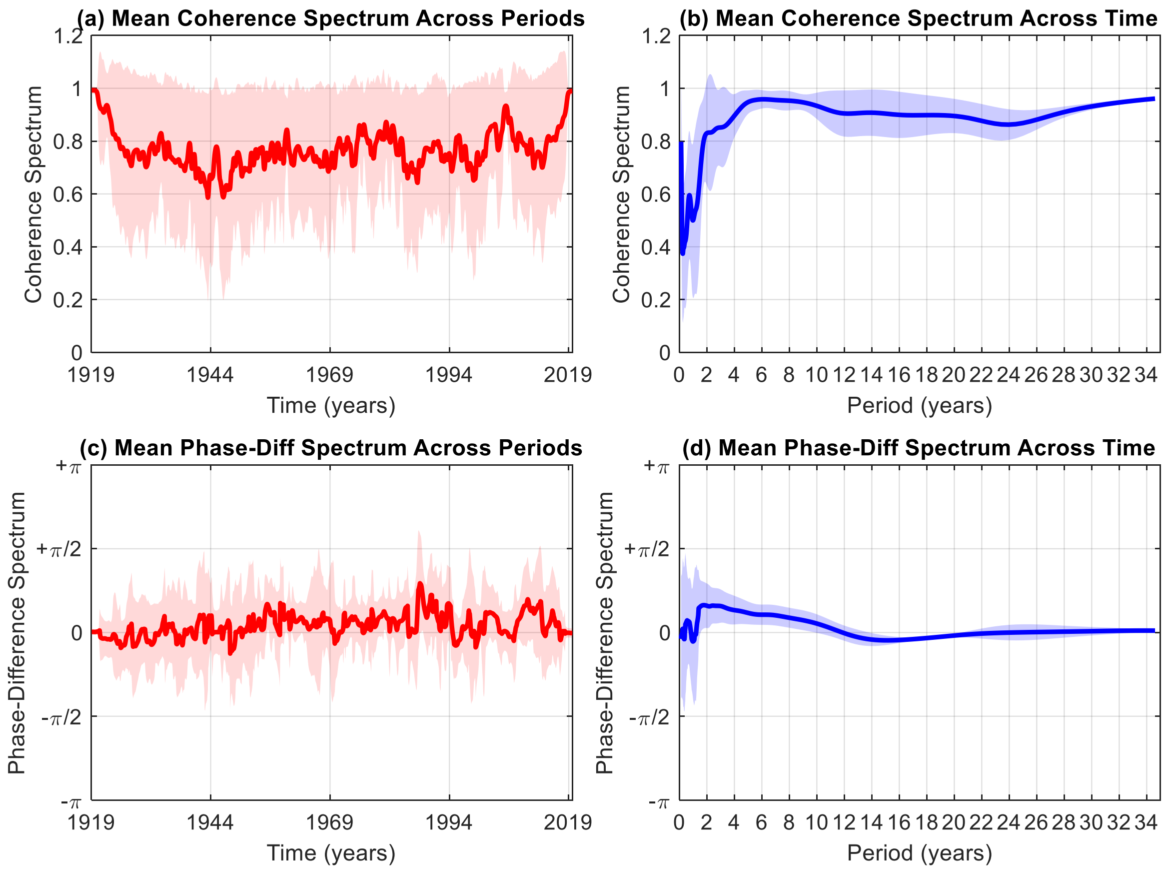

Figure 4.4. Mean Coherence and Mean Phase-Difference between the Original Trending CAB and IPI Series across Time and Frequency Domains.

In all of the subplots (Figure 4.3c-d-e and Figure 4.4a-b-c-d) the light-colored shadow bands around the solid curves (which are the mean values) are the standard-error bands computed over the data points used in calculating the mean values. The regions of x-axis corresponding to more spreaded (wide) standard-error bands localize the time zones in which the variation in the subplot quantity (coherence or mean phase difference) is high and thus one should be less sure about the mean (curve) value. Vice versa, the regions of x-axis corresponding to less spreaded (narrow) standard-error bands localize the time zones in which the variation in the subplot quantity (coherence or mean phase difference) is low and thus one can be more sure about the mean (curve) value. For instance, for this example, the standard-error bands in Figure 4.4b decreases significantly as period approaches to 8 years; indicating that the mean coherence across time (solid line) certainly represents the coherences across time for business cycles close to 8 years.

Now, the short-, medium-, and long-term behaviors can be attributed using the WCA. The motivation of applying WCA to the CAB and IPI is to discover the link (interrelations) between the time series and to find a hint for a new leading indicator. By taking simple rules of Bry and Boschan (1971), we claim that BC turning points should be revealed by looking at the short term (0.5 to one year) part of WCA image. Additionally, so as to make such a visual comparison more precisely, turning points claimed by the ACC (listed in Table 4.2) should be roughly matched on the WCA image. For this purpose, the cyan colored downward arrows are put to indicate troughs and the purple colored upward arrows are put to show peaks on the WCA image. Additionally, vertical white lines are added onto Figure 4.3b which point out the beginnings of the years written above the vertical line. Interestingly, dates of the small “zones of high coherency” located between 0.5 to one year band and dates of troughs claimed by the ACC are somehow matched. This image brings in mind an asymmetric feature of economies in general; the contagion effect. Boldin (1994) defines asymmetric quality of BCs as the dissimilar features of recession and expansion periods of the economy. Additionally, Aloui and Hkiri (2014) define the contagion effect as sudden increase in coherency during turmoil periods rather than during stable periods. Many scientists use wavelet analysis to study contagion effect such as (Gallegati, 2012; Madaleno and Pinho, 2014; Rua and Nunes, 2009).

It is important to understand the reason why Table 4.2 is constructed. Firstly, the ACC already claims that the CAB is a leading indicator of NBER's BCs. If the WCA of CAB and IPI reveals that CAB leads IPI, then it should lead NBER BC as well. Therefore, turning points of CAB are put into the table. Moreover, since our focus will be on the recession periods, these periods are put into the table as well in order to observe the size and duration relationships of "coherency zones (islands)" on the WCA image. Finally, phase difference between the peaks of CAB and peaks of NBER are put into the table, instead of phase difference of troughs, because recession periods start right after the peaks. Hence, the phase differences between CAB and IPI to be extracted from the WCA image can be compared with the phase difference between peaks of CAB and peaks of NBER.

Table 4.2. Dates of the CAB Turning Points and Phase Difference between the Peaks Claimed by ACC (CAB) and NBER.

ACC's CAB Peak Date	**ACC's CAB Trough Date**	**Recession Duration (Peak to Trough) (Month)**	**Phase Difference Between ACC's CAB Peaks and NBER Peaks (Month)**
October 1919	May 1921	7	3
December 1922	November 1923	11	5
June 1926	December 1926	6	4
December 1928	July 1932	7	8
December 1936	April 1938	4	5
August 1943	September 1945	25	18
September 1948	July 1949	10	2
May 1953	January 1954	8	2
January 1957	March 1958	14	8
June 1959	October 1960	16	11
May 1969	April 1970	11	7
February 1973	February 1975	24	9
March 1979	June 1980	15	14
December 1980	August 1982	20	8
October 1989	January 1991	15	9
March 2000	October 2001	19	12
May 2007	March 2009	22	5
			Average = 7.6

Consequently, matching "zones of high coherency" and turning points of BC as claimed by ACC are both listed in chronological order:

1. According to Table 4.2**,** at the mid of 1921 there was the first trough and the recession lasted seven months. Additionally, it is claimed by the ACC that the trough of CAB leaded the trough of NBER by three months in the first BC. On the other hand, there is a coherent region between 0.5 to one year period band on the WCA image between 1920 and 1921 with downward directed black arrows which means that CAB leads IPI roughly by two or three months (see Figure 3.5). Consequently, the WCA is successful in detection of both the first BC and the phase difference between the trough of CAB and the trough of NBER for the first BC. Additionally, for the first trough, it is not possible to say whether WCA is leading CAB or not (meaning that whether the trough observed from the WCA image is leading the through claimed by the ACC) by looking at the WCA figure because it is on the edge of the COI. Furthermore, the width of the coherent zone is roughly 26 months and it does not represent the duration of the first recession period (seven months) in Table 4.2.

2. According to Table 4.2**,** at the late of 1923 there was the second trough and the recession lasted 11 months. Additionally, it is claimed by the ACC that the trough of CAB leaded the trough of NBER by three months in the second BC. On the other hand, there is an indistinct coherent region between 0.5 to one year period band on the WCA image at 1924 with upward directed black arrows which means that IPI leads CAB roughly by two or three months (see Figure 3.5). Consequently, WCA is not successful in detection of both the second BC and the phase difference between the trough of CAB and the trough of NBER for the second BC. Additionally, for the second trough, it is clearly seen that the cyan colored downward arrow which indicates the trough of CAB prevails earlier than the coherent zone in the WCA figure. Furthermore, the width of the coherent zone is roughly 13 months and it approximately represents the duration of the second recession period (11 months) in Table 4.2.

3. According to Table 4.2**,** at the late of 1926 there was the third trough and the recession lasted six months. Additionally, it is claimed by the ACC that the trough of CAB leaded the trough of NBER by four months in the third BC. On the other hand, there is an indistinct coherent region between 0.5 to one year period band on the WCA image at 1926 with southeastward directed black arrows which means that CAB leads IPI roughly by two months (see Figure 3.5). Consequently, the WCA is successful in detection of the third BC and is partially successful in detection of the phase difference between the trough of CAB and the trough of NBER for the third BC. Additionally, for the third trough, it is roughly seen that coherent zone in the WCA figure prevails earlier than the cyan colored downward arrow which indicates the trough of CAB. Furthermore, the width of the coherent zone roughly 15 months and it does not represent the duration of the third recession period (six months) in Table 4.2.

4. According to Table 4.2**,** at the mid of 1932 there was the fourth trough and the recession lasted seven months. Additionally, it is claimed by the ACC that the trough of CAB leaded the trough of NBER by eight months in the fourth BC. On the other hand, there is a large coherent region between 0.5 to one year period band on the WCA image between 1931 and 1938 with northeastward directed black arrows which means that the IPI leads CAB roughly by two months (see Figure 3.5). Consequently, the WCA is successful in detection of the fourth BC but is not successful in detection of the phase difference between the trough of CAB and the trough of NBER for the fourth BC. Additionally, for the fourth trough point, it is roughly seen that coherent zone in the WCA figure prevails earlier than the cyan colored downward arrow which indicates the trough of CAB. Furthermore, the width of the coherent zone roughly 5.5 years and it does not represent the duration of the fourth recession period (seven months) in Table 4.2.

5. According to Table 4.2**,** at the onset of 1938 there was the fifth trough and the recession lasted four months. Additionally, it is claimed by the ACC that the trough of the CAB leaded the trough of NBER by five months in the fifth BC. On the other hand, there is a slim coherent region between 0.5 to one year period band on the WCA image at 1939 with slightly southeastward directed black arrows which

means that the CAB leads IPI by one month (see Figure 3.5). Consequently, the WCA is not successful in detection of both the fifth BC and the phase difference between the trough of CAB and the trough of NBER for the fifth BC. Additionally, for the fifth trough, it is clearly seen that the cyan colored downward arrow which indicates the trough of CAB prevails earlier than the coherent zone in the WCA figure. Furthermore, the width of the coherent zone is roughly 17 months and it does not represent the duration of the fifth recession period (4 months) in Table 4.2.

6. According to Table 4.2**,** at the late of 1945 there was the sixth trough and the recession lasted 25 months. Additionally, it is claimed by the ACC that the trough of CAB leaded the trough of NBER by 18 months in the fifth BC. On the other hand, there is a slim coherent region between 0.5 to one year period band on the WCA image between 1944 and 1946 with rightward directed black arrows which means that there is no phase difference between the CAB and IPI or the arrows are already completed 360 degree rotation and return to their initial position (see Figure 3.5). The 18 months lead of CAB claimed by the ACC is approximately equal to two full tours for arrows on the coherent region between 0.5 to one year period band on the WCA image. Consequently, the WCA is successful in detection of the sixth BC and is doubtfully successful in detection of the phase difference between the trough of CAB and the trough of NBER for the sixth BC. Additionally, for the sixth trough, it is roughly seen that the coherent zone in the WCA figure occurs earlier than the cyan colored downward arrow which indicates the trough of CAB. Furthermore, the width of the coherent zone is roughly 17 months and it does not represent the duration of the sixth recession period (25 months) in Table 4.2.

7. According to Table 4.2**,** at the mid of 1949 there was the seventh trough and the recession lasted 10 months. Additionally, it is claimed by the ACC that the trough of CAB leaded the trough of NBER by two months in the seventh BC. On the other hand, there is an indistinct coherent region between 0.5 to one year period band on the WCA image at 1950 with northeastward directed black arrows which means that the IPI leads CAB roughly by two months (see Figure 3.5). Consequently, the WCA is successful in detection of the seventh BC but is not successful in detection of the phase difference between the trough of CAB and the trough of NBER for the

seventh BC. Additionally, for the seventh trough, it is seen that the coherent zone in the WCA figure prevails slightly earlier than the cyan colored downward arrow which indicates the trough of CAB. Furthermore, the width of the coherent zone is roughly 17 months and it does not represent the duration of the seventh recession period (10 months) in Table 4.2.

8. According to Table 4.2**,** at the onset of 1954 there was the eighth trough and the recession lasted eight months. Additionally, it is claimed by the ACC that the trough of CAB leaded the trough of NBER by two months in the eighth BC. On the other hand, there is a coherent region between 0.5 to one year period band on the WCA image between 1952 and 1954 with southeastward directed black arrows which means that the IPI leads CAB roughly by two months (see Figure 3.5). Consequently, the WCA is successful in detection of both the eighth BC and the phase difference between the trough of CAB and the trough of NBER for the eighth BC. Additionally, for the eighth trough, it is clearly seen that coherent zone in the WCA figure comes earlier than the cyan colored arrow which indicates the trough of CAB. Furthermore, the width of the coherent zone is roughly 18 months and it does not represent the duration of the eighth recession period (eight months) in Table 4.2.

9. According to Table 4.2**,** at the onset of 1958 there was the ninth trough and the recession lasted 14 months. Additionally, it is claimed by the ACC that the trough of CAB leaded the trough of NBER by eight months in the ninth BC. Moreover, according to Table 4.2**,** at the late of 1960 there was the 10th trough and the recession lasted 16 months. Additionally, it is claimed by the ACC that the trough of CAB leaded the trough of NBER by 11 months in the 10th BC. On the other hand, there is a coherent region between 0.5 to one year period band on the WCA image between 1957 and 1961 with southeastward directed black arrows which means that the IPI leads CAB roughly by two months or the arrows are already completed 360 degree rotation and show the residuals (see Figure 3.5). The eight-month lead of the CAB claimed by the ACC is approximately equal to a full tour for arrows on the coherent region between 0.5 to one year period band on the WCA image and 11 months lead claimed by the ACC is equal to a full tour plus

approximately $\pi/4$ degree rotation for arrows on the coherent region between 0.5 to one year period band on the WCA image. Consequently, the WCA is successful in detection of both the ninth BC and the 10th BC. Also, the WCA is doubtfully successful for the phase difference between the trough of CAB and the trough of NBER for the ninth BC and the 10th BC. Additionally, for the ninth and 10th troughs, it is clearly seen that the coherent zones in the WCA figure prevails earlier than the cyan colored arrows which indicates the trough of CAB. Furthermore, the widths of the first part and the second part of the coherent zones are roughly 24 and 25 months, respectively, which do not represent the durations of the ninth and the 10th recession periods (14 months and 16 months) in Table 4.2.

10. According to Table 4.2**,** at the beginning of 1970 there was the 11th trough and the recession lasted 11 months. Additionally, it is claimed by the ACC that the trough of CAB leaded the trough of NBER by seven months in the 11th BC. On the other hand, there is a coherent region between 0.5 to one year period band on the WCA image between 1969 and 1973 with northeastward directed black arrows which means that the IPI leads CAB roughly by two months or the CAB leads IPI by roughly seven months (at eight months periods, leading by seven months or lagging by two months are indistinguishable because of the cyclical nature of time series) (see Figure 3.5). Seven-month lead of the CAB claimed by the ACC is almost equal to a full tour (one or two months are missing for completing the tour) for arrows on the coherent region between 0.5 to one year period band on the WCA image. Consequently, the WCA is successful in detection of both the 11th BC and the phase difference between the trough of CAB and the trough of NBER for the 11th BC. Additionally, for the 11th trough, it is clearly seen that coherent zone in the WCA figure appears earlier than the cyan colored arrow which indicates the trough of CAB. Furthermore, the width of the coherent zone is roughly 3.5 years and it does not represent the duration of the 11th recession period (11 months) in Table 4.2.

11. According to Table 4.2**,** at the onset of 1975 there was the 12th trough and the recession lasted 24 months. Additionally, it is claimed by the ACC that the trough of CAB leaded the trough of NBER by nine months in the 12th BC. On the other

hand, there is a slim coherent region between 0.5 to one year period band on the WCA image between 1975 and 1976 with rightward directed black arrows which means that there is no phase difference between CAB and IPI or the arrows are already completed 360 degree rotation and return to their initial position (see Figure 3.5). The nine months lead of the CAB claimed by the ACC is approximately equal to a full tour for arrows on the coherent region between 0.5 to one year period band on the WCA image. Consequently, the WCA is successful in detection of both the 12th BC and the phase difference between the trough of CAB and the trough of NBER for the 12th BC. Additionally, for the 12th trough, it is roughly seen that the coherent zone in the WCA figure emerges slightly earlier than the cyan colored arrow which indicates the trough of CAB. Furthermore, the width of the coherent zone is roughly 15 months and it does not represent the duration of the 12th recession period (24 months) in Table 4.2.

12. According to Table 4.2**,** at the mid of 1980 there was the 13th trough and the recession lasted 15 months. Additionally, it is claimed by the ACC that the trough of CAB leaded the trough of NBER by 14 months in the 13th BC. Moreover, according to Table 4.2**,** at the mid of 1982 there was the 14th trough and the recession lasted 20 months. Additionally, it is claimed by the ACC that the trough of CAB leaded the trough of NBER by eight months in the 14th BC. On the other hand, there is a coherent region between 0.5 to one year period band on the WCA image between 1979 and 1983. At the left hand side of the coherent zone which corresponds to 13th trough have southeastward directed black arrows which means that the CAB leads IPI roughly by two months or the arrows are already completed 360 degree rotation and show the residuals (see Figure 3.5). The 14-month lead of the CAB claimed by the ACC is equal to a full tour plus approximately $\pi/4$ degree rotation for arrows on the coherent region between 0.5 to one year period band on the WCA image. On the other hand, the right hand side of the coherent zone which corresponds to 14th trough have northeastward directed black arrows which means that the IPI leads CAB roughly by a month or the CAB leads IPI by roughly eight months (at nine months periods, leading by eight months or lagging by one moths are indistinguishable because of the cyclical nature of time series) (see Figure 3.5). The eight-month lead of the CAB claimed by the ACC is almost equal to a full tour

(one or two months are missing for completing the tour) for arrows on the coherent region between 0.5 to one year period band on the WCA image. Consequently, the WCA is successful in detection of both the 13th BC and the 14th BC. Also, the WCA is successful in detection of the phase difference between the trough of CAB and the trough of NBER for the 13th and 14th BCs. Additionally, for the 13th and 14th troughs, it is clearly seen that coherent zones in the WCA figure prevail earlier than the cyan colored arrows which indicates the trough of CAB. Furthermore, the widths of the first and second parts of the coherent zones are roughly 34 months and 12 months, respectively which do not represent the durations of the 13th and the 14th recession periods (15 months and 20 months) in Table 4.2.

13. According to Table 4.2**,** at the opening of 1991 there was the 15th trough and the recession lasted 15 months. Additionally, it is claimed by the ACC that the trough of CAB leaded the trough of NBER by nine months in the 15th BC. On the other hand, there is a coherent region between 0.5 to one year period band on the WCA image between 1990 and 1992 with southeastward directed black arrows which means that the CAB leads IPI roughly by two months or the arrows are already completed 360 degree rotation and show the residuals (see Figure 3.5). The nine-month lead of the CAB claimed by the ACC is equal to a full tour plus approximately $\pi/8$ degree rotation for arrows on the coherent region between 0.5 to one year period band on the WCA image. Consequently, the WCA is successful in detection of both the 15th BC and the phase difference between the trough of CAB and the trough of NBER for the 15th BC. Additionally, for the 15th trough, it is clearly seen that the coherent zone in the WCA figure arises earlier than the cyan colored arrow which indicates the trough of CAB. Furthermore, the width of the coherent zone is roughly 3.8 years and it does not represent the duration of the 15th recession period (15 months) in Table 4.2.

14. According to Table 4.2**,** at the late of 2001 there was the 16th trough and the recession lasted 19 months. Additionally, it is claimed by the ACC that the trough of CAB leaded the trough of NBER by 12 months in the 16th BC. On the other hand, there is a coherent region between 0.5 to one year period band on the WCA image between 2001 and 2004 with southeastward directed black arrows which

means that the CAB leads IPI roughly by two months or the arrows are already completed 360 degree rotation and show the residuals (see Figure 3.5). The 14-month lead of the CAB claimed by the ACC is equal to a full tour plus approximately $\pi/2$ degree rotation for arrows on the coherent region between 0.5 to one year period band on the WCA image. Consequently, the WCA is successful in detection of the 16th BC and WCA is doubtfully successful in detection of the phase difference between the trough of CAB and the trough of NBER for the 16th BC. Additionally, for the 16th trough, it is clearly seen that the coherent zone in the WCA figure appears earlier than the cyan colored arrow which indicates the trough of CAB. Furthermore, the width of the coherent zone is roughly 3 years and it does not match the duration of the 16th recession period (19 months) in Table 4.2.

15. According to Table 4.2**,** at the beginning of 2009 there was the 17th trough and the recession lasted 22 months. Additionally, it is claimed by the ACC that the trough of CAB leaded the trough of NBER by five months in the 17th BC. On the other hand, there is a coherent region between 0.5 to one year period band on the WCA image between 2005 and 2007 with randomly directed black arrows. However, it is hard to claim that the 17th trough and the "coherent zone" correspond to each other. Consequently, the WCA is not successful in detection of both the 17th BC and the phase difference between the trough of CAB and the trough of NBER for the 17th BC. Subsequently, 17th it is clearly seen that the coherent zone in the WCA figure is not a leading indicator for the 17th trough.

Table 4.3 is constructed to sum up the abovementioned performance of the WCA on the CAB and IPI data with regard to CAB being a leading indicator of IPI, the success in catching the phase relationship between CAB and IPI and in capturing the recession durations claimed by the ACC. The zeros in the table indicate inconclusive cases.

Table 4.3. Performance Summary of WCA on the Original Trending CAB and IPI Data.

BC	Success in Being Leading Indicator of Troughs Claimed by ACC	Success in Capturing Phase Relationship Between CAB and IPI	Success in Capturing Recession Duration Claimed by ACC
1.	0	+	–
2.	–	–	+
3.	+	+	–
4.	+	–	–
5.	–	–	–
6.	+	+	–
7.	+	–	–
8.	+	+	–
9.	+	+	–
10.	+	+	–
11.	+	+	–
12.	+	+	–
13.	+	+	–
14.	+	+	–
15.	+	+	–
16.	+	+	–
17.	0	0	0
	Σ+ = 13 Σ– = 2	Σ+ = 12 Σ– = 4	Σ+ = 1 Σ– = 15

As shown in Table 4.3, the WCA successfully reacts earlier than the occurrences of troughs from second BC to 16th BC with the exception of the third BC. Similarly, one can successfully predict phase relationship between troughs claimed by the ACC and troughs claimed by the NBER from eighth BC to 16th BC. However, the WCA totally fails to bring a comment to recession durations claimed by the ACC or NBER. Moreover, the WCA fails in identifying the last BC claimed by the ACC, therefore performance of the WCA is still questionable.

Furthermore, the interpretation of Figure 4.3b under medium-term scope (between three to 12 years period band) enables to shed light on association between CAB and IPI over a different scale. Clearly, the CAB and IPI are highly coherent between three to 12 years period throughout the time line which means that the analysis is on the right track. In other words, the analysis of the CAB is promising to predict changes in the IPI. Elaborate investigation of the medium-term periods of Figure 4.3b depicts that the CAB and IPI are "in phase" along the time line and there is no phase difference between the time series until 1945 (the same result roughly can be extracted from Figure 4.3e), excluding the two to four years period band after 1939 (arrows point to southeast direction which means that the CAB leads IPI by approximately five months). However, between 1945 and 1975, arrows on the three to 12 years period band point almost downwards, which means that the CAB leads IPI by approximately 3.5 years. Whereas, arrows point to southeast in the 1.5 to three year period band in between 1945-1975, which means that the CAB leads IPI by approximately 5.5 months. Additionally, from 1965 to 2000, the CAB keeps leading the IPI yet with small phase angle (approximately few months) at medium-term scale. However, from 2000 on, the phase between the CAB and IPI returns to its initial position and the CAB leads the IPI by about 1.5 year. On the other hand, there are two less coherent zones and one blue (almost totally incoherent) zone in medium-term region. The first less coherent zone is located at four years period in between 1933 and 1939 and the second less coherent zone is located at two to four years period band in between 1950 and 1955. Furthermore, the incoherent zone is located at four years period band in between 1986 and 1985. Arrows around those less coherent regions do not point the same direction with the rest of the adjacent arrows in the medium-term. These regions may be attributed to unexplained economic incidents in those years. Furthermore, there is a large less coherent zone in between 12 and 20 year periods band between 1962 and 1975.

Additionally, it can be inferred that the CAB and IPI are highly coherent at higher periods. Nevertheless, only small part of the long-term period is implicit in COI in which the time series are coherent and the arrows point to southeast direction. This averagely corresponds to the fact that the CAB leads IPI by about four years.

It should be noted that the coherent regions below 0.25 year period are disregarded since the distinction between noise and meaningful data is not precise at that scale. Additionally, coherent regions over 32 year period are disregarded as well, because coherency analysis becomes statistically insignificant out of the COI.

In addition, Figure 4.5 shows the image of the quantized distribution of the phase differences between CAB and IPI. In Figure 4.5, light-blue areas ($0 < \varphi_{x,y} < -\pi/2$) and yellow areas ($0 < \varphi_{x,y} < \pi/2$) correspond to the “in phase” condition. While the light-blue area indicates that the IPI leads CAB, the yellow area indicates that the CAB leads IPI. Blue areas ($-\pi/2 < \varphi_{x,y} < -\pi$) and red areas ($\pi/2 < \varphi_{x,y} < \pi$) correspond to the “out of phase” condition. The blue area indicates that the IPI leads CAB (or the troughs of the CAB lead the peaks of IPI), while the red area indicates that the CAB leads IPI (or the troughs of the IPI lead the peaks of the CAB). Consequently, the CAB leads the IPI almost everywhere between two to eight year period band, around 32 year period and at the periods larger than 64 year. On the other hand, the IPI leads the CAB around 16 year period and between 40 to 64 year period band.

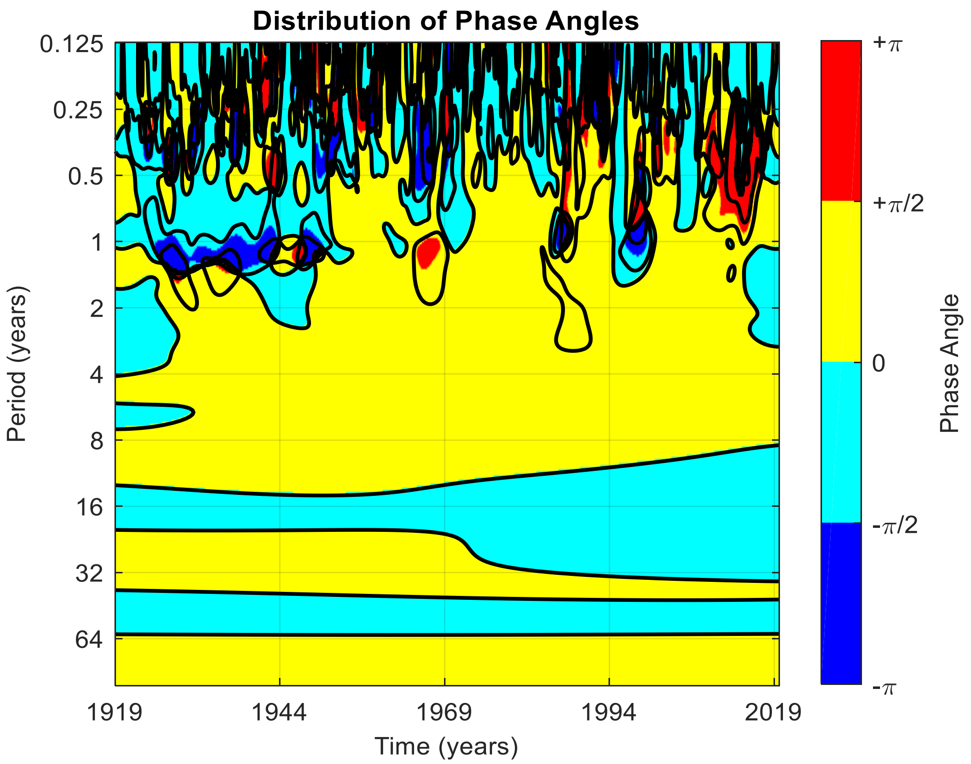

Figure 4.5. Quantized Distribution of Phase Angles between the Original Trending CAB and IPI Series.

4.5. Univariate Wavelet-Based Analysis of the Detrended CAB and IPI Series

In this section, the detrended CAB and IPI series, as shown in Figure 4.1b, will be used. In order to detrend the time series, linear trend lines of the two time series were individually subtracted from the original time series and we have left with cyclical part of the time series. Firstly, dominant sub-cycles of the detrended time series were explored by using two separate univariate analyses, WPS and PSD. While WPSs of the time series are computed using CWT of the series, the PSDs of the time series are computed by adjusting an ARMA(P,Q) model to the series Aguiar-Conraria et al. (2008). “Q” parameter is set to zero as it is suggest in the paper Aguiar-Conraria et al. (2008) whereas a suitable “P” parameter is experimentally found to be 210 by comparing the WPS and PSD methods and to obtain smooth and well-defined spectrum peaks.

In Figure 4.6, there are horizontal red bands at 10-year period of the WPSs of the CAB and IPI along the time span which means that both time series consist of common sub-cycles with 10-year periods. Moreover, the same conclusion can be drawn for the horizontal red bands in both WPSs located at around 20-year period which means that both time series consist of common sub-cycles with 20-year periods. There are clear red lines located at 30-year period and they are also sub-cycles. Similarly, horizontal red bands located between 32-year period and 64-year period along the time span in WPSs elucidate that both time series consist of common sub-cycles with roughly 48-year period, but it must be kept in mind that these sub-cycles are slightly outside of the significant region (COI) and thus they are questionable. Additionally, at the period larger than 64 year, there are solid intense red lines. It is hard to tell that they are also sub-cycles, because they are far from the significant region outlined by the COI.

On the other hand, PSD peaks around 8-period are noteworthy for CAB and IPI. Moreover, peaks located at 5-year period and 10-year period are remarkable only on the PSDs of CAB. Additionally, when one goes to larger periods, continuous increases starting from 20-year period are remarkable on the PSDs of the both time series which can be addressed to obvious red zone of WPS figures. However, since the time data is lost in FT-based PSD analysis, it is not possible to say something about time localization of the peaks. Thus, although WPSs and PSDs give some limited information on the nature of the time series, unfortunately they do not give any information about probable associations between them.

Furthermore, comparison WPS figures of detrended and original trending series depicts that there are small differences among them. For example, the red line located around 10 year period in WPS figures of detrend CAB and IPI is slightly thicker than the red line located around 10 year period in WPS figures of original trending CAB and IPI. Nevertheless, PSD figures show indifferent results.

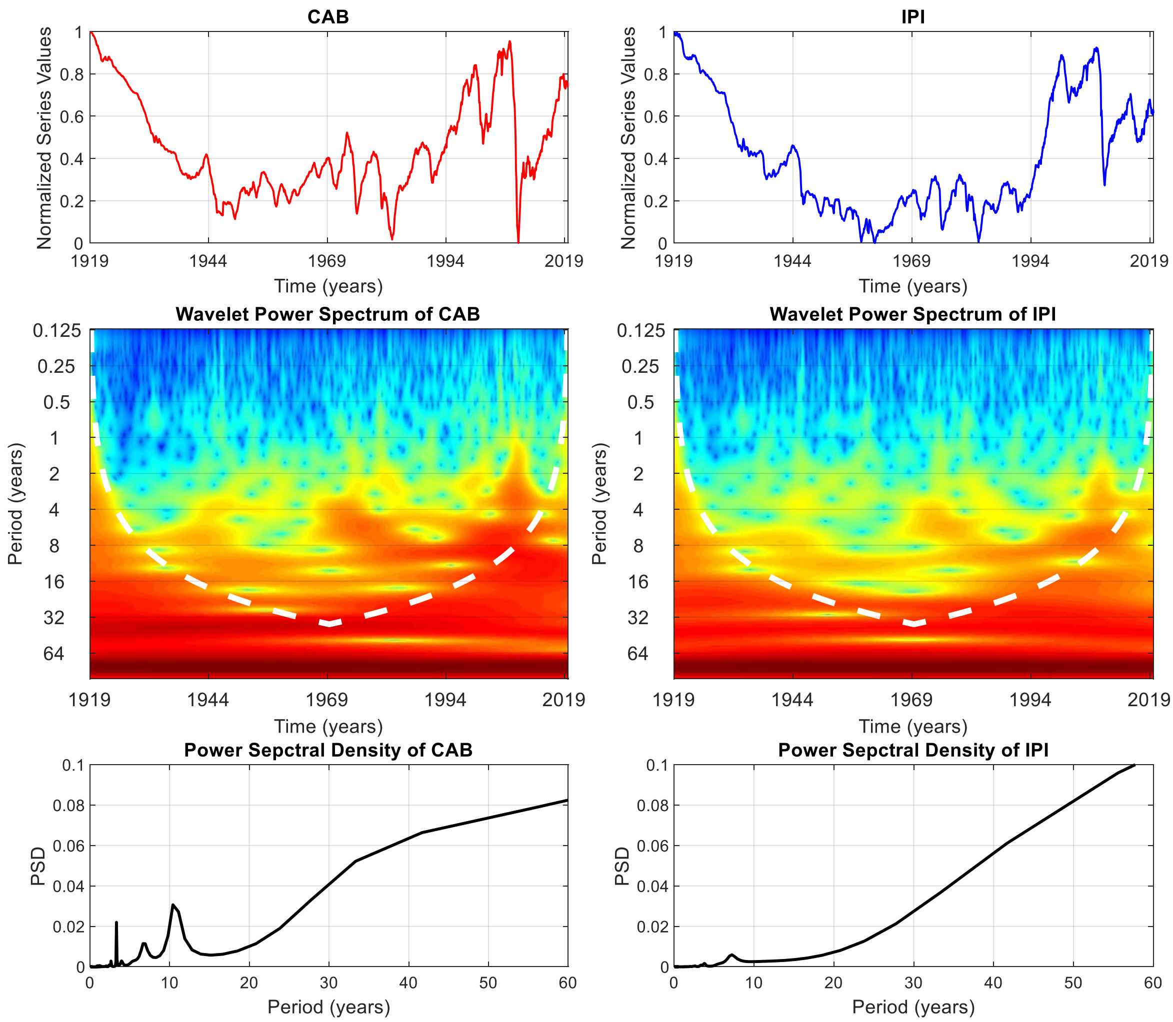

Figure 4.6. Wavelet Power Spectra and Power Spectral Densities of the Detrended CAB and IPI Series.

4.6. Wavelet Coherence Analysis of the Detrended CAB and IPI Series

In this section, WCA of the detrended CAB and IPI series will be used. Subsequently, results of WCA will be compared to NBER's BC turning points to decide whether WCA of the CAB and IPI reveals a leading indicator or not and whether the CAB leads IPI as claimed by the ACC.

Table 4.4 lists the values of some of the important parameters used in the WCA computation in this section.

Table 4.4. Values of Some Important Parameters used in the WCA Computations.

Parameter	**Explanation**	**Value**
dt	sampling interval	1/12 years
DJ	number of octaves per scale	1/32
LPer	lower level of period	1/12 years
UPer	upper level of period	100.42 years
LPhaseDif	lower levels of phase-difference bands	[0.5, 1.0, 3.0] years
UPhaseDif	upper levels of phase-difference bands	[1.0, 2.0, 12] years
MinScale	minimum scale	0.12 years
MaxScale	maximum scale	100.42 years
Mother	mother wavelet	Morlet
MonteCarloCount	number of surrogate sets	10
ArrowDensity	densitiy of arrow on WCA figure	[60 60]

Fıgure 4.7 contains plots of normalized values of the detrended CAB and IPI series (individually detrended via the removal of their individual linear trends/fits), their WCA image, and average phase difference between two series over the three particular period bands (0.5-1, 1-2, and 3-12 year period bands). WCA encompasses valuable information on the interrelation of the two series. In order to advance without missing a point and to be companionable with real-life analysis habits of the economists, the WCA figure will be studied under the short-, medium-, and long-term perspectives.

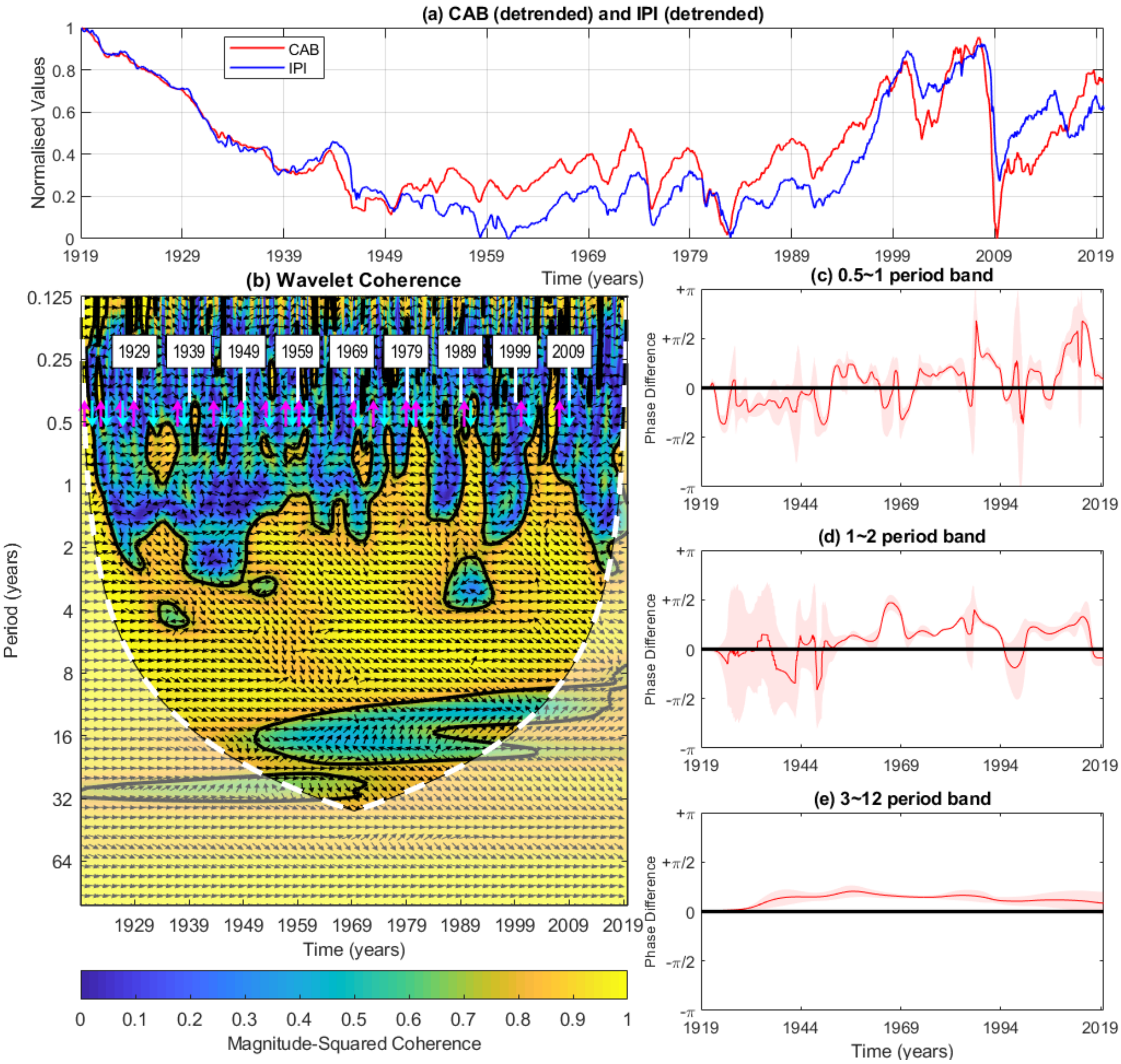

Figure 4.7. Wavelet Coherence Analysis and Phase-Difference Plots of the Detrended CAB and IPI Series.

Figure 4.8 was generated to identify more crisply the range of these short, medium, and long terms and to behold overall time-wise and frequency-wise mean of phase difference and coherency of the CAB and IPI series. From Figure 4.8a, it can be deduced that average coherency between two series is approximately 0.7 along the timeline, which means they are highly coherent. On the other hand, Figure 4.8b contains critical information for the WCA. The peaks in this sub-figure can be used for designation of short-, medium-, and long-term behavior. In this context, the peaks located at 1 and 6 years are attributed to short and medium while periods are longer than 24 years can be attributed to long terms. It is hard to deduce a lot from Figure 4.8c whereas Figure 4.8d roughly shows that in (business) cycles between 2- and 12-year period band and between 19- and

34-year period band, the CAB leads IPI by approximately $\pi/8$ phase angle, but at the rest of the timeline the two series are in-phase. Nevertheless, just by looking at the mean coherency spectrum and phase difference spectrum across time plots can be deceptive because two dimensional coherency plots disregard the degree of coherency. Importance of the true (un-averaged) WCA analysis and the WCA image in Figure 4.7 arises in this situation.

Furthermore, comparison of mean coherency and mean phase difference figures of detrended and original trending series depicts that there are minor differences between them. For instance, in Figure 4.8b, coherency decreases to 0.7 between 10 to 24 year period bands whereas there is no such a decrease in Figure 4.4b.

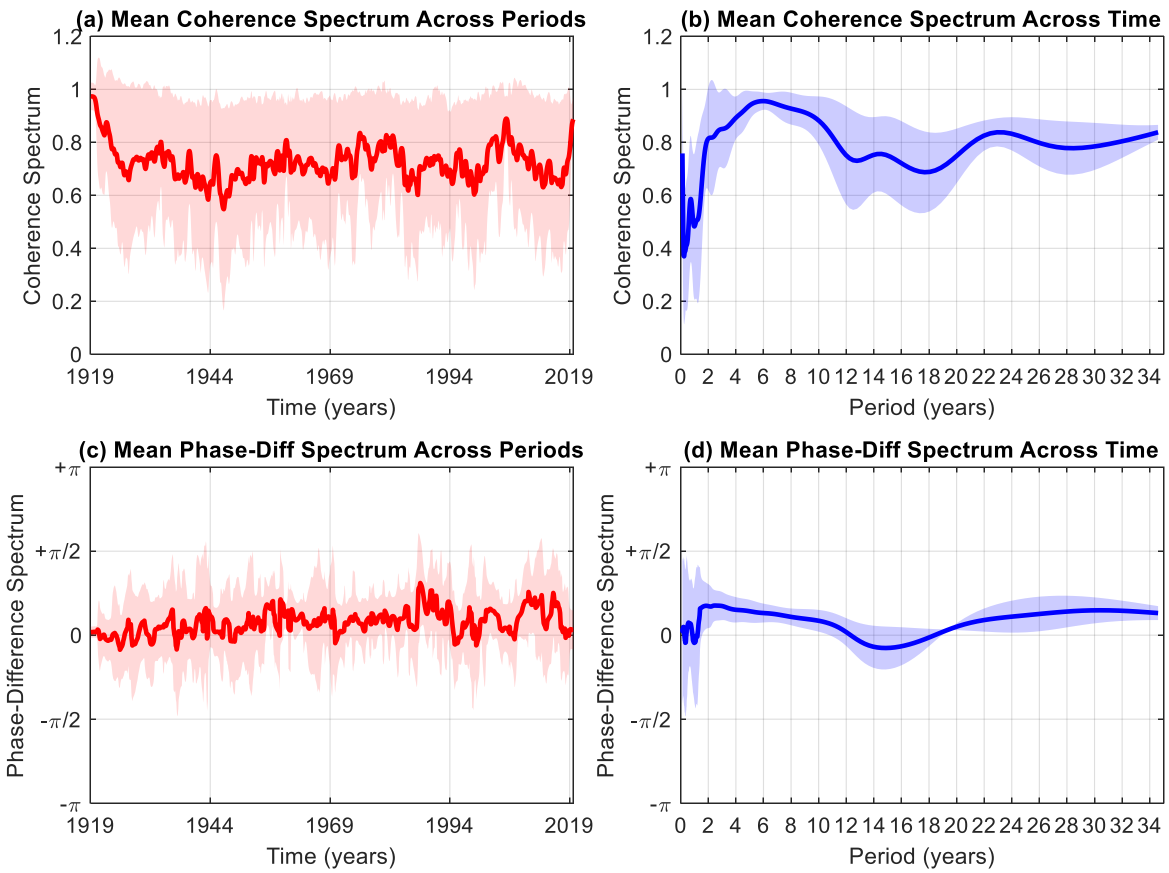

Figure 4.8. Mean Coherence and Mean Phase-Difference between the Detrended CAB and IPI Series across Time and Frequency Domains.

Now, the short-, medium-, and long-term behaviors can be analyzed using the WCA. The motivation for application of the WCA to the CAB and IPI is to discover the link (interrelations) between the time series and to find a hint for a new leading indicator. As discussed in the former section, by considering the simple rules of Bry and Boschan (1971), we claim that BC turning points should be revealed by looking at the short term (0.5 to one year) part of the WCA image. Additionally, so as to make such a visual comparison more precisely, turning points claimed by the ACC (listed in Table 4.2) should be roughly matched on the WCA image. For this purpose, the cyan colored downward arrows are put to indicate troughs and the purple colored upward arrows are put to show peaks on the WCA image. Additionally, vertical white lines are added onto Figure 4.7b which point out the beginnings of the years written above the vertical line. Similar to Figure 4.3b of the previous section, in Figure 4.7b dates of the small "zones of high coherency" located between 0.5 to one year band and dates of troughs claimed by the ACC are somehow matched here as well. The aim of this section is to study if the widely-accepted asymmetric feature of economies in general and the CAB being a leading indicator of NBER's BCs can be captured by the WCA of the detrended CAB and IPI data as well and to compare the results with those of the previous section that belong to the original trending data. Consequently, matching "zones of high coherency" and turning points of BC as claimed by the ACC are both listed in chronological order:

1. According to Table 4.2**,** at the mid of 1921 there was the first trough and the recession lasted seven months. Additionally, it is claimed by the ACC that the trough of CAB leaded the trough of NBER by three months in the first BC. On the other hand, there is a coherent region between 0.5 to one year period band on the WCA image between 1920 and 1921 with downward directed black arrows which means that the CAB leads IPI roughly by two or three months (see Figure 3.5). Consequently, the WCA is successful in detection of both the first BC and the phase difference between the trough of CAB and the trough of NBER for the first BC. Additionally, for the first trough, it is not possible to declare whether WCA is leading CAB or not by looking at the WCA figure because it is on the edge of the COI. Furthermore, the width of the coherent zone is roughly 26 months and it does not represent the duration of the first recession period (seven months) in Table 4.2.

2. According to Table 4.2**,** at the late of 1923 there was the second trough and the recession lasted 11 months. Additionally, it is claimed by the ACC that the trough of CAB leaded the trough of NBER by three months in the second BC. On the other hand, there is an indistinct coherent region between 0.5 to one year period band on the WCA image at 1924 with upward directed black arrows which means that the IPI leads CAB roughly by two or three months (see Figure 3.5). Consequently, the WCA is not successful in detection of both the second BC and the phase difference between the trough of CAB and the trough of NBER for the second BC. Additionally, for the second trough, it is clearly seen that the cyan colored downward arrow which indicates the trough of CAB prevails earlier than the coherent zone in the WCA figure. Furthermore, the width of the coherent zone is roughly 13 months and it approximately represents the duration of the second recession period (11 months) in Table 4.2.

3. According to Table 4.2**,** at the late of 1926 there was the third trough and the recession lasted six months. Additionally, it is claimed by the ACC that the trough of CAB leaded the trough of NBER by four months in the third BC. On the other hand, there is an indistinct coherent region between 0.5 to one year period band on the WCA image at 1926 with southeastward directed black arrows which means that the CAB leads IPI roughly by two months (see Figure 3.5). Consequently, the WCA is successful in detection of the third BC and is partially successful in detection of the phase difference between the trough of CAB and the trough of NBER for the third BC. Additionally, for the third trough, it is roughly seen that coherent zone in the WCA figure prevails earlier than the cyan colored downward arrow which indicates the trough of CAB. Furthermore, the width of the coherent zone roughly 15 months and it does not represent the duration of the third recession period (six months) in Table 4.2.

4. According to Table 4.2**,** at the mid of 1932 there was the fourth trough and the recession lasted seven months. Additionally, it is claimed by the ACC that the trough of CAB leaded the trough of NBER by eight months in the fourth BC. On the other hand, there is a large coherent region between 0.5 to one year period band on the WCA image between 1931 and 1938 with northeastward directed black

arrows which means that the IPI leads CAB roughly by two months (see Figure 3.5). Consequently, the WCA is successful in detection of the fourth BC but is not successful in detection of the phase difference between the trough of CAB and the trough of NBER for the fourth BC. Additionally, for the fourth trough point, it is roughly seen that coherent zone in the WCA figure prevails earlier than the cyan colored downward arrow which indicates the trough of CAB. Furthermore, the width of the coherent zone roughly 5.5 years and it does not represent the duration of the fourth recession period (seven months) in Table 4.2.

5. According to Table 4.2**,** at the onset of 1938 there was the fifth trough and the recession lasted four months. Additionally, it is claimed by the ACC that the trough of CAB leaded the trough of NBER by five months in the fifth BC. On the other hand, there is a slim coherent region between 0.5 to one year period band on the WCA image at 1939 with slightly southeastward directed black arrows which means that the CAB leads IPI by one month (see Figure 3.5). Consequently, the WCA is not successful in detection of both the fifth BC and the phase difference between the trough of CAB and the trough of NBER for the fifth BC. Additionally, for the fifth trough, it is clearly seen that the cyan colored downward arrow which indicates the trough of CAB prevails earlier than the coherent zone in the WCA figure. Furthermore, the width of the coherent zone is roughly 17 months and it does not represent the duration of the fifth recession period (4 months) in Table 4.2.

6. According to Table 4.2**,** at the late of 1945 there was the sixth trough and the recession lasted 25 months. Additionally, it is claimed by the ACC that the trough of CAB leaded the trough of NBER by 18 months in the fifth BC. On the other hand, there is a slim coherent region between 0.5 to one year period band on the WCA image between 1944 and 1946 with rightward directed black arrows which means that there is no phase difference between the CAB and IPI or the arrows are already completed 360 degree rotation and return to their initial position (see Figure 3.5). The 18 months lead of CAB claimed by the ACC is approximately equal to two full tours for arrows on the coherent region between 0.5 to one year period bands on the WCA image. Consequently, the WCA is successful in detection of the sixth BC and is doubtfully successful in detection of the phase difference between

the trough of CAB and the trough of NBER for the sixth BC. Additionally, for the sixth trough, it is roughly seen that the coherent zone in the WCA figure occurs earlier than the cyan colored downward arrow which indicates the trough of CAB. Furthermore, the width of the coherent zone is roughly 17 months and it does not represent the duration of the sixth recession period (25 months) in Table 4.2.

7. According to Table 4.2**,** at the mid of 1949 there was the seventh trough and the recession lasted 10 months. Additionally, it is claimed by the ACC that the trough of CAB leaded the trough of NBER by two months in the seventh BC. On the other hand, there is an indistinct coherent region between 0.5 to one year period band on the WCA image at 1950 with northeastward directed black arrows which means that the IPI leads CAB roughly by two months (see Figure 3.5). Consequently, the WCA is successful in detection of the seventh BC but is not successful in detection of the phase difference between the trough of CAB and the trough of NBER for the seventh BC. Additionally, for the seventh trough, it is seen that the coherent zone in the WCA figure prevails slightly earlier than the cyan colored downward arrow which indicates the trough of CAB. Furthermore, the width of the coherent zone is roughly 17 months and it does not represent the duration of the seventh recession period (10 months) in Table 4.2.

8. According to Table 4.2**,** at the onset of 1954 there was the eighth trough and the recession lasted eight months. Additionally, it is claimed by the ACC that the trough of CAB leaded the trough of NBER by two months in the eighth BC. On the other hand, there is a coherent region between 0.5 to one year period band on the WCA image between 1952 and 1954 with southeastward directed black arrows which means that the IPI leads CAB roughly by two months (see Figure 3.5). Consequently, the WCA is successful in detection of both the eighth BC and the phase difference between the trough of CAB and the trough of NBER for the eighth BC. Additionally, for the eighth trough, it is clearly seen that coherent zone in the WCA figure comes earlier than the cyan colored arrow which indicates the trough of CAB. Furthermore, the width of the coherent zone is roughly 18 months and it does not represent the duration of the eighth recession period (eight months) in Table 4.2.

9. According to Table 4.2**,** at the onset of 1958 there was the ninth trough and the recession lasted 14 months. Additionally, it is claimed by the ACC that the trough of CAB leaded the trough of NBER by eight months in the ninth BC. Moreover, according to Table 4.2**,** at the late of 1960 there was the 10th trough and the recession lasted 16 months. Additionally, it is claimed by the ACC that the trough of CAB leaded the trough of NBER by 11 months in the 10th BC. On the other hand, there is a coherent region between 0.5 to one year period band on the WCA image between 1957 and 1961 with southeastward directed black arrows which means that the IPI leads CAB roughly by two months or the arrows are already completed 360 degree rotation and show the residuals (see Figure 3.5). The eight-month lead of the CAB claimed by the ACC is approximately equal to a full tour for arrows on the coherent region between 0.5 to one year period band on the WCA image and 11 months lead claimed by the ACC is equal to a full tour plus approximately $\pi/4$ degree rotation for arrows on the coherent region between 0.5 to one year period band on the WCA image. Consequently, the WCA is successful in detection of both the ninth BC and the 10th BC. Also, the WCA is doubtfully successful for the phase difference between the trough of CAB and the trough of NBER for the ninth BC and the 10th BC. Additionally, for the ninth and 10th troughs, it is clearly seen that the coherent zones in the WCA figure prevails earlier than the cyan colored arrows which indicates the trough of CAB. Furthermore, the widths of the first part and the second part of the coherent zones are roughly 24 and 25 months, respectively, which do not represent the durations of the ninth and the 10th recession periods (14 months and 16 months) in Table 4.2.

10. According to Table 4.2**,** at the beginning of 1970 there was the 11th trough and the recession lasted 11 months. Additionally, it is claimed by the ACC that the trough of CAB leaded the trough of NBER by seven months in the 11th BC. On the other hand, there is a coherent region between 0.5 to one year period band on the WCA image between 1969 and 1973 with northeastward directed black arrows which means that the IPI leads CAB roughly by two months or the CAB leads IPI by roughly seven months (at eight months periods, leading by seven months or lagging by two months are indistinguishable because of the cyclical nature of time series) (see Figure 3.5). Seven-month lead of the CAB claimed by the ACC is almost equal

to a full tour (one or two months are missing for completing the tour) for arrows on the coherent region between 0.5 to one year period band on the WCA image. Consequently, the WCA is successful in detection of both the 11th BC and the phase difference between the trough of CAB and the trough of NBER for the 11th BC. Additionally, for the 11th trough, it is clearly seen that coherent zone in the WCA figure appears earlier than the cyan colored arrow which indicates the trough of CAB. Furthermore, the width of the coherent zone is roughly 3.5 years and it does not represent the duration of the 11th recession period (11 months) in Table 4.2.

11. According to Table 4.2**,** at the onset of 1975 there was the 12th trough and the recession lasted 24 months. Additionally, it is claimed by the ACC that the trough of CAB leaded the trough of NBER by nine months in the 12th BC. On the other hand, there is a slim coherent region between 0.5 to one year period band on the WCA image between 1975 and 1976 with rightward directed black arrows which means that there is no phase difference between the CAB and IPI or the arrows are already completed 360 degree rotation and return to their initial position (see Figure 3.5). The nine months lead of the CAB claimed by the ACC is approximately equal to a full tour for arrows on the coherent region between 0.5 to one year period band on the WCA image. Consequently, the WCA is successful in detection of both the 12th BC and the phase difference between the trough of CAB and the trough of NBER for the 12th BC. Additionally, for the 12th trough, it is roughly seen that the coherent zone in the WCA figure emerges slightly earlier than the cyan colored arrow which indicates the trough of CAB. Furthermore, the width of the coherent zone is roughly 15 months and it does not represent the duration of the 12th recession period (24 months) in Table 4.2.

12. According to Table 4.2**,** at the mid of 1980 there was the 13th trough and the recession lasted 15 months. Additionally, it is claimed by the ACC that the trough of CAB leaded the trough of NBER by 14 months in the 13th BC. Moreover, according to Table 4.2**,** at the mid of 1982 there was the 14th trough and the recession lasted 20 months. Additionally, it is claimed by the ACC that the trough of CAB leaded the trough of NBER by eight months in the 14th BC. On the other

hand, there is a coherent region between 0.5 to one year period band on the WCA image between 1979 and 1983. At the left hand side of the coherent zone which corresponds to 13th trough have southeastward directed black arrows which means that the CAB leads IPI roughly by two months or the arrows are already completed 360 degree rotation and show the residuals (see Figure 3.5). The 14-month lead of the CAB claimed by the ACC is equal to a full tour plus approximately $\pi/4$ degree rotation for arrows on the coherent region between 0.5 to one year period band on the WCA image. On the other hand, the right hand side of the coherent zone which corresponds to 14th trough have northeastward directed black arrows which means that the IPI leads CAB roughly by a month or the CAB leads IPI by roughly eight months (at nine months periods, leading by eight months or lagging by one moths are indistinguishable because of the cyclical nature of time series) (see Figure 3.5). The eight-month lead of the CAB claimed by the ACC is almost equal to a full tour (one or two months are missing for completing the tour) for arrows on the coherent region between 0.5 to one year period band on the WCA image. Consequently, the WCA is successful in detection of both the 13th BC and the 14th BC. Also, the WCA is successful in detection of the phase difference between the trough of CAB and the trough of NBER for the 13th and 14th BCs. Additionally, for the 13th and 14th troughs, it is clearly seen that coherent zones in the WCA figure prevail earlier than the cyan colored arrows which indicates the trough of CAB. Furthermore, the widths of the first and second parts of the coherent zones are roughly 34 months and 12 months, respectively which do not represent the durations of the 13th and the 14th recession periods (15 months and 20 months) in Table 4.2.

13. According to Table 4.2**,** at the start of 1991 there was the 15th trough and the recession lasted 15 months. Additionally, it is claimed by the ACC that the trough of CAB leaded the trough of NBER by nine months in the 15th BC. On the other hand, there is a coherent region between 0.5 to one year period band on the WCA image between 1990 and 1992 with southeastward directed black arrows which means that the CAB leads IPI roughly by two months or the arrows are already completed 360 degree rotation and show the residuals (see Figure 3.5). The nine-month lead of the CAB claimed by the ACC is equal to a full tour plus approximately $\pi/8$ degree rotation for arrows on the coherent region between 0.5

to one year period band on the WCA image. Consequently, the WCA is successful in detection of both the 15th BC and the phase difference between the trough of CAB and the trough of NBER for the 15th BC. Additionally, for the 15th trough, it is clearly seen that the coherent zone in the WCA figure arises earlier than the cyan colored arrow which indicates the trough of CAB. Furthermore, the width of the coherent zone is roughly 3.8 years and it does not represent the duration of the 15th recession period (15 months) in Table 4.2.

14. According to Table 4.2**,** at the late of 2001 there was the 16th trough and the recession lasted 19 months. Additionally, it is claimed by the ACC that the trough of CAB leaded the trough of NBER by 12 months in the 16th BC. On the other hand, there is a coherent region between 0.5 to one year period band on the WCA image between 2001 and 2004 with southeastward directed black arrows which means that the CAB leads IPI roughly by two months or the arrows are already completed 360 degree rotation and show the residuals (see Figure 3.5). The 14-month lead of the CAB claimed by the ACC is equal to a full tour plus approximately $\pi/2$ degree rotation for arrows on the coherent region between 0.5 to one year period band on the WCA image. Consequently, the WCA is successful in detection of the 16th BC and WCA is doubtfully successful in detection of the phase difference between the trough of CAB and the trough of NBER for the 16th BC. Additionally, for the 16th trough, it is clearly seen that the coherent zone in the WCA figure appears earlier than the cyan colored arrow which indicates the trough of CAB. Furthermore, the width of the coherent zone is roughly 3 years and it does not match the duration of the 16th recession period (19 months) in Table 4.2.

15. According to Table 4.2**,** at the beginning of 2009 there was the 17th trough and the recession lasted 22 months. Additionally, it is claimed by the ACC that the trough of CAB leaded the trough of NBER by five months in the 17th BC. On the other hand, there is a coherent region between 0.5 to one year period band on the WCA image between 2005 and 2007 with unsystematically directed black arrows. However, it is hard to claim that the 17th trough and the “coherent zone” correspond to each other. Consequently, the WCA is not successful in detection of both the 17th BC and the phase difference between the trough of CAB and the

trough of NBER for the 17th BC. Subsequently, 17th it is clearly seen that the coherent zone in the WCA figure is not a leading indicator for the 17th trough.

Table 4.5 is constructed to sum up the abovementioned performance of the WCA on the CAB and IPI with regard to CAB being a leading indicator of IPI, the success in catching the phase relationship between CAB and IPI and in capturing the recession durations claimed by the ACC. The zeros in the table indicate inconclusive cases.

Table 4.5. Performance Summary of WCA on the Detrended CAB and IPI Data.

BC	**Success in Being Leading Indicator of Troughs Claimed by ACC**	**Success in Capturing Phase Relationship Between CAB and IPI**	**Success in Capturing Recession Duration Claimed by ACC**
1.	0	+	–
2.	–	–	+
3.	+	+	–
4.	+	–	–
5.	–	–	–
6.	+	+	–
7.	+	–	–
8.	+	+	–
9.	+	+	–
10.	+	+	–
11.	+	+	–
12.	+	+	–
13.	+	+	–
14.	+	+	–
15.	+	+	–
16.	+	+	–
17.	0	0	0
	$\Sigma+ = 13$ $\Sigma- = 2$	$\Sigma+ = 12$ $\Sigma- = 4$	$\Sigma+ = 1$ $\Sigma- = 15$

As shown in Table 4.5, the WCA successfully reacts earlier than the occurrences of troughs from second BC to 16th BC with the exception of the third BC. Similarly, one can successfully predict phase relationship between troughs claimed by the ACC and troughs claimed by the NBER from eighth BC to 16th BC. However, the WCA totally fails to bring a comment to recession durations claimed by the ACC or NBER. Moreover, the WCA fails in identifying the last BC claimed by the ACC, therefore performance of the WCA is still questionable. Consequently, comparison short-term interpretation of the WCA figures of the detrended and original trending series depicts that there is almost no differences among them.

Furthermore, the interpretation of Figure 4.7b under medium-term scope (between three to 12 years period band) depicts that the CAB and IPI are highly coherent between three to 12 years period throughout the time line which means that the analysis is on the right track. In other words, the analysis of the CAB is promising to predict changes in the IPI. Elaborate investigation of the medium-term periods of Figure 4.7b depicts that the CAB and IPI are “in phase” along the time line and there is no phase difference between the time series until 1945 (the same result roughly can be extracted from Figure 4.7e), excluding the two to four years period band after 1939 (arrows point to southeast direction which means that the CAB leads IPI by approximately five months). However, between 1945 and 1975, arrows on the three to 12 years period band point almost downwards, which means that the CAB leads IPI by approximately 3.5 years. Whereas, arrows point to southeast in the 1.5 to three year period band in between 1945-1975, which means that the CAB leads IPI by approximately 5.5 months. Additionally, from 1965 to 2000, the CAB keeps leading the IPI yet with small phase angle (approximately few months) at medium-term scale. However, from 2000 on, the phase between the CAB and IPI returns to its initial position and the CAB leads the IPI by about 1.5 year. On the other hand, there are two less coherent zones and one blue (almost totally incoherent) zone in medium-term region. The first less coherent zone is located at four years period in between 1933 and 1939 and the second less coherent zone is located at two to four years period band in between 1950 and 1955. Furthermore, the incoherent zone is located at four years period band in between 1986 and 1985. Arrows around those less coherent regions do not point the same direction with the rest of the adjacent arrows in the medium-term. These regions may be attributed to unexplained economic incidents in those years. Furthermore, there is a large blue “no coherency region” in between 10 and 20 year periods band from 1950 till the end. Addition to large “no coherency region”, there is les coherent region between 22 to 32 year period band between 1919 and 1970. Interestingly, these “incoherent” and “less coherent” regions do not exist in Figure 4.3b of the previous section related to the original trending series and thus they can be attributed to the effects of detrending.

Additionally, it can be inferred that the CAB and IPI are highly coherent at higher periods. Nevertheless, only small part of the long-term period is implicit in the COI in which the time series are coherent and the arrows point to southeast direction. This averagely corresponds to the fact that the CAB leads IPI by about four years. Also, unlike Figure 4.3b of the previous section related to the original trending series, arrows on 48 to 64 year period band point to southeast direction too which averagely corresponds to the fact that the CAB leads IPI by about eight years.

It should be noted that the coherent regions below 0.25 year period are disregarded since the distinction between noise and meaningful data is not precise at that scale. Additionally, coherent regions over 32 year period are disregarded as well, because coherency analysis becomes statistically insignificant out of the COI.

In addition, Figure 4.9 shows the image of the quantized distribution of the phase differences between CAB and IPI. In Figure 4.9, light-blue areas $(0 < \varphi_{x,y} < -\pi/2)$ and yellow areas $(0 < \varphi_{x,y} < \pi/2)$ correspond to the “in phase” condition. While the light-blue area indicates that the IPI leads CAB, the yellow area indicates that the CAB leads IPI. Blue areas $(-\pi/2 < \varphi_{x,y} < -\pi)$ and red areas $(\pi/2 < \varphi_{x,y} < \pi)$ correspond to the “out of phase” condition. The blue area indicates that the IPI leads CAB (or the troughs of CAB lead the peaks of IPI), while the red area indicates that the CAB leads IPI (or the troughs of IPI lead the peaks of CAB). Consequently, the CAB leads the IPI almost everywhere between two to eight year period band, and at the periods larger than 32 year. On the other hand, the IPI leads the CAB between 20 to 30 year period band between 1919 and 1940, and between 10 to 20 year period band beyond 1962. Furthermore, quantized phase-difference distribution figures of the detrended and original trending series depict that there are considerable differences between them especially at the mid-term and long-term periods.

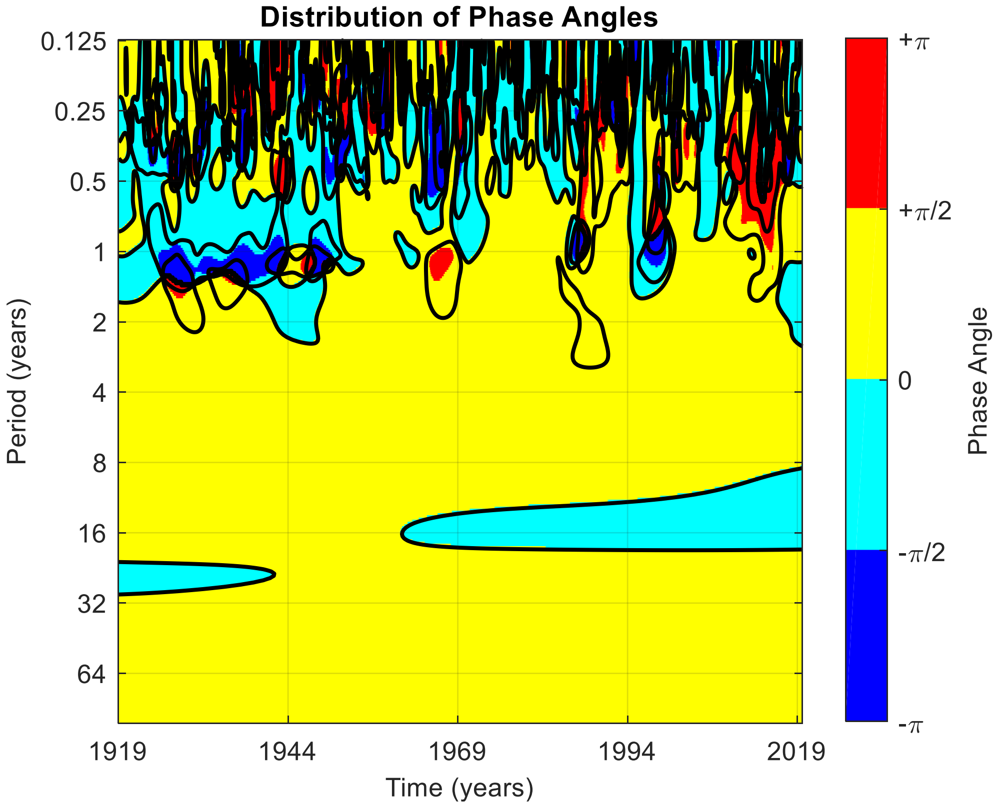

Figure 4.9. Quantized Distribution of Phase Angles between the Detrended CAB and IPI Series.

Overall, the focus of this chapter was on BC periods, i.e., the short-term periods. Therefore, for short-term periods, the comparisons between Figure 4.3 and Figure 4.7, Figure 4.4 and Figure 4.8, and Figure 4.5 and Figure 4.9 depicted that detrending the data did not affect the WCA results. On the other hand, this was not a valid inference for the longer periods. Especially between 8- to 32-year periods, the effects of detrending became evident. While the differences between Figure 4.3 and Figure 4.7 within 8- to 32-year periods showed that the detrending increased the resolution, the differences between Figure 4.5 and Figure 4.9 for 8- to 64-year periods showed that the detrending also influenced the phase-difference between the time series. Subsequently, Figure 4.8, which contained the mean phase-difference and mean coherence showed dissimilarities with Figure 4.4 as well.

4.7. Univariate Wavelet-Based Analysis of the Moving-Average-Smoothed First-Order Differenced CAB and IPI Series

The ACC uses moving-average-smoothed first-order differenced transformations of the CAB and IPI in their analysis (*Chemical Activity Barometer vs. Industrial Production*, 2019). Although, moving average (MA) is a powerful tool to eliminate noise in time series, it also generates artificial lags in the series (Bai et al., 2015). In this section, the WPS and PSD of the year-to-year change of the three-month MA of the CAB and IPI will be investigated.

In Figure 4.10, there are horizontal red bands at/around 2-, 4-, 10-, 20-, and 30-year periods and at larger periods of the WPSs of the CAB and IPI along the time span. However, among them, the horizontal red bands located at shorter than 8-year period can not be observed in Figure 4.2 and Figure 4.6 of the previous sections. Similarly, there are few peaks at the shorter than 8-year period in the PSD figures which is unlike of the original trending and detrended series. This can be the result of artificial lags introduced in smoothing by MA.

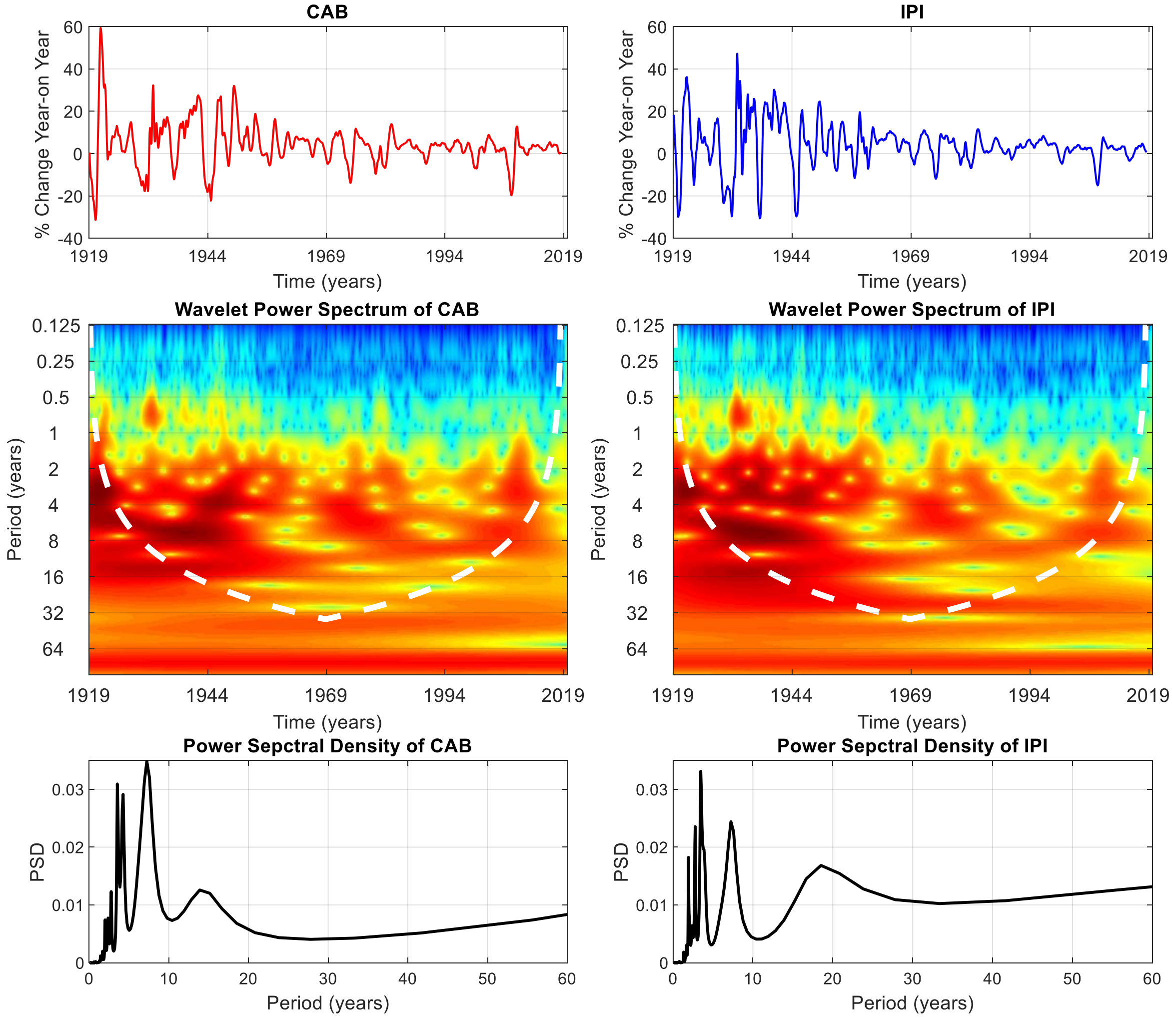

Figure 4.10. Wavelet Power Spectra and Power Spectral Densities of the Year-to-Year Change of Three-Month MA of the CAB and IPI Series.

4.8. Wavelet Coherence Analysis of the Moving-Average-Smoothed First-Order Differenced CAB and IPI Series

Similar to previous sections on the original trending and detrended series, the WCA of the year-to-year change of the three-month MA of the CAB and IPI will be investigated concisely in this section.

When Figure 4.11 is compared with the former WCA figures (Figure 4.3 for the original trending data and Figure 4.7 for the detrended data), at first sight, it seems like there are no striking differences among them for low periods (0.5 to one year period). Since we analyze BCs for these low periods (since typical BCs fall in this period range as elaborated at the begining of this chapter), our BC analyses and their conclusions with regard to BC issues are similar as well. However, when one prudently compares the figures, it can be seen that there are significant dissimilarities among them. For instance, shapes of the “zones of high coherency” are different. Also, in Figure 4.11 “zones of high coherency” shifted to the left hand side compared to Figure 4.3 and Figure 4.7. This shifting to the left hand side can be observed by comparing the 11th BC located at 1970 in different figures. On the other hand, the effects of detrending and MA prevail theselves for the longer periods (2 to 64 years)**.** Th**e** blue-colored “incoherent region” located between 8- to 40-year periods is much larger than the WCA figure of the detrended data and some arrows are differently oriented as well. Furthermore, the arrows on 48- to 64-year period bands are also differently oriented than the arrows in the WCA figure of the detrended data. Moreover, the sizes of the “less coherent” zones located at the four-year period in between 1933 and 1939, and located at two- to four-year period band in between 1950 and 1955, are larger than the sizes in the WCA figure of the detrended data. Furthermore, the “incoherent zone” is located at the four-year period band in between 1986 and 1985 has a larger size as well.

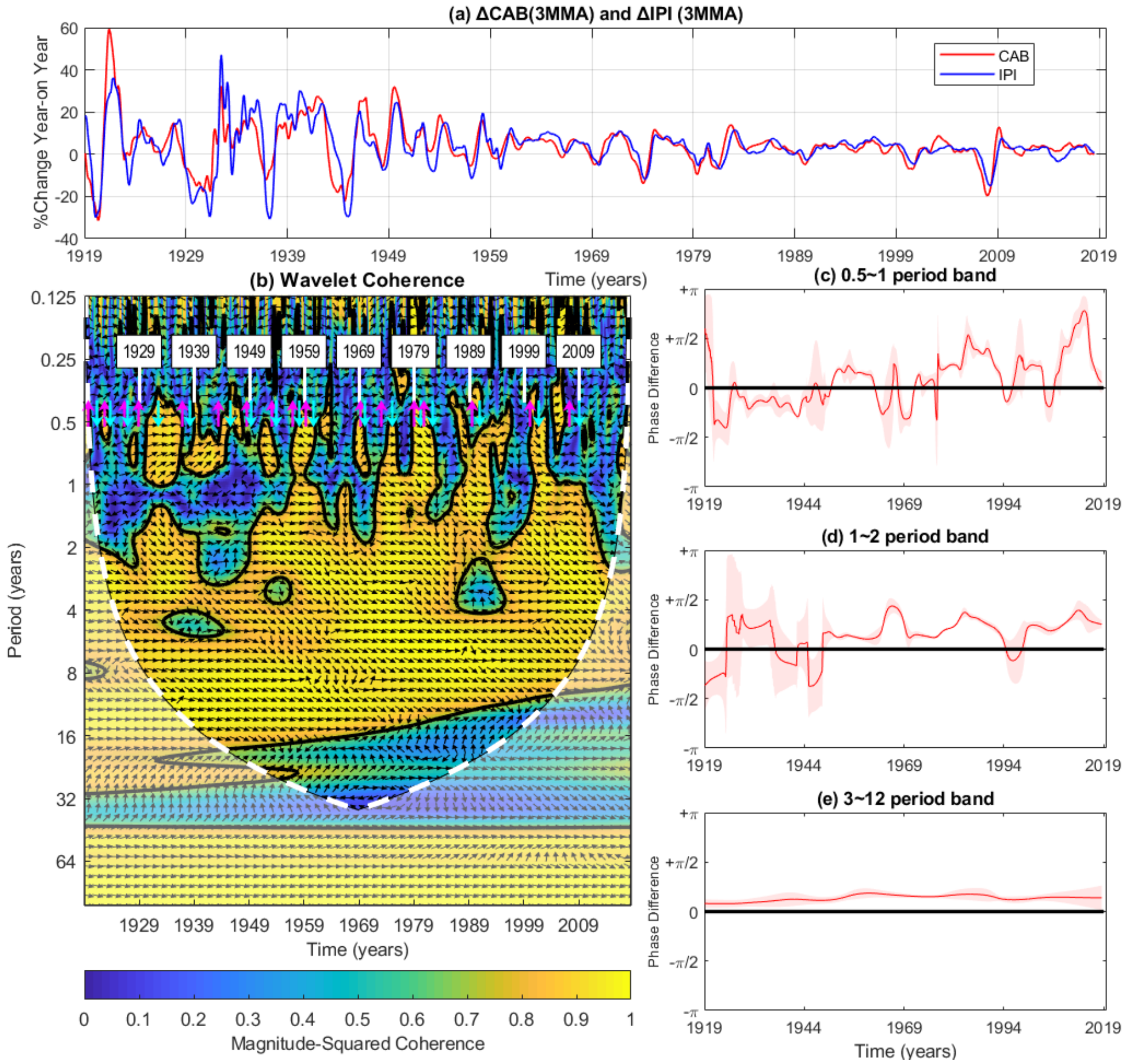

Figure 4.11. Wavelet Coherence Analysis of the Year-to-Year Change of the Three-Month MA of the CAB and IPI Series.

Since Figure 4.12 is generated from Figure 4.11, there are differences between the figures of mean coherence and mean phase-difference between Figure 4.12 and Figure 4.4 and Figure 4.8 (previous sections on the original trending and detrended data, respectively) across time and frequency domains. For instance, these differences can be captured by comparing periods larger than 24 year in Figure 4.12b and Figure 4.8b or by comparing periods larger than 14 year in Figure 4.12d and Figure 4.8d.

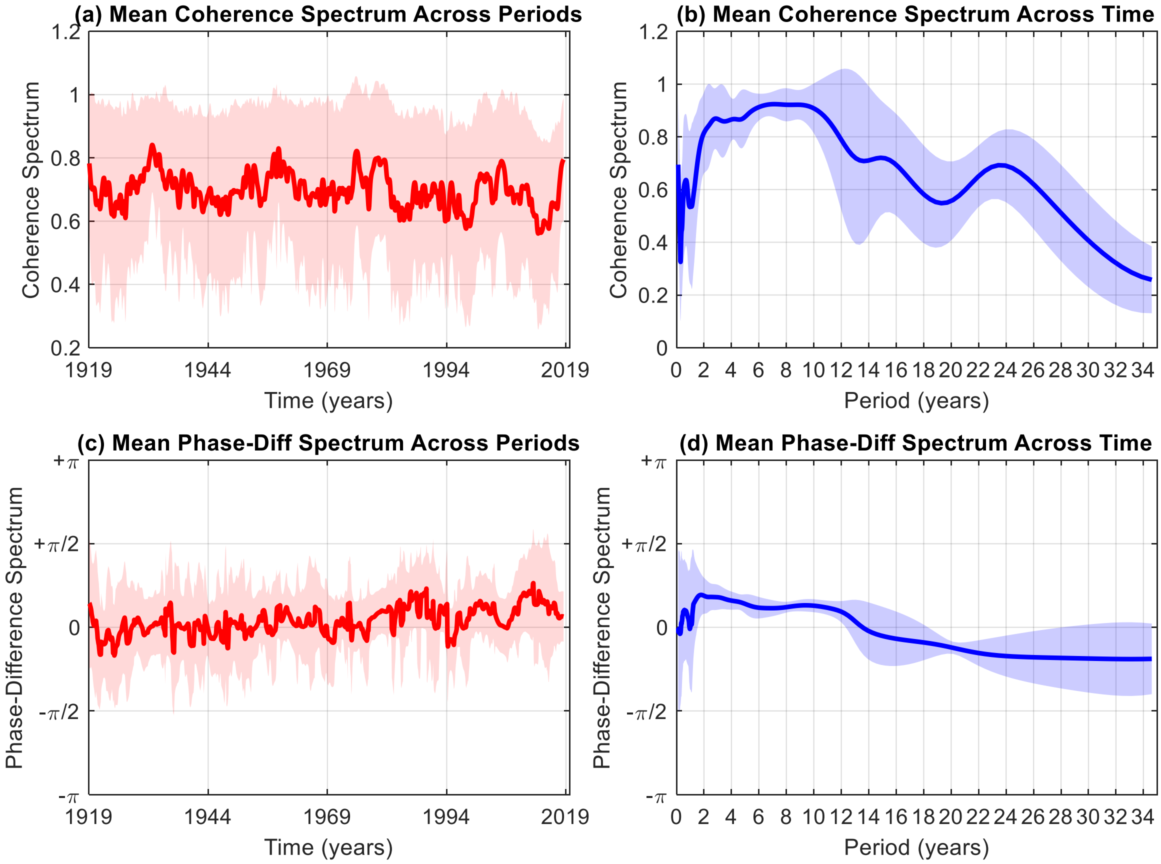

Figure 4.12. Mean Coherence and Mean Phase-Difference between the Year-to-Year Change of the Three-Month MA of the CAB and IPI Series across Time and Frequency Domains.

Finally, Figure 4.13 is created by using the year-to-year change of the three-month MA of the CAB and IPI series. Figure 4.13 depicts that the smoothing increases the size of the region in which the IPI leads the CAB on the phase distributions between 16- to 64-year period bands as compared to Figure 4.5 and Figure 4.9 of the previous sections on the original trending and detrended data, respectively.

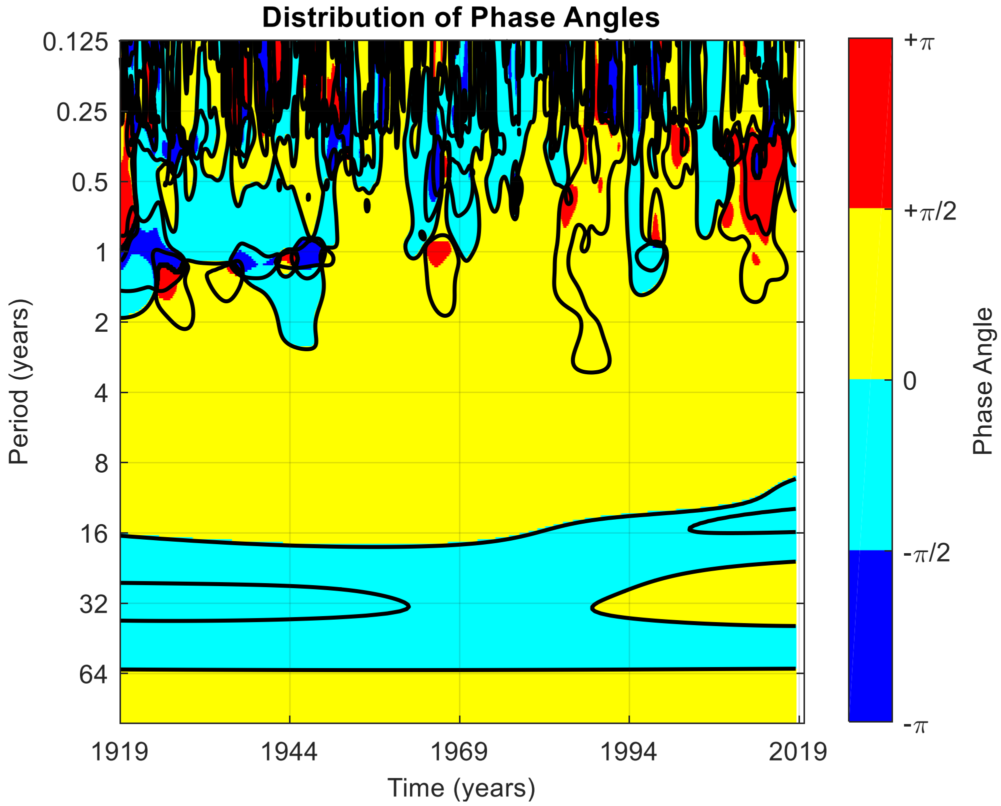

Figure 4.13. Quantized Distribution of Phase Angles between the Year-to-Year Change of the Three-Month MA of the CAB and IPI Series.

Overall, the focus of this chapter was on the BC periods, i.e., the short-term periods as above-mentioned. Therefore, the short-term periods comparison of Figure 4.11 with Figure 4.3 and Figure 4.7 depicted that the three-month MA impacted the WCA figure at the short-term periods. At the same time, comparison of the longer periods (of 8- to 64-year periods) of Figure 4.11 with Figure 4.3 and Figure 4.7, and Figure 4.13 with Figure 4.5 and Figure 4.9 depicted that the WCA of the three-month MA differed from the original trending and detrended time series in two circumstances. First, they showed different levels of coherency, and, second, they showed different phase-angle relationships between the two time series. It is known that MA smoothing generates artificial lag and we assume that this artificial lag can be attributed for the dissimilarities between the WCA figures. On the other hand, the ACC still uses three-month MA smoothing in their analyses. The reason can be that the MA-smoothed time series can be used for detection of turning points simply by eye, without further analysis. For instance, from Figure 4.11a it can be confirmed just by observation that some definite, well-defined turning points (troughs and/or peaks) located around 2007, 2001, 1991, 1982, 1980, and 1975 and so on, coincide with the turning points disclosed by the NBER.

4.9. Summary of the Effects of Detrending and Three-Month MA Smoothing

In this section, dissimilarities resulting from detrending and MA smoothing are encapsulated. Firstly, comparison of the univariate analyses (contrasting Figure 4.2, Figure 4.6 and Figure 4.10) reveals that the sub-cycles located at shorter than 30-year period become more visible in Figure 4.6 of the detrended time series compared to the sub-cycles in Figure 4.2 of the original trending time series. Whereas, in Figure 4.10 of the time series smoothed by the simple MA, those sub-cycles are much more visible than the sub-cycles of the detrended and original trending time series. Secondly, comparison of the WCA figures (contrasting Figure 4.3, Figure 4.7 and Figure 4.11) exposes that the coherency levels in the WCA of the detrended series (Figure 4.7) and original trending series (Figure 4.3) are almost perfectly the same over the BC periods (0.5- to one-year periods), whereas the “high coherency zones” in the WCA (Figure 4.11) of the time series smoothed by MA show small but critical differences. Since, adjacent data points have effects on each data point of time series smoothed by MA, the “high coherency zones” are shifted to the left and their shapes are slightly different than the “high coherency zones” in the WCAs of the detrended and original trending time series. Moreover, for the longer periods (eight- to 64-year periods), the effects of detrending and MA smoothing are more obvious. The resolution for these particular period ranges is higher for the WCA of the detrended series (Figure 4.7) is higher than for the WCA of the original trending series (Figure 4.3). On the other hand, MA smoothing increases the resolution more than detrending.

Finally, as in shown Figure 4.5, Figure 4.9, and Figure 4.13, the phase relationships between the CAB and IPI are not significantly affected by detrending or MA smoothing over the BC periods (0.5- to one-year periods). On the other hand, for the longer periods (eight- to 64- year periods), the detrending increases the region in which the IPI leads the CAB in comparison with the original trending series, whereas, MA smoothing further increases the region in which the IPI leads the CAB in comparison with the detrended time series. The WCA, on the other hand, does not necessitate detrending and does not introduce artificial lags as in MA smoothing in exploring the lead-lag relationships between time series.

5. WAVELET COHERENCE ANALYSES FOR THE YEARLY CEPCI, CAB, AND IPI DATA

5.1. Description of Cost Indices and the CEPCI

Cost estimation is a critical step in the design of chemical processes. Process or cost engineers use cost indices to estimate the total cost of a project. There are several cost indices which are used for process engineers in different fields. The Nelson-Farrar Refinery Cost Index, which is used in the oil and gas industry, can be found in the (*Oil and Gas Journal*, 2020). The Marshall and Swift equipment cost index which is used in allied industries. The Process Engineering Plant Cost Index which is originated from UK covers data for the 16 OECD countries and published monthly in the (*Process Engineering*, 2020). The Chemical Engineering Plant Cost Index (CEPCI) (Mignard, 2014) is perhaps the best known and the most widely used index. In cost estimation, these indices are fed to the following equation to estimate the present cost:

$$Present\ Cost\ Estimate = Original\ Cost \times \left(\frac{Index\ Value\ at\ Present\ Time}{\substack{Index\ Value\ at\ the\ Time\ the \\ Original\ Cost\ was\ Obtained}} \right). \quad (5.1)$$

CEPCI is widely used by process engineers and is published monthly in the (*Chemical Engineering - Chemical Engineering essentials for the global chemical processing industries (CPI)*, 2020). At the end of the year, the mean of the monthly indices are calculated to construct the annual indices. Although CEPCI is constructed from US cost data, it is used worldwide due to dominancy of the US economy and acceptance of US dollar as an international currency. CEPCI has been available since 1963 and was revised several times, two of them are major revisions (1982 and 2002) (Jenkins, 2018; Vatavuk, 2002). CEPCI is a composite index which is constructed from weighed sum of normalized four sub-indices. They are *i)* equipment, *ii)* construction labor, *iii)* buildings, and *iv)* engineering and supervision. The equipment sub-index is also generated by seven different sub-indices, they are *i)* process machinery, *ii)* heat exchangers and tanks, *iii)* pumps and compressors, *iv)* pipes, valves and fittings, *v)* process instruments, *vi)* electrical equipment, *vii)* structural supports and miscellaneous (Mignard, 2014). Current formulation of CEPCI is as follows:

$$CEPCI = 0.50675E + 0.04575B + 0.1575ES + 0.290CL \tag{5.2}$$

where E, B, ES, and CL are the equipment index, buildings index, engineering and supervision index, and construction labor index, respectively (Vatavuk, 2002).

When the CEPCI's indices and sub-indices are calculated, 54 inputs are used. One of those inputs is the productivity factor which is defined as the effect of prediction of technological developments. Moreover, 41 of 54 inputs are Producer Price Indices (PPIs). US Department of Labor's Bureau of Labor Statistics (BLS) announces the PPIs monthly and the PPIs cover sectors such as agriculture, forestry, manufacturing, mining, and selected service sectors. 41 PPIs are selected from 13000 indices. These 13000 indices are generated from 100000 price quotations coming from 25000 private foundations. Furthermore, there are also 12 inputs used in the CEPCI sub-indices which are related to labor-costs. These inputs are published by the BLS as well and include changes in labor rates and special labor costs as designers and engineers etc. (Vatavuk, 2002). Due to difficulties in following and forecasting the 53 PPIs and due to missing or modified data, economists try to find indicators to estimate the value of the CEPCI. There are two different approaches. Microeconomic approach is one of them and it tries to estimate the value of the CEPCI with few BLS parameters. (Caldwell and Ortego, 1975) used five BLS parameters in order to estimate CEPCI, they are namely general purpose machinery and equipment price index, metal tanks price index, processing materials and components price index, electrical machinery and equipment price index, and one chemical engineering labor index. On the other hand, macroeconomic approach as well was used by economist, such as (Cran, 1976) and (Caldwell and Ortego, 1975). Cran (1976)uses weighted average of two general economic indicators (steel cost and labor indices) to track CEPCI, whereas Caldwell and Ortego (1975) check for linear relation between the CEPCI and price indices (the consumer and the wholesale price indices) also between the CEPCI and the Gross National Product (GNP) deflator. Although they showed the correlation among them, actual value prediction of the CEPCI was not successful. (Mignard, 2014) also tries to predict the CEPCI by using macro-economic indicators. He used yearly interest rate on US bank prime loans, and yearly price of US domestic oil to generate a composite index. The composite index was successful to predict the CEPCI data but its parameters had to be changed in some specific years. It was claimed that these changes were caused by oil shocks in the 1970s, high interest rates in the 1980s, and changes in the formulation of the CEPCI in 1982 and 2002.

5.2. Description of the Yearly Data

In the previous chapter, performance of the Chemical Activity Barometer (CAB) as a leading indicator for US economy was investigated. Comparison of the WCA of the CAB and IPI considering the turning points announced by the ACC has disclosed that the CAB was a leading indicator for the IPI as well as for the troughs announced by the ACC since 1945. In this chapter, the potential of CEPCI as a leading indicator of IPI will be studied and compared with that of the CAB using WCA. However, only the yearly data are available for CEPCI from 1950 to 2019. So as to make a healthy comparison, monthly data of the CAB and IPI are transformed to yearly data and WCA of the CAB and IPI are re-performed using this yearly data as well. Therefore all the analyses in this chapter are performed on yearly basis.

The original trending values of the CEPCI, CAB, and IPI are depicted in Figure 5.1a. It can be immediately deduced that three time series have common positive trend. However, while the CAB and IPI increase more closely with each other with time, the CEPCI notably deviate from them. It is also observed that the CAB and IPI moves correlated but it is not that much easy to bring similar comment for the CEPCI. The three time series are detrended (linear trend removal) individually and plotted in Figure 5.1b. The values above the linear trend become positive and the values below the trend become negative. This detrended figure better shows the years when the CAB and IPI move together and gives insight about the positioning of the CEPCI according to the CAB and IPI. For instance, around 1970, 1980, 2000, and 2009 there are obvious negative correlations between CEPCI and the CAB/IPI pair. Nevertheless, Figure 5.1 is not adequate to conclude on further interrelationship among the three time series. To reveal possible hidden relationships between CEPCI, CAB, and IPI, the WCA will be performed in the following sections of this chapter. Since the WCA is a binary analysis, it is not possible to analyze three time series simultaneously on one WCA image. Therefore, following sections contain WCA of binary combination of the CEPCI, CAB and IPI. Moreover, detrended series are used in the following sections. The reason is twofold: firstly, since in the Chapter 4 it was shown that detrending increases resolution of the WCA at the higher periods, and secondly, the trend of the CEPCI has completely different characteristic than trends of the CAB and IPI.

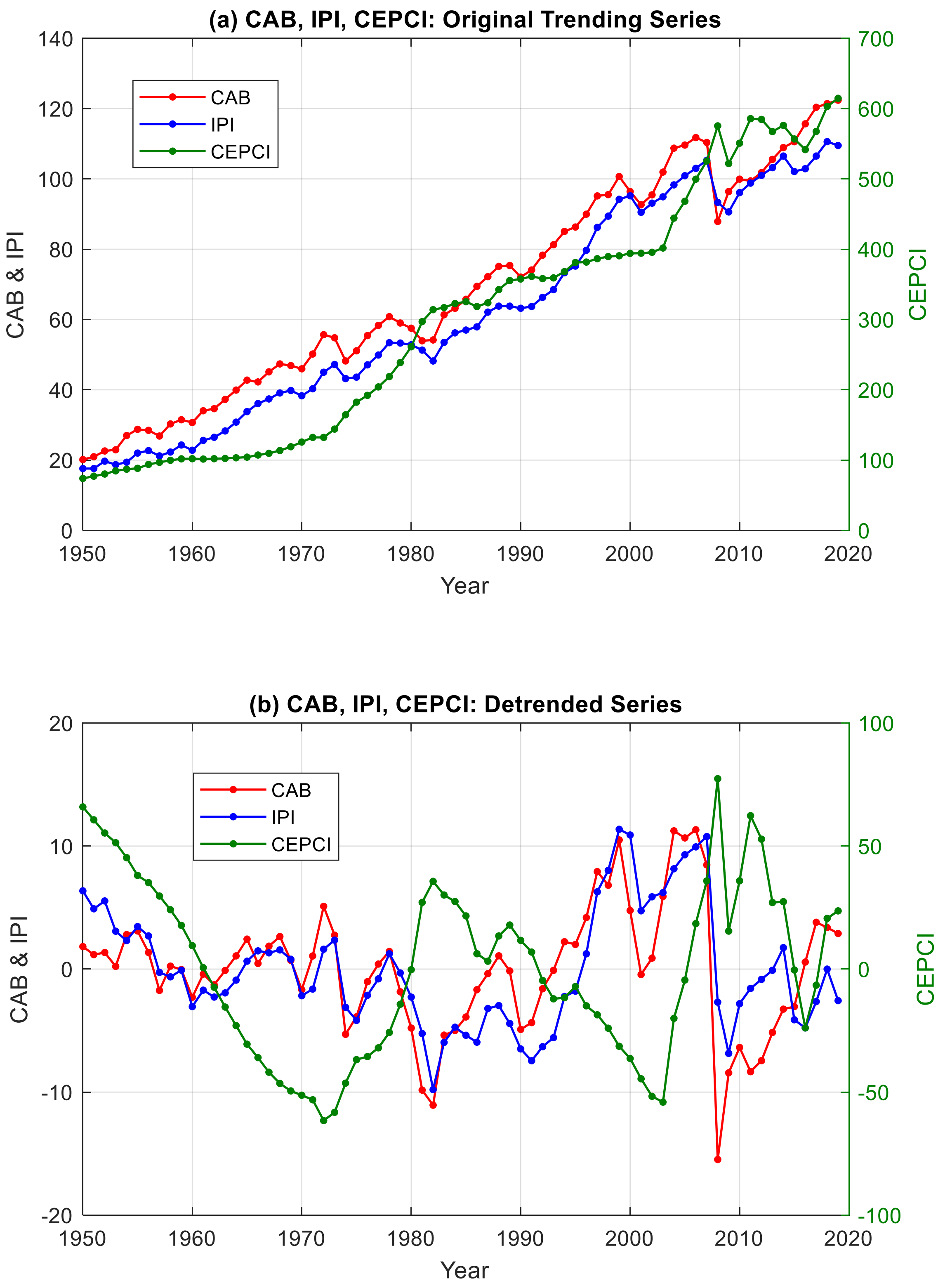

Figure 5.1 Original Trending and Detrended Yearly CEPCI, CAB and IPI Series.

5.3. WCA of the Detrended Yearly CAB and IPI Series

In Chapter 4, an extensive WCA has been executed to reveal hidden relationship between CAB and IPI. Since the recession periods of Business Cycles (BC) mostly have durations less than one year, we focused on the short-term periods on the WCA figure for the CAB and IPI. Fortunately, data collection frequency of the CAB and IPI is high enough to study such short-term BCs. On the other hand, we have only the yearly data for the CEPCI. In this section, WCA of the CAB and IPI is considered again, this time, however, with the yearly data, and the results are compared with the WCA outcomes presented in Chapter 4 so that effects of the data frequency will be also be apprehended. After this yearly version of the WCA for the CAB and IPI, the WCA for the other binary pairs (CEPCI/CAB, and CEPCI/IPI) will be performed taking data collection frequency into consideration. Table 5.1 lists the values of some of the important parameters used in this chapter for the WCA computations of the yearly CAB and IPI.

Table 5.1. Values of Some Important Parameters used in the WCA Computations.

Parameter	Explanation	Value
dt	sampling interval	1 year
DJ	number of octaves per scale	1/32
LPer	lower level of period	1 year
UPer	upper level of period	70 years
LPhaseDif	lower levels of phase-difference bands	[1.0, 3.0, 16] years
UPhaseDif	upper levels of phase-difference bands	[2.0, 8.0, 24] years
MinScale	minimum scale	1 year
MaxScale	maximum scale	70 years
Mother	mother wavelet”	Morlet
MonteCarloCount	number of surrogate sets	10
ArrowDensity	densitiy of arrow on WCA figure	[60 60]

Fıgure 5.2 contains plots of the detrended yearly CAB and IPI series, their WCA image, and average phase difference between two series over the three particular period bands (1-2, 3-8, and 16-24 year period band). WCA comprises much valuable information

on the interrelation of the two series. In order to advance without missing a point and to be companionable with real-life analysis habits of the economists, the WCA figure will be studied under the short-, medium-, and long-term perspectives.

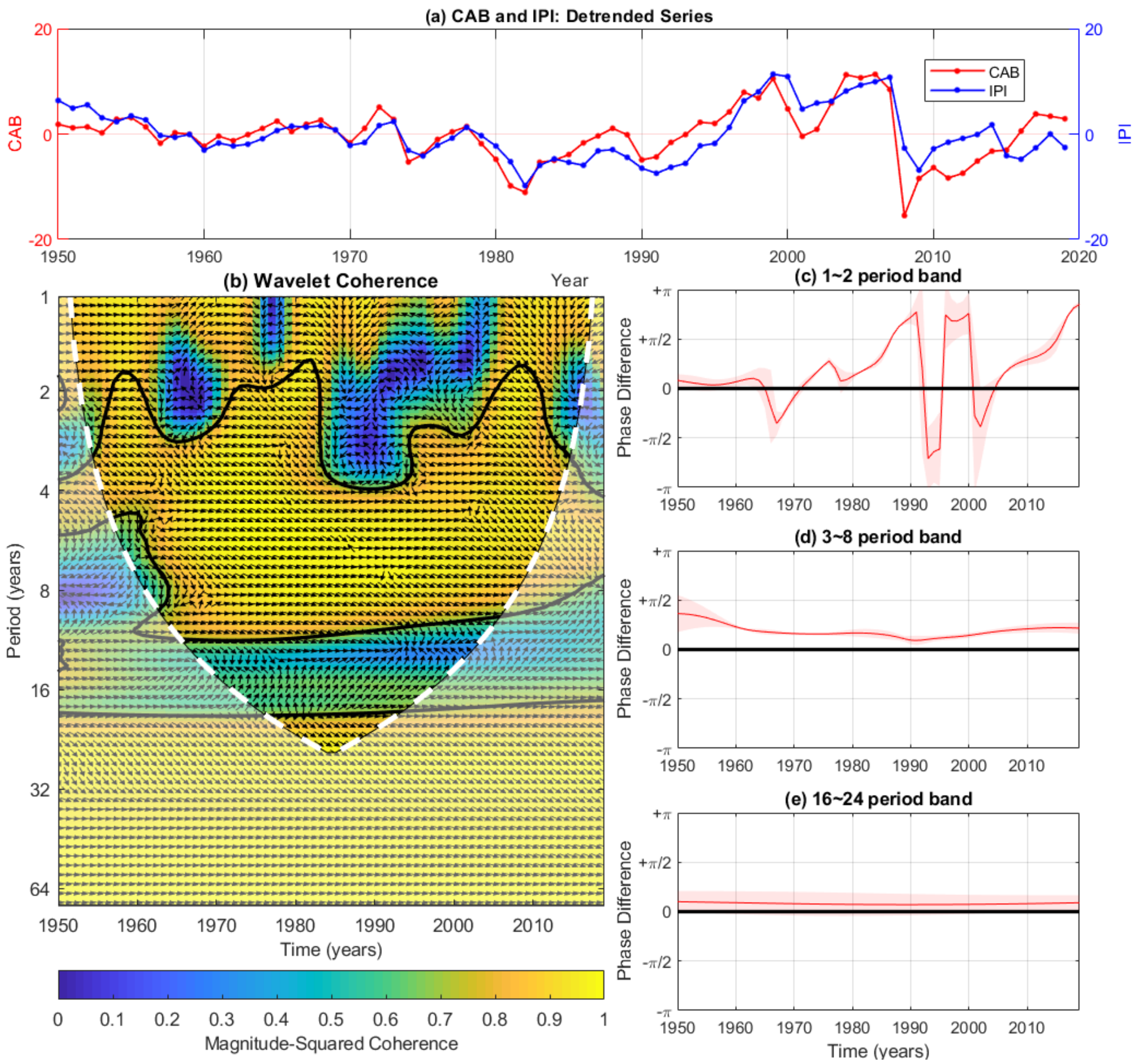

Figure 5.2. Wavelet Coherence Analysis and Phase-Difference Plots of the Detrended Yearly CAB and IPI Series.

Figure 5.3 was generated to identify more crisply the range of these short, medium, and long terms and to behold overall time-wise and frequency-wise mean of phase difference and coherency of the yearly CAB and IPI series. From Figure 5.3a, it can be deduced that average coherency between the CAB and IPI is approximately 0.85 along the timeline, which means they are highly coherent. In Chapter 4, this average coherency was approximately 0.7 (see Figure 4.8a). This difference can be the result of the fact that Figure

5.2b does not cover periods less than one year, however those lower periods had been covered in Figure 4.7b and they contained less coherent zones with respect to higher periods. On the other hand, Figure 5.3b contains critical information for WCA. The peaks in this sub-figure can be used for designation of short-, medium-, and long-term behavior. In this context, the peaks located at one and five years can be attributed to short and medium terms, while periods longer than 24 years can be attributed to long terms, as almost the same as in the Chapter 4 (see Figure 4.8b). It is hard to deduce something from Figure 5.3c (it looks like a smoothed version of the analogous figure in Chapter 4, see Figure 4.8c). Whereas, Figure 5.3d roughly shows that in (business) cycles, from the beginning to 12-year period band and between 18- and 34-year period band, the CAB leads IPI by approximately $\pi/8$ phase angle, but at the rest of the timeline the IPI leads CAB by approximately $\pi/8$ phase angle which is almost the same as in Chapter 4 (see Figure 4.8d). Nevertheless, just by looking at the mean coherency spectrum and phase-difference spectrum across time plots can be deceptive because these two dimensional averaged coherency plots omit many details. Importance of the true (un-averaged) WCA analysis and the WCA image in Figure 5.2b arises in this situation.

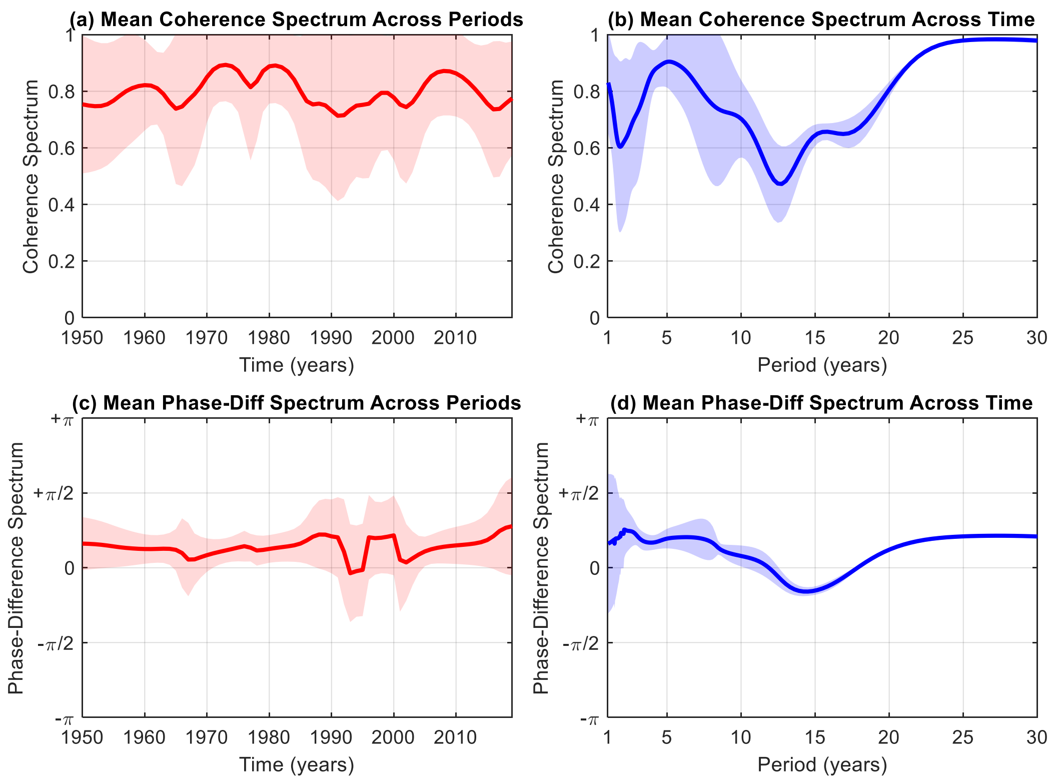

Figure 5.3. Mean Coherence and Mean Phase-Difference between the Detrended Yearly CAB and IPI Series across Time and Frequency Domains.

Now, the short-, medium-, and long-term behaviors can be analyzed using the WCA. Unlike the analysis in Chapter 4, Figure 5.3b does not comprise periods less than one year, since the data used in this chapter are yearly. However 1- to 2-year period band can give insight about short-term periods. There is an intermittent "zone of high coherency" along the time located at 1- to 2-year period band. Between 1950 and 1965, there is a coherent zone with rightward directed arrows, which means the two series are in phase (see Figure 5.2c). On the other hand, in Chapter 4 (Figure 4.7b), there is the same coherent zone located at 1- to 2-year period band between 1950 and 1965 with arrows which have the same direction, however the resolution is higher in Chapter 4. Between 1965 and 1970, there is another coherent zone located at roughly 1- to 1.5-year period band with northeastward directed arrows, which means that the IPI leads the CAB by three months (see Figure 5.2c). On the other hand, in Chapter 4 (Figure 4.7b), there is no such a coherent zone. Between 1970 and 1975, there is another coherent zone with some rightward directed arrows between 1970 and 1973, which means that the two series are in phase, and some southeastward directed arrows between 1973 and 1975, which means that the CAB leads the IPI by three months (see Figure 5.2c). There is a "no coherency zone" between 1975 and 1979 and another "high coherency zone" between 1979 and 1982 with arrows rightward directed, which means that the two series are in phase (see Figure 5.2c). On the other hand, in Chapter 4 (Figure 4.7b), there is similar coherent zone located at 1- to 2-year period band between 1972 and 1983 with arrows which have roughly the same direction, however, Figure 4.7b does not have "incoherent region " between 1975 and 1979. There is another coherent zone between 1983 and 1990 with some southwestward directed arrows between 1983 and 1985, some downward directed arrows between 1970 and 1988, and some southeastward directed arrows between 1989 and 1991, which means that the CAB leads the IPI averagely five months between 1983 and 1991 (see Figure 5.2c). On the other hand, there is no corresponding coherent zone in Figure 4.7b. Between 1991 and 2002, there is another coherent zone located at roughly 1- to 1.5-year period band with leftward directed arrows, which means two series are out-of-phase (see Figure 5.2c). On the other hand, there is no corresponding coherent zone in Figure 4.7b. There is another coherent zone between 2003 and 2005 with rightward directed arrows, which means the series are in phase. On the other hand, there is a coherent zone at similar years with similarly directed arrows in Figure 4.7b. There is another coherent zone between 2008 and 2019 with some southwestward directed arrows between 2008 and 2010, some downward directed arrows between 2010 and 2016, and some southeastward directed arrows between 2016 and 2019, which means that the CAB leads the IPI averagely five months between 2008 and 2019 (see Figure 5.2c). On the other hand, there is no corresponding coherent zone in Figure 4.7b.

Comparing the coherency and phase relations between the yearly CAB and IPI, as deduced from the short-term (1- to 2-year period band) part of the WCA and from the short-term part of the WCA figure of the monthly CAB and IPI (Chapter 4, Figure 4.7b), it is seen that they significantly differ from each other. Therefore, it can be said that the WCA at just above the data collection periods is not very reliable.

Furthermore, the interpretation of Figure 5.2b under medium-term scope (between 3- to 12-year period band) depicts that the CAB and IPI are highly coherent between 3- to 12-year periods throughout the time line, except the incoherent zone between 1950-1963 for periods between five to 11 year. A comparison of the “high coherency zone” located at the medium-term region with the “high coherency zone” located at the medium term in Figure 4.7b (monthly data) depicts that these two zones are almost the same but the one in Figure 5.2b looks like a trimmed form of the one in Figure 4.7b. Additionally, the arrows on these two zones mostly show the same direction. Hence, it can be inferred that increasing the data collection frequency does not affect high coherency zone for medium-term periods, especially periods larger than three years.

Additionally, long-term interpretation of Figure 5.2b show that, as is the case in the medium term, there is almost no difference between the high periods of Figure 5.2b and the high periods of Figure 4.7b (monthly data). There is a large “incoherent region” between 10- and 20-year periods along the time and it can be inferred that the CAB and IPI are highly coherent at the periods higher than 20 years. However, only a small part of the “high coherency region” falls in the COI. Moreover, almost all arrows in Figure 5.2b and Figure 4.7b show the same direction.

In addition, Figure 5.4 shows the image of the quantized distribution of the phase differences between the yearly CAB and IPI. Since WCA of the yearly CAB and IPI are not significant for short-term periods, it is not easy to say something for periods shorter than two years. Although it seems like the CAB leads the IPI (phase angle is between 0 to $\pi/2$, yellow regions) almost everywhere between 1- to 2-year period, between 1950 and 1960, and between 1962 and 1972, the IPI leads the CAB. Moreover, between 1986 and 2005, the two series are out-of-phase (phase angle is between $\pi/2$ to π at the red regions and phase angle is between -$\pi/2$ to -π at the blue regions) between 1- to 2-year periods. Furthermore, between 2014 and 2016, the two series are out-of-phase (phase angle is between $\pi/2$ to π at the red regions). At the rest of the figure, the CAB leads the IPI almost everywhere between 2- to 10-year period band (phase angle is between 0 to $\pi/2$, yellow regions), and at the periods larger than 20 years (phase angle is between 0 to $\pi/2$, yellow regions). On the other hand, the IPI leads the CAB between 10- to 20-year period band (phase angle is between 0 to -$\pi/2$, cyan regions) along the time. A comparison of Figure 5.4 with Figure 4.9 shows that they are almost identical at the periods greater than two years.

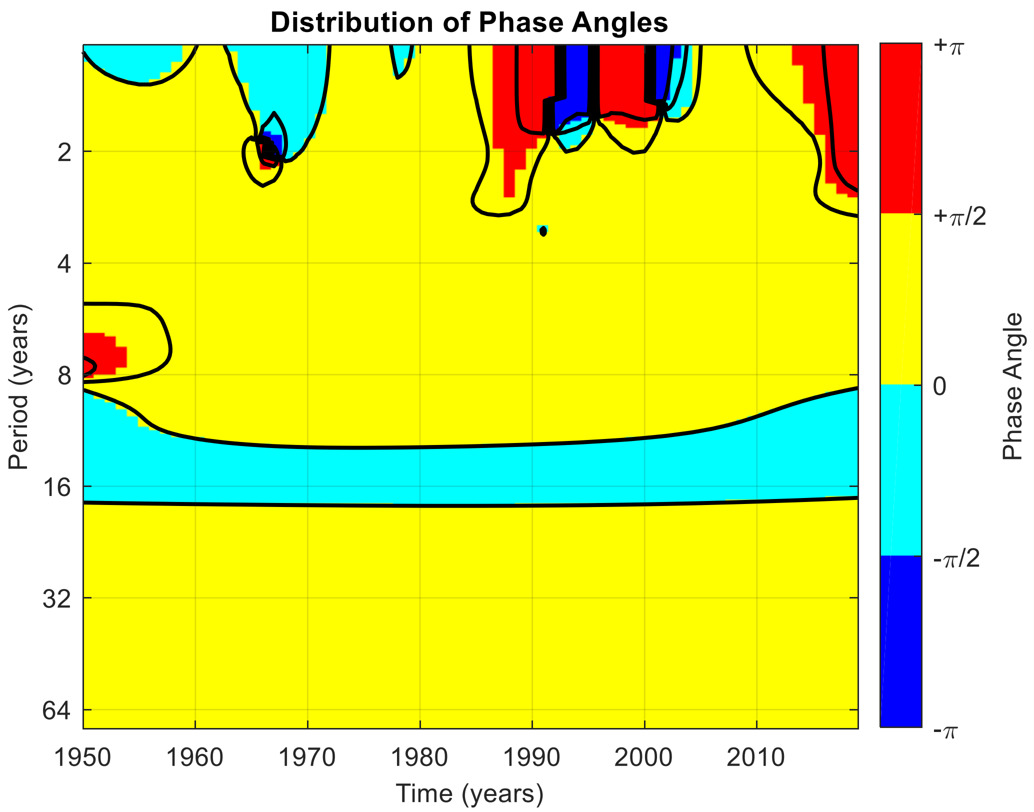

Figure 5.4. Quantized Distribution of Phase Angles between the Detrended Yearly CAB and IPI Series.

5.4. WCA of the Detrended Yearly CAB and CEPCI Series

In this section, the WCA of the detrended yearly CAB and CEPCI series will be carried out. As mentioned above (in Section 5.2), the ACC claims that the CAB is a leading indicator for the US economy and there is no doubt that the CEPCI has a strong relation with the US economy. However, unlike the CAB, the CEPCI is not constructed primarily for tracking the IPI, but it is constructed to track the plant-construction costs in the US (Vatavuk, 2002). Therefore**,** it will be interesting to analyze the interrelationships between the CAB and CEPCI via WCA. Accordingly, if the CEPCI leads the CAB, the CEPCI may be counted as a better US economy leading indicator. If not however, it will be hard to say something strong about leading indicator characteristic of the CEPCI and it requires further analyses.

Table 5.2 lists the values of some of the important parameters used in the WCA computations of the yearly CAB and CEPCI in this chapter.

Table 5.2. Values of Some Important Parameters used in the WCA Computations.

Parameter	**Explanation**	**Value**
Dt	sampling interval	1 year
DJ	number of octaves per scale	1/32
LPer	lower level of period	1 year
UPer	upper level of period	70 years
LPhaseDif	lower levels of phase-difference bands	[1.0, 3.0, 16] years
UPhaseDif	upper levels of phase-difference bands	[2.0, 8.0, 24] years
MinScale	minimum scale	1 year
MaxScale	maximum scale	70 years
Mother	mother wavelet	Morlet
MonteCarloCount	number of surrogate sets	10
ArrowDensity	densitiy of arrow on WCA figure	[60 60]

Fıgure 5.5 contains plots of the detrended yearly CAB and CEPCI series, their WCA image, and average phase difference between two series over the three particular

period bands (1-2, 3-8, and 16-24 year period bands). WCA comprises much valuable information on the interrelation of the two series. In order to advance without missing a point and to be companionable with real-life analysis habits of the economists, the WCA figure will be studied under the short-, medium-, and long-term perspectives.

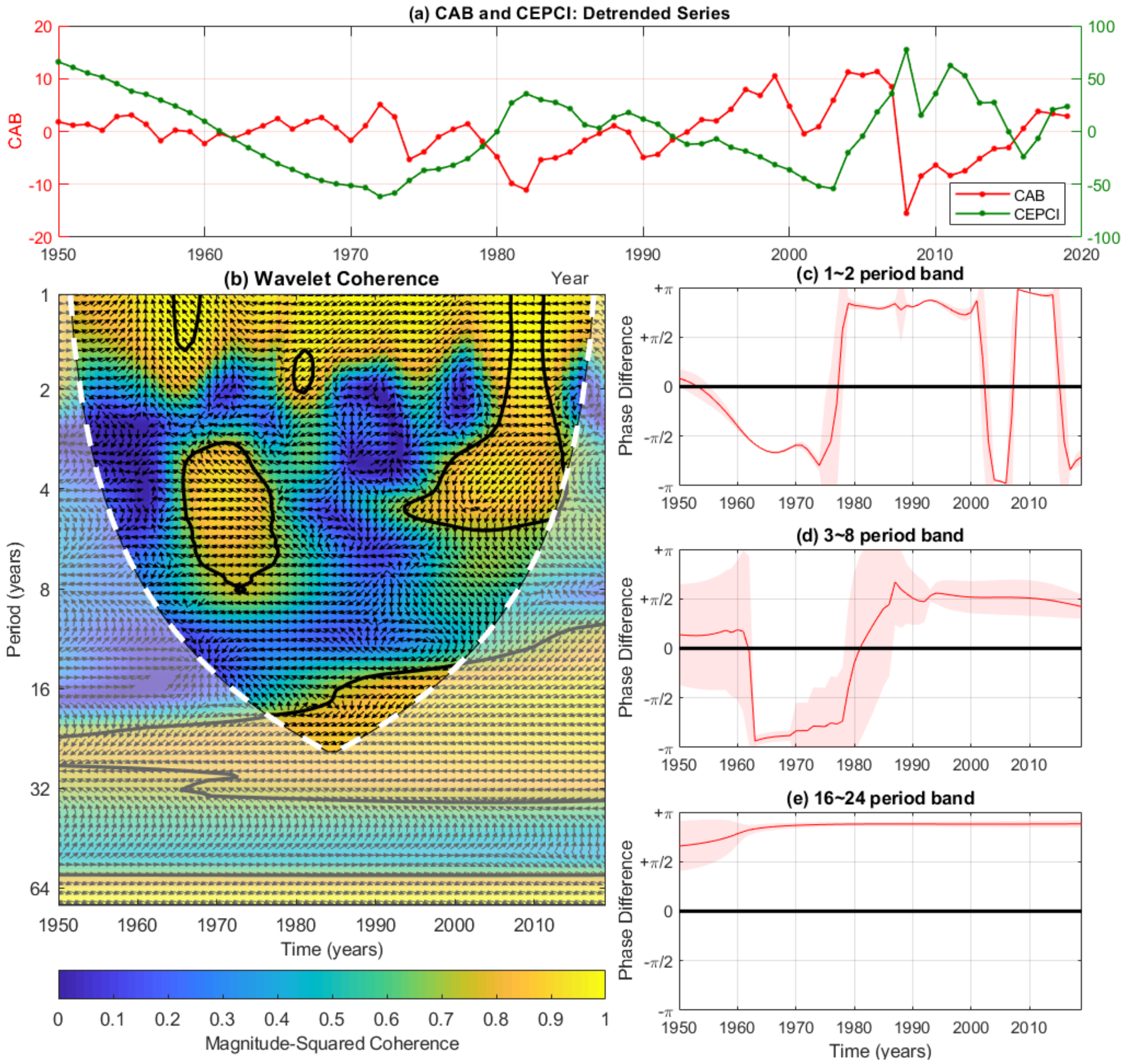

Figure 5.5. Wavelet Coherence Analysis and Phase-Difference Plots of the Detrended Yearly CAB and CEPCI Series.

Figure 5.6 was generated to identify more crisply the range of these short, medium, and long terms and to behold overall time-wise and frequency-wise mean of phase difference and coherency of the CAB and CEPCI series. From Figure 5.6a, it can be deduced that average coherency between the CAB and CEPCI does not show a constant mean value and the overall coherency can be analyzed in five parts. In the first part, the coherency varies around roughly 0.4 from 1950 to about 1962. In the second part, the coherency varies slightly above 0.6 from 1965 to early 1980. In the third part, the coherency varies around roughly 0.7 from early 1980 to early 1995. In the fourth part, the coherency varies around roughly 0.7 from mid 1995 to 2002. In the final part, the coherency increases to 0.8 from 2005 to 2012 and returns to back to roughly 0.7 from 2012 to date. On the other hand, Figure 5.6b contains critical information for the WCA. The peaks in this sub-figure can be used for the designation of short-, medium-, and long-term behavior. In this context, the peaks located at one and four years can be attributed to the short- and medium-term periods while the peak at 22 year can be attributed to the long-term period. Figure 5.6c says that the CAB and CEPCI are in phase from 1950 to about 1955, however, the CEPCI starts to lead the CAB from about 1955 to approximately 1977 by an average of $\pi/4$ phase angle. From 1977 to 2014, the CAB leads the CEPCI by slightly less than $\pi/4$ phase angle, however, roughly from 2002 to 2006, the phase angle decreases to $\pi/8$. Finally, from 2015 to date, the CAB leads the IPI by $\pi/8$ phase angle. On the other hand, Figure 5.6d roughly shows that in shorter periods from 1- to 8-year period band, the CAB leads the CEPCI with a small phase difference. However from 8- to 13-year periods, the CAB leads the CEPCI by about $\pi/8$ phase angle. From 13- to 27-year periods, the phase difference between the CAB and CEPCI keeps increasing (indicating that the CAB leads the CEPCI more and more with time). However, in Figure 5.6d, this increase suddenly ceases around 27-year period and the mean phase difference suddenly decreases to $-\pi$, indicating that beyond 27-year period the CEPCI leads the CAB. The cause of this sudden decrease may be explained by the cyclical nature of the phase angle; the phase angle completes a full tour. Nevertheless, just looking at the mean coherency spectrum and phase difference spectrum across time plots can be deceptive because these two dimensional averaged coherency plots omit many details. Importance of the true (un-averaged) WCA analysis and the WCA image in Figure 5.5b arises in this situation.

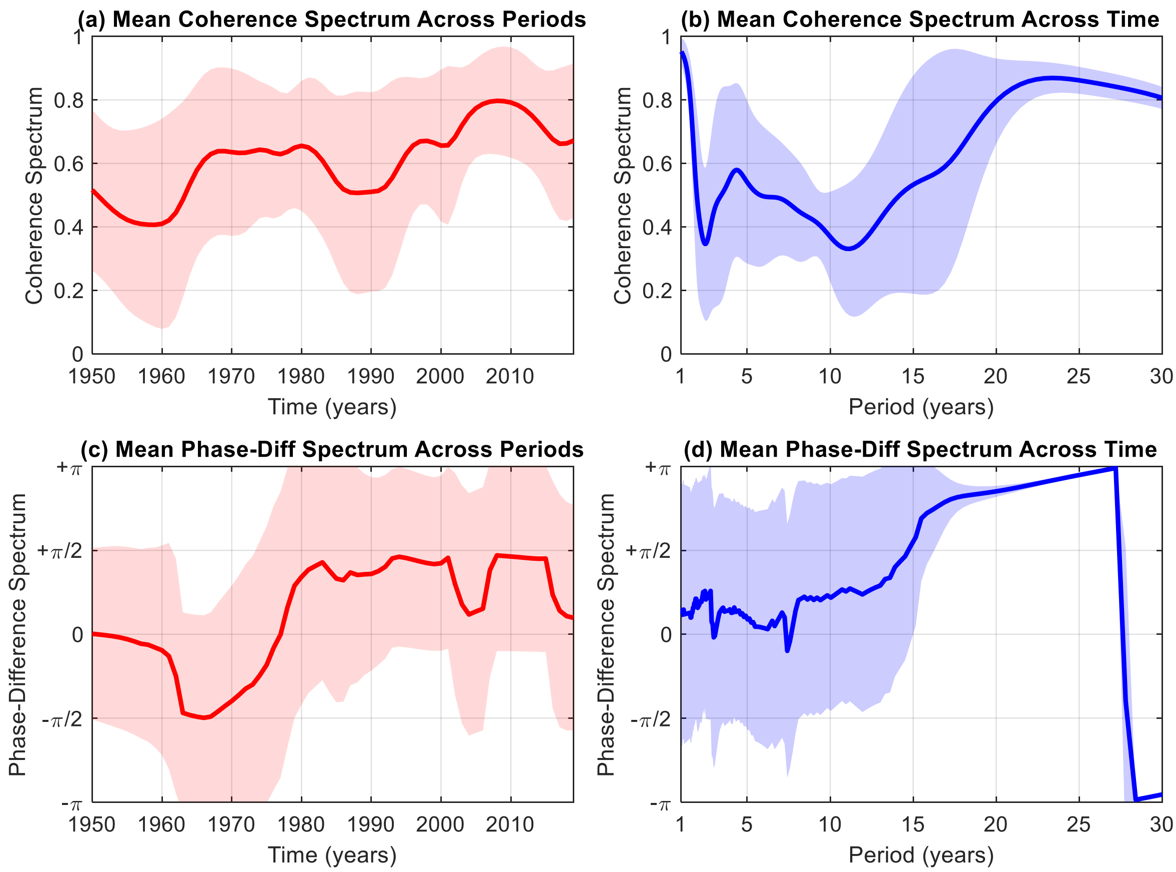

Figure 5.6. Mean Coherence and Mean Phase-Difference between the Detrended Yearly CAB and CEPCI Series across Time and Frequency Domains.

Now, the short-, medium-, and long-term behaviors can be analyzed using the WCA. In the former section (Section 5.3) it was shown that increasing data collection period from month to year has effected the short-term periods (1- to 2-year period band). Although we know that it is not statistically significant, there is a large "high coherency region" located roughly between 1- to 2-year period band along the time. Arrows on the region have different directions. The arrows from 1950 to 1955 are rightward directed, which means the two series are in phase. The arrows from 1955 to 1975 are averagely upward directed, which means that the CEPCI leads the CAB roughly by five months (the lead duration is in months since it leads about one fourth of 1.5 years). The arrows from 1975 to 1981 are leftward directed, which means the two series are out-of-phase. The arrows from 1981 to 2002 are averagely southwestward directed, which means the CAB leads the CEPCI roughly by seven months (the lead duration is in months since it leads about one third of 1.5 years), or the two series are out-of-phase and the CEPCI leads the CAB for three months (the lead duration is in months since it leads about one sixth of 1.5

years). The arrows located from 2002 to 2017 are leftward directed, which means that the two series are out-of-phase. Finally, the arrows from 2017 to date are northwestward directed, which means that the CEPCI leads the CAB by seven months (the lead duration is in months since it leads about one third of 1.5 years), or the two series are out-of-phase and the CAB leads the CEPCI by three months (the lead duration is in months since it leads about one sixth of 1.5 years).

Furthermore, the interpretation of Figure 5.5b under medium-term scope (between 3- to 12-year period band) depicts that the CAB and CEPCI are highly coherent for two specific zones. The first "high coherency zone" is located between 3- to 8-year period band in between 1966 and mid of 1979. The reason of this zone can be the oil shock of 1970s which affected both the CAB and CEPCI. The arrows on the zone can be investigated in four different groups. The first group is the arrows located between 3- to 4-year period band. Those arrows are northwestward directed, which means that the CEPCI leads the CAB averagely by 15 months (or the two series are out-of-phase and the CAB leads the CEPCI by six months. The rationality behind these leads in month units can be explained as follows. 3.5 years is the average for the 3- to 4-year period band, and this corresponds to 42 months, which is the one whole tour of the phase angle. The angles in this zone are about 145 degrees. Therefore, since 145/360 is about 3/8, the 3/8th of 42 months corresponds to about 15 months.

The second group is the arrows located between 4- to 6-year period band. Those arrows are leftward directed until 1973, which means that two series are out-of-phase. The third group is the arrows located between 4- to 6-year period band from 1973 to mid 1979. Those arrows are northwestward directed, which means that the CEPCI leads the CAB averagely by 20 months (or, the two series are out-of-phase and the CAB leads the CEPCI by 10 months). The fourth group is the arrows located between 6- to 8-year period band. Those arrows are leftward directed along the zone, which means that two series are out-of-phase. The second "high coherency zone" is located between 3- to 8-year period band between 1993 and to date (note that from 2014 to 2019 and from 5.5- to 8-year period band the color of the zone becomes green, which means there is a decrease in coherency between two time series) The reason behind this zone can be the change in formulation of the CEPCI that took place in 2002. On the other hand, the arrows on this zone show two different characteristics as well and they can be investigated in two different groups. The first group of arrows is between 3- to 5-year period band. Those arrows are southwestward directed, which means that the CAB leads the CEPCI averagely by 15 months (or, the two series are out-of-phase and the CEPCI leads the CAB by six months). The second group of arrows between 5- to 8-year period band. Those arrows are downward directed, which means that the CAB leads the CEPCI by about 1.5 year.

Additionally, long-term interpretation of Figure 5.5b shows that there is a large "high coherency region" between roughly 16- and 32-year periods along the time. However, only small part of the "high coherency region" is inside the COI. On the other hand, the arrows on this zone show two different characteristics as well and they can be investigated in two different groups. The first group of arrows is between 16- to 21-year period band. Those arrows are southwestward directed, which means that the CAB leads the CEPCI by about 12 years (or, the two series are out-of-phase and the CEPCI leads the CAB by 6 about years). The second group arrows are between 21- to 32-year period band. Those arrows are leftward directed, which means that the two series are out-of-phase.

In addition, Figure 5.7 shows the image of the quantized distribution of the phase differences between the yearly CAB and CEPCI. Although there is no dominant color between 1- to 16-year period band from 1950 to early 1960s, there is a blue-colored region between 1- to 16-year period band from early 1960s to roughly 1980 (phase angle is between $-\pi/2$ to $-\pi$ at the blue regions). Moreover, there is the red colored region between 1- to 16-year period band roughly from 1980 to 2019 (phase angle is between $\pi/2$ to π at the red regions). However, there are cyan- and blue-colored zones from 1983 to 1993 between 2- to 4-year period band in which the CEPCI leads the CAB, a blue-colored zone from 2001 to 2007 between 1- to 2.5-year period band in which the phase angle is between $-\pi/2$ to $-\pi$, another blue colored zone from 2014 to 2019 between 1- to 2.5-year period band in which the phase angle is between $-\pi/2$ to $-\pi$, and, finally, a yellow-colored zone from 1993 to 2019 between 5- to 10-year period band in which the phase angle is between 0 to $\pi/2$. The yellow-colored zone can be critical because the coherency of this region is significant (see Figure 5.5b) and apparently there the CAB leads the CEPCI. Finally, there are a red zone throughout the time line located at 16- to 28-year period band, a blue zone throughout the time line located at 28- to 44-year period band, a cyan zone throughout the time line located at 44- to 57-year period band, and, lastly, a yellow zone throughout the time line located at 57- to 72-year period band.

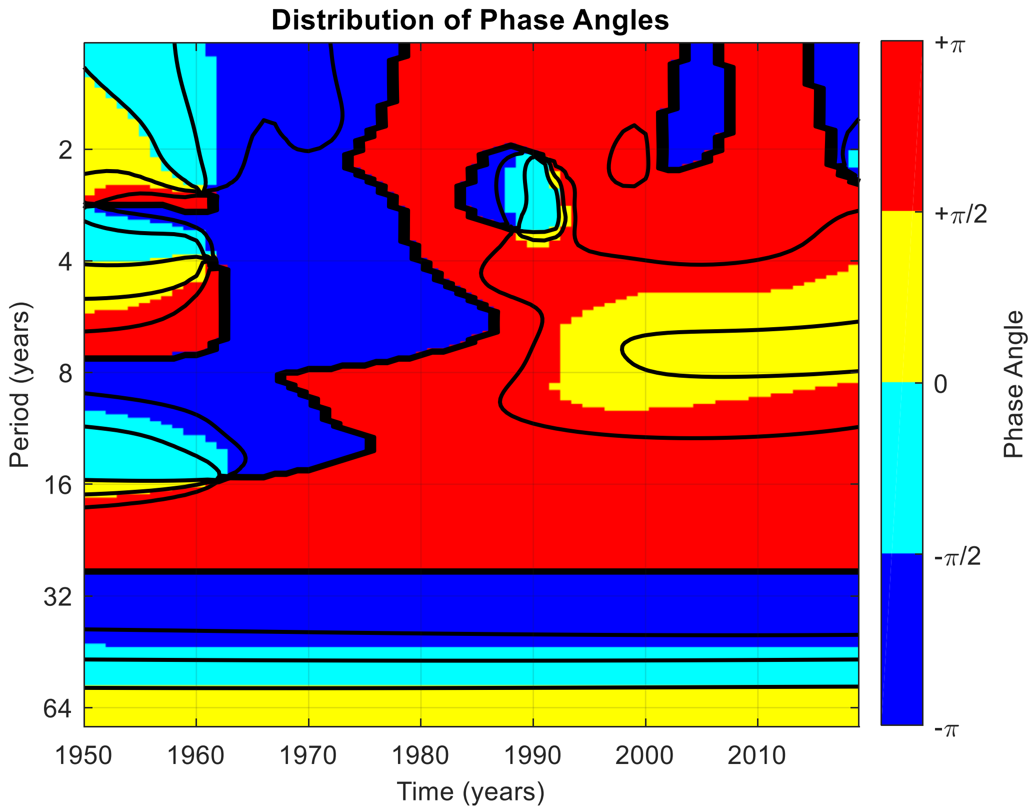

Figure 5.7. Quantized Distribution of Phase Angles between the Detrended Yearly CAB and CEPCI Series.

Consequently, it is not possible to say something on whether the CEPCI is a leading indicator of the US economy or not, for the short-term (less than two years). Similarly, it is not possible to draw a conclusion for the medium-term (between 3- to 12-year), for years before 1993. On the other, from 1993 to date there becomes a significant coherency between the two time series and from the analysis it seems that the CAB leads the CEPCI at this medium-term. Hence, there is no strong evidence to call CEPCI as a leading indicator in the medium-term. Finally, there is a very significant coherency for the long-term periods between the two time series. In the long-term periods, the two time series are mostly out-of-phase. Therefore it is not possible to make decision about the leading-indicator potential of the CEPCI.

5.5. WCA of the Detrended Yearly IPI and CEPCI Series

In this section, the WCA of the detrended yearly IPI and CEPCI series will be considered. In Section 5.4, it was questioned whether the CEPCI leads the CAB or not. Since the data collection frequency is low, no conculusive comment had been made for the short-term (less than two years) and deductions, in general, were not in the direction of that the CEPCI is a better leading indicator for the US economy than the CAB for larger periods (longer than three years). Consequently, interrelation between the IPI and CEPCI gains importance. It is expected that WCA of the IPI and CEPCI will give an idea on whether the CEPCI is a leading indicator for the US economy or not. Table 5.3 lists the values of some of the important parameters used in the WCA computations of the yearly IPI and CEPCI in this chapter.

Table 5.3. Values of Some Important Parameters used in the WCA Computations.

Parameter	Explanation	Value
dt	sampling interval	1 year
DJ	number of octaves per scale	1/32
LPer	lower level of period	1 year
UPer	upper level of period	70 years
LPhaseDif	lower levels of phase-difference bands	[1.0, 3.0, 16] years
UPhaseDif	upper levels of phase-difference bands	[2.0, 8.0, 24] years
MinScale	minimum scale	1 year
MaxScale	maximum scale	70 years
Mother	mother wavelet	Morlet
MonteCarloCount	number of surrogate sets	10
ArrowDensity	densitiy of arrow on WCA figure	[60 60]

Fıgure 5.8 contains plots of the detrended yearly IPI and CEPCI series, their WCA image, and average phase difference between two series over the three particular period bands (1-2, 3-8, and 16-24 year period bands). WCA comprises much valuable information on the interrelation of the two series. In order to advance without missing a point and to be companionable with real-life analysis habits of the economists, the WCA figure will be studied under the short-, medium-, and long-term perspectives.

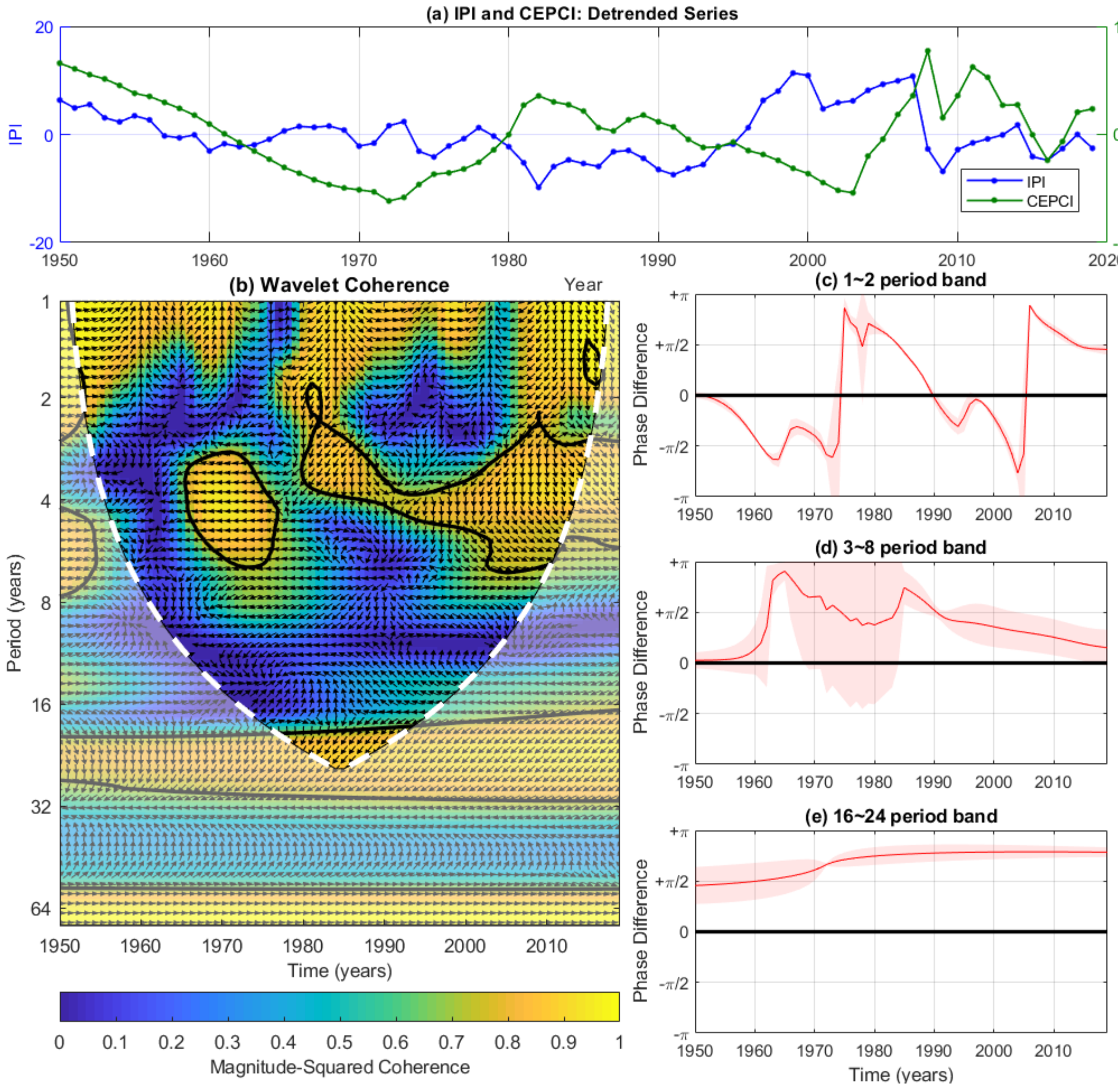

Figure 5.8. Wavelet Coherence Analysis and Phase-Difference Plots of the Detrended Yearly IPI and CEPCI Series.

Figure 5.9 was generated to identify more crisply the range of these short, medium, and long terms and to behold overall time-wise and frequency-wise mean of phase difference and coherency of the IPI and CEPCI series. From Figure 5.9a, it can be deduced that average coherency between the IPI and CEPCI does not varies around a constant mean value and the overall coherency can be divided into four parts. In the first part, the coherency is around 0.7 at 1950 and it decreases to about 0.4 towards the early 1960s. In the second part, coherency varies roughly between 0.5 and 0.6 from mid 1960s to 2005. In the third part, coherency increases from 0.6 to 0.7 from roughly 2005 to 2008. In the final part, the coherency varies around 0.7 from 2009 to date. On the other hand, Figure 5.9b contains critical information for the WCA. The peaks in this sub-figure can be used for the designation of short-, medium-, and long-term behaviors. In this context, the peaks located at one year and four year can be attributed to short and medium terms while periods longer than 22 years can be attributed to long terms. Figure 5.9c says that the IPI and CEPCI are in phase from 1950 to early 1960s, however the IPI starts to lead the CEPCI from early of 1960s to date averagely by a phase angle of $\pi/4$. On the other hand, Figure 5.9d roughly shows that, in shorter periods from 1- to 4-year period band, the phase angle between IPI and CEPCI increases from 0 to $\pi/2$. From 4- to 11-year period band, the IPI leads the CEPCI by an average of $\pi/2$ phase angle. However, from 4- to 7-year period band, the phase angle decreases to $\pi/4$. From 11- to 16-year period, the CEPCI leads the IPI, increasingly. However, in Figure 5.6d, the increase was until 22-year period and there was a sudden drop to about $\pi/4$ phase angle afterwards. Finally, from 16- to 30-year period, the IPI leads the CEPCI by $3\pi/4$ phase angle (or, the two series are out-of-phase and the CEPCI leads the IPI by $\pi/4$ phase angle). Nevertheless, just by looking at the mean coherency spectrum and phase difference spectrum across time plots can be deceptive because these averaged plots hinder the details of coherency phenomenon. Importance of the true (un-averaged) WCA analysis and the WCA image in Figure 5.8b arises in this situation.

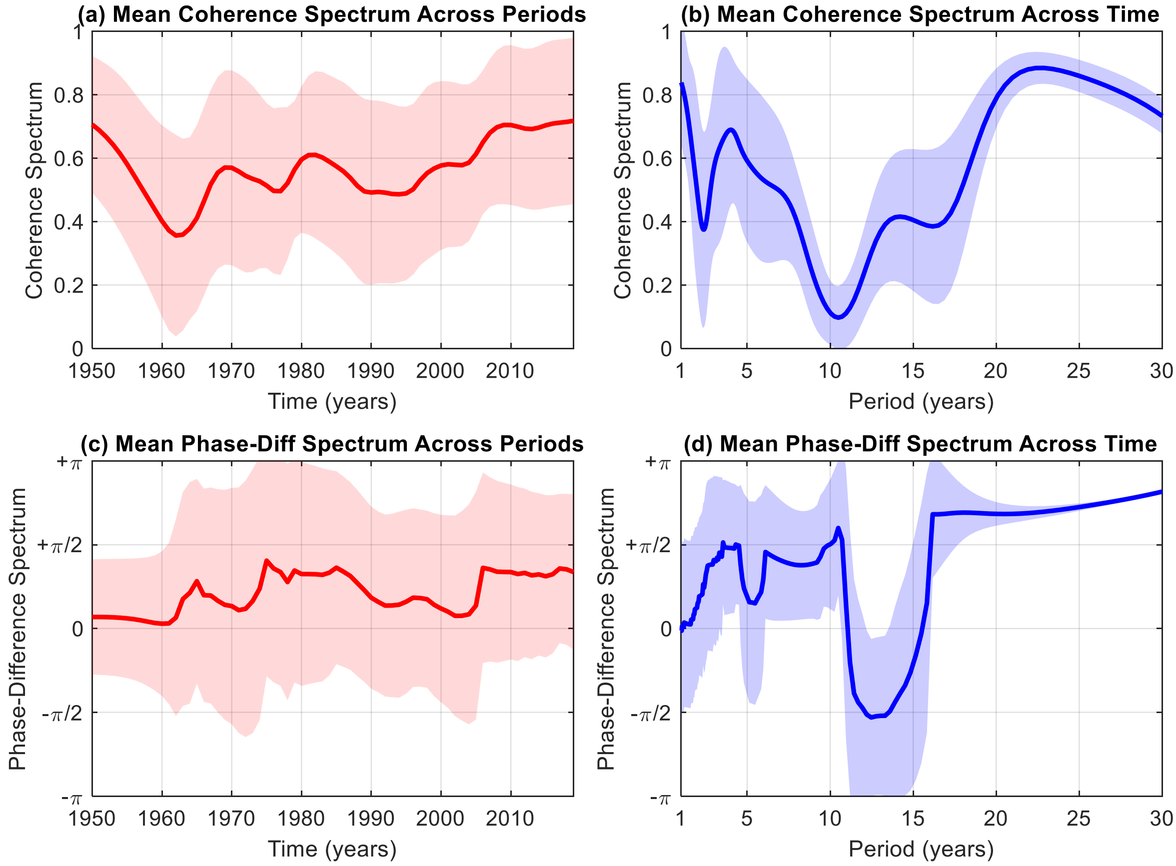

Figure 5.9. Mean Coherence and Mean Phase-Difference between the Detrended Yearly IPI and CEPCI Series across Time and Frequency Domains.

Now, the short-, medium-, and long-term behaviors can be analyzed using the WCA. In Section 5.3 it had been shown that increasing the data collection frequency from month to year had effected the short-term periods (1- to 2-year period band). Although we know that it is not statistically significant, in Figure 5.8d there is a large "high coherency region" located roughly between 1- to 2-year period band along the time. This region is interrupted between 1976 and 1980 by an "incoherent region". Arrows on the region have different directions. The arrows from 1950 to 1955 on this region are rightward directed, which means the two series are in phase. The arrows located from 1955 to 1975 are averagely upward directed, which means that the CEPCI leads the IPI roughly by five months. The arrows located from 1973 to 1976 are leftward directed, which means the two series are out-of-phase. The arrows located from 1980 to 1989 are averagely downward directed, which means the IPI leads the CEPCI roughly by five months. The arrows from 1989 to 1994 on the region are rightward directed, which means the two series are in phase. The arrows located from 1994 to 1997 on the region are averagely northeastward directed, which means the CEPCI leads the IPI roughly by three months. The arrows from 1997 to 2001 on the region are rightward directed, which means the two series are in phase. The arrows from 2001 to 2005 on the region are upward directed, which means the CEPCI leads the IPI roughly by five months. The arrows located from 2005 to 2008 are leftward directed, which means the two series are out-of-phase. From 2008 on, the arrows are downward directed, which means the IPI leads the CEPCI roughly by five months. A comparing short-term periods (1- to 2-year period band) of Figure 5.5b with Figure 5.8b portrays that the short-term interrelation between CAB and CEPCI, and between IPI and CEPCI have dissimilarities, especially after 1980.

Furthermore, the interpretation of Figure 5.8b under medium-term scope (between 3- to 12-year period band) depicts that the IPI and CEPCI are highly coherent for four specific regions. The first "high coherency zone" is located between 4- to 8-year period band in between 1950 and 1956. Those arrows on the region are averagely rightward directed, which means that two series are in phase. The second "high coherency zone" is located between 3- to 8-year period band in between 1965 and mid 1978. The reason behind this zone can be the oil shock of 1970s which affected both the IPI and the CEPCI. The arrows on this zone are leftward directed, which means that the two series are out-of-phase. The third "high coherency zone" is located between 2- to 4-year period band. The reason behind this zone can be the occurrence of very high interest rates in 1980s which affected both the IPI and the CEPCI. The arrows on this zone are southwestward directed along the zone, which means that the IPI leads the CEPCI by roughly 15 months (or, the two series are out-of-phase and the CEPCI leads the IPI by six months). The fourth "high coherency zone is located between 3- to 8-year period band from 1993 to date. The reason behind this zone can be the change in the formulation of CEPCI in 2002. On the other hand, arrows on the zone show two different characteristics as well and they can be investigated in two different groups. The first group of arrows is located between 3- to 5-year period band. Those arrows are downward directed, which means that the IPI leads the CEPCI roughly by one year. The second group of arrows is located between 5- to 8-year period band. Those arrows are southeastward directed, which means that the IPI leads the CEPCI averagely by nine months. A comparison of the medium-term periods of Figure 5.5b with Figure 5.8b depicts that the IPI and CEPCI pair have more coherent regions than the CAB and CEPCI pair, at medium-term periods. Additionally, the phase difference between IPI and CEPCI is roughly $\pi/8$ degree (the shifted version of the phase difference between CAB and CEPCI), at medium-term periods. The reason of this shift is the $\pi/8$ phase angle between the CAB and IPI at medium-term periods (see Figure 4.7e).

Additionally, long-term interpretation of Figure 5.8b shows that there is a large “high coherency region” between roughly 16- and 32-year periods along the time. However, only small part of the “high coherency region” falls into the COI. The arrows located on this region are southwestward directed, which means that the IPI leads the CEPCI by an average of 16 years (or, the two series are out-of-phase and the CEPCI leads the IPI by 8 years). A comparing of the long-term periods of Figure 5.5b with Figure 5.8b indicates that the CAB and CEPCI have slightly more coherent region than the IPI and CEPCI at long-term periods, and, between 16- and 21-year period band, the phase relationship is different. The CAB and CEPCI pair has more coherent regions than the IPI and CEPCI pair, at long-term periods.

In addition, Figure 5.10 shows the image of the quantized distribution of the phase differences between the yearly IPI and CEPCI. Since the phase distribution between two series is too complex, especially for periods less than four years or so, the detailed interpretation of Figure 5.10 will not be undertaken. However, in general, at medium-term periods, the yellow-colored region (phase angle is between 0 to $\pi/2$ at the yellow regions) is dominant from 1950 to early 1960. From early of 1960 to 1990, the red-colored region (phase angle is between $\pi/2$ to π at the red regions) is dominant. Finally, from 1990 to date, the yellow-colored region is dominant again. Hence, it can nearly be said that the IPI leads the CEPCI at medium-term periods. However, between 10- and 16-year periods, the CEPCI leads the IPI. From 10- to roughly 32-year period band, there is a solid red region, which means the IPI leads the CEPCI in those periods. From 32-year period to higher periods there are the blue, cyan and yellow regions in succession, which means that the phase relationship between the IPI and CEPCI alternates at higher periods.

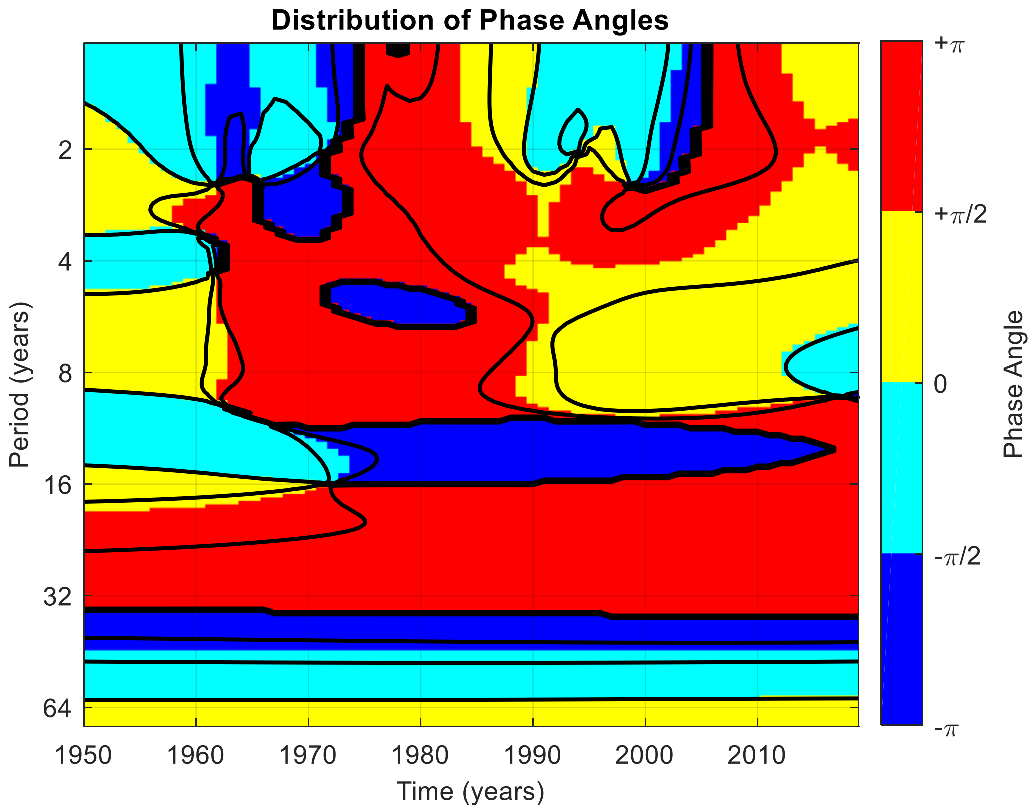

Figure 5.10. Quantized Distribution of Phase Angles between the Detrended Yearly IPI and CEPCI Series.

Consequently, it is again not possible indeed to say something about the performance of the CEPCI as a leading indicator for the US economy for the short-terms (less than two years). Since there is more coherent region in the medium-term periods (between 3- to 12-year) on the WCA figure of the IPI and CEPCI compared to that on the WCA figure of the CAB and CEPCI, it is more possible to draw a conclusion for the medium-term. In the medium-term, it can be said that the IPI leads the CEPCI, in other words, the CEPCI is not a leading indicator of the US economy for the medium-term periods. Finally, there is a very significant coherency for the long-term periods between the two time series. In the long-term periods, the two time series are, most of the time, out-of-phase. Therefore it is not possible to make decision about the leading-indicator characteristics of the CEPCI.

5.6. Summary on the Performance of CEPCI as a Leading Indicator for the US Economy

CEPCI is the most widely used cost index in chemical engineering world. It is a composite index and contains many US economy-related parameters, and thus, it was presumed to be good candidate for being a leading indicator of the US economy. This chapter has shed a light on the CEPCI’s potential as a leading indicator.

Effects of the data frequency (monthly versus yearly) on the WCA was a key element. This chapter begun with a comparison of the WCAs of the monthly and yearly data of the CAB and IPI. The results show that, data frequency has significant effect on the short-term periods, especially for periods close to the data frequency. For our case, the WCA results for the periods less than two years are considered as questionable.

Furthermore, the ACC claims that the CAB is a good leading indicator for the US economy. Therefore, it was checked whether the CEPCI leads the CAB or not. The motivation behind this analysis was simple. Since the CAB is a leading indicator of the IPI, it was thought that if the CEPCI leaded the CAB, naturally the CEPCI would have been considered as a better leading indicator of the IPI (actually a leading indicator of the CAB as well). Unfortunately, there is no evidence to show that the CEPCI leads the CAB in Figure 5.5b at periods larger than two years and it is not possible to securely comment for periods less than two years due to insufficient data frequency. On the other hand, the CEPCI may still be considered as a leading indicator for the IPI (it can be a leading indicator which has a performance worse than the CAB).

Lastly, so as to test whether the CEPCI is a leading indicator for the IPI or not, the WCA of the IPI and the CEPCI has beenexecuted (Figure 5.8b). It is clearly seen that the IPI leads the CEPCI at periods larger than two years. Since, we can not say anything significant for the shorter periods, it can be concluded that the CEPCI is not a leading indicator for the IPI and thus for the US economy for periods larger than two years.

6. APLICATION OF WCA TO FAULT DETECTION

With the developing technology, plant operations have become more complex than ever. However, the sophisticated plant operations stimulate undesirable process events and according to Venkatasubramanian et al. (2003) these events end up with casualty of 20 billion dollars in US petrochemical industry annually. Due to these losses, attention of researchers and practitioners turned into the finding a solution to minimize the losses caused by abnormal evets. The Process Fault Detection and Diagnosis (FDD) has been firstly conceptualized in 1970s and, Bread and Jones filter is firstly used in fault detection (Ding, 2008). Although the basic elements of process control (PID controllers, MPC controllers etc.) keep the process as much as at optimum by eliminating disturbances, they fail to cope with changes occurred during the course of the technological adaption and some insidious process changes which are called “faults”. The major faults may be counted as process drifts (e.g., due to catalyst deactivation), stochastic changes (e.g., due to ambient temperature changes), measurement problems (e.g., due to biased sensors), and actuator problems (e.g., due to valve sticking). These faults can cause economic, environmental and safety drawbacks. On the other hand, there are still needs for human operators for mostly manual checking in order to detect and diagnose faults. Because of range of failures and excessive number of variables generated from highly integrated processes, human operators are likely to fail to detect all faults. As reported by Venkatasubramanian et al. (2003) 70% of industrial accidents are triggered by human mistakes.

Process Monitoring (PM) methods have been introduced in order to eliminate human effects and improve fault detection tasks. PM consists of four procedures: fault detection, fault identification, fault diagnosis, and process recovery. The first procedure is concerned with the detection of faults. The second is oriented with the identification of the variables which are likely to be the cause of fault. The third procedure is concerned with the diagnosis of the causes underlying a fault. Finally, the last procedure focuses on the recovery of the process from faulty operation to normal operation.

PM may be approached from several dimensions ranging from statistics, pattern recognition and classification, information theory, and system theory (Chiang et al., 2001). The measurements reflect the states of the process and PM supports operators and engineers to unveil helpful information obtained from large process measurements. Process operators or engineers follow the process using PM techniques and can intervene with the process if necessary. Different sources give different names but Chiang et al. (2001) classifies the PM techniques as “data-driven” and “analytical”.

Data-driven techniques are based on process history data. Therefore, quantity and quality of the process data are critical for a data-driven model. Since a complex process generates very large data, data-driven techniques may become very useful due to possibility for dimension reduction. On the other hand, inadequate and untrustworthy measurements can influence the data-driven techniques directly and adversely. Data-driven techniques can be divided into two groups which are “qualitative” and “quantitative”. Moreover, quantitative methods can be classified as “statistical” or “non-statistical”. While a neural network is an example for non-statistical quantitative data-driven technique, the Principal Component Analysis is an example for statistical quantitative data-driven technique.

Analytical techniques mostly utilize the first-principle mathematical models. Since the analytical techniques rely on physical considerations, it can represent the reality much better than the data-driven model. However, in order to apply an analytical technique successfully, a system which has sufficient data collection ability (i.e., sufficient number of sensors and indicators) is needed. Therefore, analytical techniques are mostly used in small systems which can be easily followed. Diagnostic observers for dynamic systems, parameter estimation, and Kalman filtering are among the mostly used strategies for fault detection and isolation whose working principal depends on a priori knowledge.

According to Venkatasubramanian et al. (2003), there is no perfect technique which successfully diagnoses all faults. It sounds fair because PM models are mostly developed to detect some particular faults. Therefore such PM models are highly biased and they are likely to fail to detect faults other than they are modeled and trained for. In order to benchmark alternative strategies, Venkatasubramanian et al. (2003) suggest 10 prominent features that a successful FDD technique should possess. Some of the important ones that are also relevant to this thesis work are as follows: *i)* Quick fault detection and diagnosis ability for rapid response to malfunctions, *ii)* Fault isolation ability to discriminate known faults from unknown ones, *iii)* Fault explanation ability to interpret root causes of the fault and how the fault spreads, and *iv)* Simplicity to implement in real world.

On the other hand, there are also signal-processing based fault diagnosis techniques. It is believed that signals carry characteristics of the malfunction and with the correct signal-processing algorithm the fault can be diagnosed (Ding, 2008). Typically, signal-processing based fault-diagnosis techniques are performed for steady state system and it is expected to define deviation from the steady state as faults.

Since the Wavelet Coherence Analysis (WCA) is successful in both time and frequency domains, it is worthy to test the usability of the WCA in FDD tasks. As a matter of fact, in Chapter 3, while the features of WCA have been tested, a change-point detection related problem has already been studied. Since a FDD problem is also a change-point detection problem, Chapter 3 actually contains a FDD application of the WCA. Therefore, comparison of Eq. 3.1 and 3.2 with Figure 3.1 and 3.6 is a good point to start assessing the potential of WCA as a FDD tool. In Eq. 3.2 there was a sudden change after the 25th year. On the other hand, Eq. 3.1 had no change along the time line. Therefore, if Eq. 3.1 is assumed as reference time series (normal, unfaulty, operating template), any deviation from this template can be attributed as a fault occurring in due to Eq. 3.2. In Figure 3.1, the instantaneous change occurring at 25th year had been caught for this simple case. In Figure 3.6b, cycles and the changes in these cycles had been shown. If it is assumed that Eq. 3.2 corresponds to operation without fault until 25th year, the change in the Eq. 3.2 at the 25th year is detected in two ways; as an alteration in the coherency level and as a shift in the phase relationship between two series (changes in direction of the arrows on the coherent zones). Figure 3.6b explicitly shows that there is a discontinuity around 25th year that matches with the position at which the fault was introduced through Eq. 3.2. Moreover, at the 25th year, the directions of the arrows begin to change, i.e. the phase relationship between the reference time series and faulty time series changes and this change is permanent because the fault persists thereafter to the end of the series. Thus, the phase-difference arrows can be used to identify hidden phase-shift faults as well as to assess whether the effect of the fault persists or not.

6.1. Definition of the Synthetic Time Series

For a preliminary exhibition of the aptitudes of WCA in the field of FDD, a modified version of the synthetic data generating model for the Swiss-Roll Data Set is used (Musulin, 2014). Firstly, the original series $x_1(t)$ and $x_2(t)$ are defined as follows for the normal (unfaulty) operation:

$$x_1(t) = \frac{\mathrm{t}\cos(\mathrm{t})}{5} \tag{6.1}$$

$$x_2(t) = \frac{\mathrm{t}\sin(\mathrm{t})}{5} \tag{6.2}$$

where,

$$t = \frac{3\pi}{2}\left(1 + 2\in(i)\right), \qquad 1 < i \leq 500 \tag{6.3}$$

and where $\in$ is the disturbance represented by uniform random numbers U(0,1) of dimension 500 (thus, the dimension of t is 500 as well). $x_1(t)$ is depicted in Figure 6.1a and $x_2(t)$ is depicted in Figure 6.1b.

For the first faulty data set, the following two different step faults are replaced with the normal operation data, as follows:

$$x_{1_{f1}}(t) = \frac{\mathrm{t}\cos(\mathrm{t} - 0.5)}{5} \qquad \begin{array}{l} \text{for } 200 < i \leq 500, \\ \text{otherwise } x_{1_{f1}}(t) = x_1(t) \end{array} \tag{6.4}$$

$$x_{2_{f1}}(t) = \frac{\mathrm{t}\sin(\mathrm{t} + 1.0)}{5} \qquad \begin{array}{l} \text{for } 200 < i \leq 500, \\ \text{otherwise } x_{2_{f1}}(t) = x_2(t). \end{array} \tag{6.5}$$

$x_{1_{f1}}(t)$ is depicted in Figure 6.1c and $x_{2_{f1}}(t)$ is depicted in Figure 6.1d.

For the second partially faulty data set, a temporarily occurring fault is replaced with $x_1(t)$ only and $x_2(t)$ is left faultless, as follows:

$$x_{1_{f2}}(t) = \frac{\mathrm{t}\cos(\mathrm{t} - \mathrm{d})}{5} \qquad \begin{array}{l} \text{for } 100 < i \leq 400, \\ \text{otherwise } x_{1_1}(t) = x_1(t) \end{array} \tag{6.6}$$

$$x_{2_{f2}}(t) = x_2(t) \qquad 1 < i \leq 500 \tag{6.7}$$

where d is a fault vector of uniform random numbers, U(0,1) of dimension 50, yet generated with a different seed. $x_{1_{f2}}(t)$ is depicted in Figure 6.1e and $x_{2_{f2}}(t)$, is depicted in Figure 6.1f (which is identical to Fig.6.b).

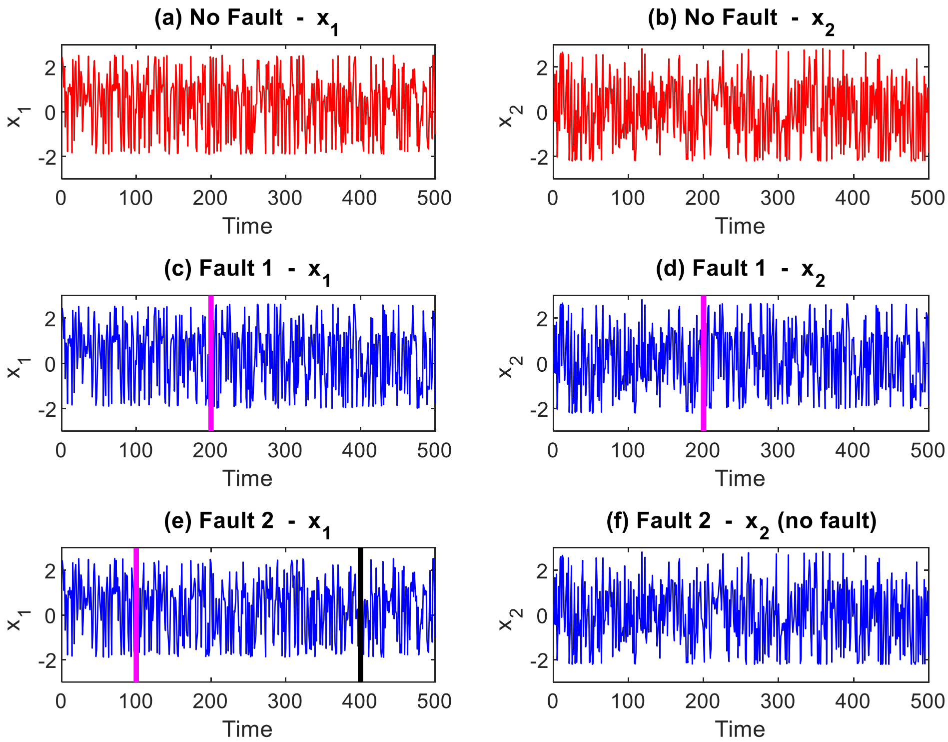

Figure 6.1. Normal and Fault-Added Synthetic Time Series.

The two original (unfaulty) series $x_1(t)$ and $x_2(t)$ are shown in red color in Figure 6.1a and 6.1b respectively. Different fault-added version of $x_1(t)$ and $x_2(t)$ are shown in the rest of Figure 6.1. The vertical pink bars on the figures indicate starting points of the added faults, whereas the vertical black bar indicates the end of the added fault. There is no fault in Figure 6.1f and thus it is identical to Figure 6.1b. As can be appreciated from Fig.6.1 it is highly difficult to detect the exact beginning and ending locations of the faulty operation zones just by eye inspection if these locations had not been marked with vertical bars, since the generated faults are not simply identifiable mean or trend changes but are obscure random-number sequence changes in the first and second faulty sets.

6.2. Application of WCA to Fault Detection

In this section, WCA will be performed over these conscientiously prepared synthetic series to decide whether WCA is a promising tool for process fault detection. The normal (unfaulty) series are used as the "normal operation template" (as the first series of the WCA) and the faulty series are used as the "abnormal operation" or "query series" (as the second series of the WCA). Therefore, the WCA of this binary series (normal and faulty) may actually be considered as the application of WCA on "template matching" problems which are very important in the operation of batch chemical plants.

Table 6.1 lists the values of some of the important parameters used in the WCA computations in this chapter.

Table 6.1. Values of Some Important Parameters used in the WCA Computations.

Parameter	Explanation	Value
dt	sampling interval	1
DJ	number of octaves per scale	1/32
MinScale	minimum scale	0.95
MaxScale	maximum scale	256
Mother	mother wavelet	Morlet
MonteCarloCount	number of surrogate sets	10
ArrowDensity	densitiy of arrow on WCA figure	[25 25]

Firstly, WCA of $x_2(t)$ and $x_{2_{f2}}(t) = x_2(t)$ will be observed to see the behavior of WCA when there is no fault. Figure 6.2 contains plots of $x_2(t)$ (red) and $x_{2_{f2}}(t)$ (blue), it also contains WCA of $x_2(t)$ and $x_{2_{f2}}(t)$. Unsurprisingly, WCA of a series with itself gives one unique yellow region with rightward directed arrows, which means the two series are in phase. It can be deduced that when there is no fault or when a perfect template matching occurs, WCA will show a homogeneous region with rightward directed arrows.

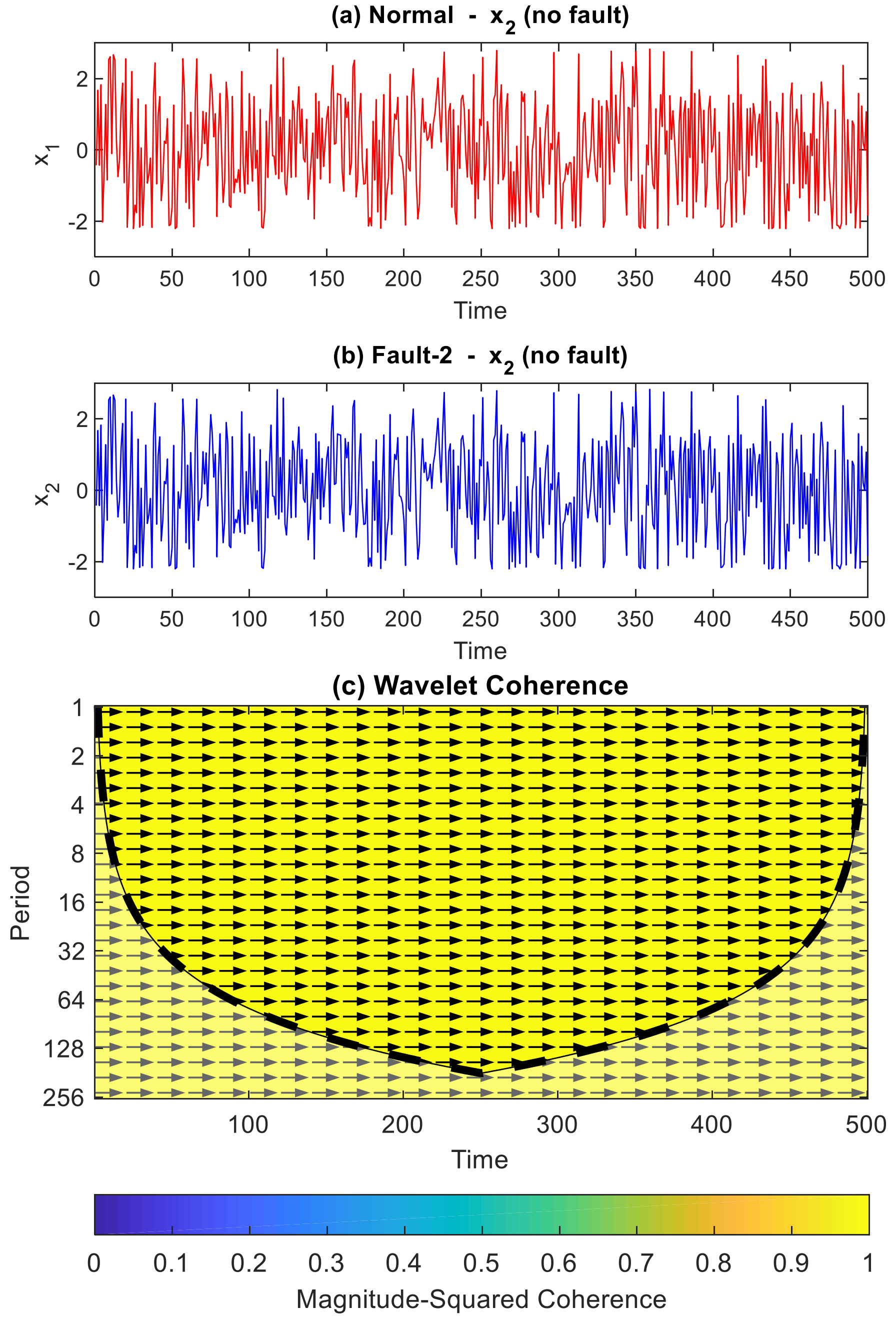

Figure 6.2. WCA of Series $x_2(t)$ (no fault) and $x_{2_{f2}}(t)$ (no fault).

Secondly, WCA of $x_1(t)$ and $x_{1_{f1}}(t)$ will be observed to see the behavior of WCA when there is permanent fault after a particular point in time. From Eq. 6.4, it is know that fault is added to the system at time 200. Figure 6.3 contains plots of $x_1(t)$ (red) and $x_{1_{f1}}(t)$ (blue), it also contains WCA of $x_1(t)$ and $x_{1_{f1}}(t)$. The starting point of the fault is indicated by a vertical pink bar at t=200 in Figure 6.3b and c. Although it is not possible to detect the initiation of the fault in Figure 6.3b by naked eye, in the WCA image it is clearly identified by the disruption of the smooth yellow zone right at the bar for periods between one and about 58 year. Additionally, color of periods larger than 90 years become blue which indicates no coherency and only small portion of this region located in COI. We have observed similar “no coherency zone” at larger periods in Figure 4.7b and it may be caused from increase in resolution because of elimination of trends. The disrupted zones can be investigated under three groups. The first disrupted coherent zone is located at between 32- to 58-year period band. This zone firstly responses to the fault and it is the most persisting disrupted zone. However, the left tail of this disrupted zone, located around 34-year period is interestingly starts just before the fault, 10 time units before. This can be caused by tail effects of sliding wavelets in wavelet transformation. There is a “perfect coherency zone” located at 19- to 32-year period band, which interestingly occupies the entire time range and separates the first group from the second one. The second group of disputed zones is located between 2- to 19- year period band. These are unsystematically distributed with different sizes. This disorderly appearance is most probably due to the injection of random numbers as fault sources in Eq. 6.1 and 6.4. The third group of disrupted zones is located at less than two-year period. They may be residuals and can be assumed as noise. On the other hand, arrows after the fault are mostly rightward directed. It can be said that phase relationship between original and fault-added series is not affected from fault. In short, the vicinity of the 34-year period is more sensitive to the fault than the others in this case.

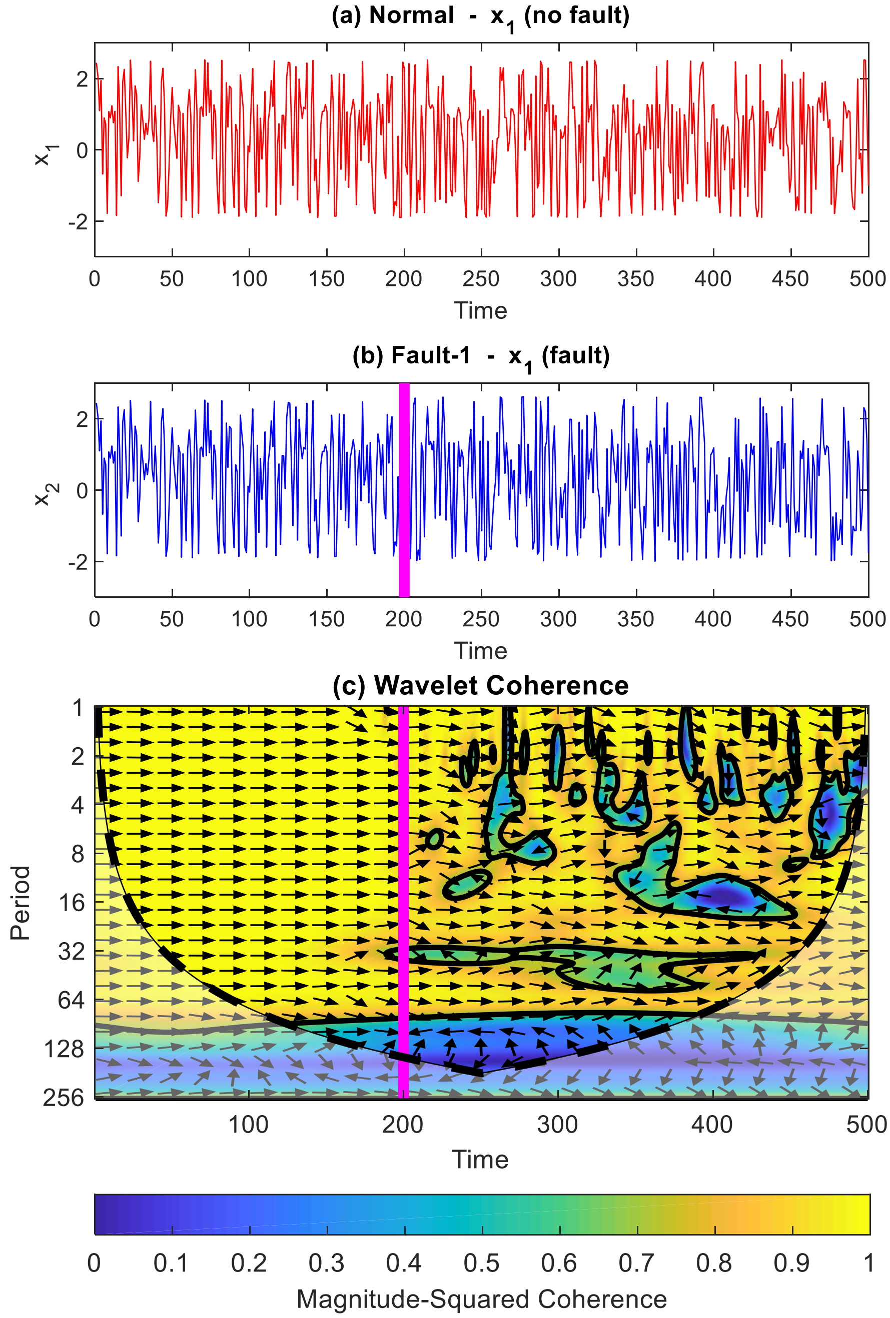

Figure 6.3. WCA of Series $x_1(t)$ (no fault) and $x_{1_{f_1}}(t)$ (fault-1).

Thirdly, WCA of $x_2(t)$ and $x_{2_{f1}}(t)$ will be observed to see the behavior of WCA when there is permanent fault after a particular point in time. From Eq. 6.5 it is know that fault is added to the system at time 200. Figure 6.4 contains plots of $x_2(t)$ (red) and $x_{2_{f_1}}(t)$ (blue), it also contains WCA of $x_2(t)$ and $x_{2_{f1}}(t)$. The starting point of the fault is indicated by a vertical pink bar at t=200 in Figure 6.4b and c. Although it is not possible to detect the initiation of the fault in Figure 6.4b by naked eye, in the WCA image it is clearly identified by the disruption of the smooth yellow zone right at the fault bar for periods between one and about 97 years. Additionally, the colors of periods larger than 128 years become blue which indicates incoherency, and only small portion of this region is located in COI. Similar “incoherent zones” at larger periods in Figure 4.7b may be observed and these may be caused by the increase in resolution as a result of detrending. Unlike Figure 6.3c, “incoherent zones” are much larger in Figure 6.4c. This can be resulted from higher magnitude (+1.0) of fault incurred. The magnitude of the fault in Eq. 6.5 is twofold of that in Eq. 6.4 (-0.5). The disrupted zones can be investigated under two groups. The first disrupted coherent zone is located at 70- to 100-year period band between $255<t<440$. Unlike Figure 6.3c, larger periods failed to detect the fault. There is a “perfect coherency zone” located at 19- to 32-year period band which interestingly occupies the entire time range and separates the first group from the second one. The second group is the large disrupted zones located between 2- to 60-year period band and it indicates the detection of the fault. Once again, there is a minor “incoherent zone” located around 17-year period, which is interestingly starts just (10 time units) before the fault is presented and is similar to minor “incoherent zone” around 34th time period in Figure 6.3c. On the other hand, the arrows after the fault are very much unsystematically directed compared to Figure 6.3c in which the magnitude of fault was less (half) than the magnitude of fault in Figure 6.4c. By comparing the behavior of the phase-difference arrows in Figure 6.3c and Figure 6.4c, it can be said that phase relationships between original and faulty series are affected after a threshold level of fault magnitude.

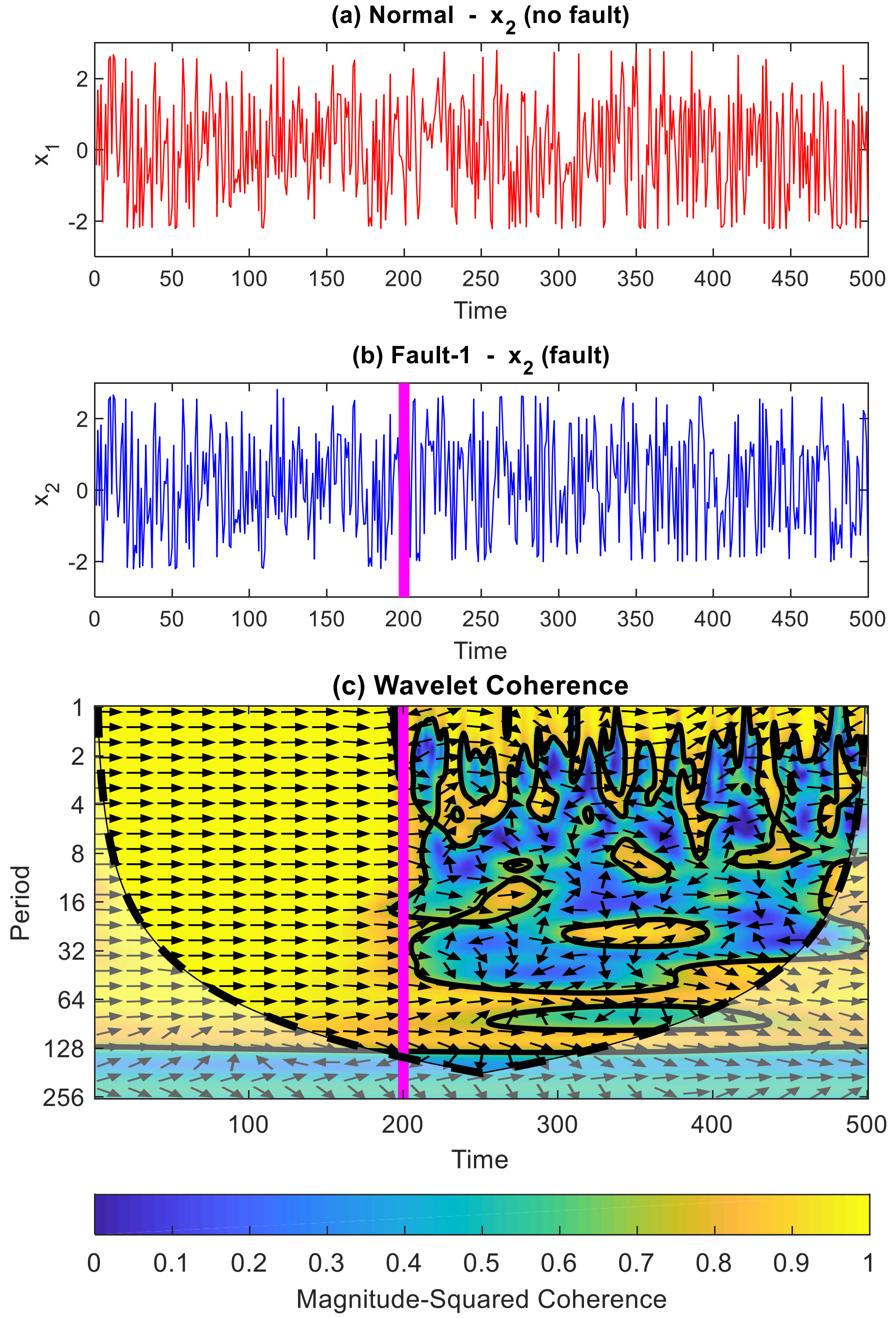

Figure 6.4. WCA of Series $x_2(t)$ (no fault) and $x_{2_{f_1}}(t)$ (fault-1).

Finally, WCA of $x_1(t)$ and $x_{1_{f2}}(t)$ will be observed to see the behavior of WCA when the fault is introduced abruptly at a particular point in time and removed at another future point in time. From Eq. 6.6, it is known that the fault is added to the system temporarily, only in between 100 < t < 400. Figure 6.5 contains plots of $x_1(t)$ (red) and $x_{1_{f_2}}(t)$ (blue), it also contains WCA of $x_1(t)$ and $x_{1_{f2}}(t)$. The starting points of the fault is indicated by a vertical pink bar and the termination of the fault is indicated by a vertical black bar in Figure 6.5b and c. Although it is not possible to detect the faulty zone in Figure 6.5b by comparing it with Figure 6.5a via naked eye, in the WCA image, the faulty zone is clearly identified by the definite presence of the “incoherent zone” that occurs right after the pink bar until the black bar. Additionally, “incoherent zones” are distributed between 1st and 128th time instances, and for this example, the color code for periods larger than 128 years are also yellow even though a small part it is located inside the COI. Since the magnitude of the fault is random for this case, it is observed that sizes of the “incoherent zones” are in between Figure 6.4c and Figure 6.5c. The disrupted zones can be investigated under three groups. The first group is located at 50- to 85-year period band. This “incoherent zone” starts from the pink bar and it crosses the black bar (termination of the fault) by 56 time unit and it is a successful precursor to detect the fault on time. Interestingly, there is another “incoherent zone” located between 85- to 11- year period band between $0<t<279$. Since its starting point is outside the COI, and is much before the starting point of the fault, it is not counted as a consequential disruption of coherent zone. There is again a “perfect coherency zone” located at 41- to 50-year period band, which interestingly occupies the entire time range and separates the first group from the second one. The second group of disrupted zones is located between 9- to 41-year period band and these zones may also be attributed to detection of the fault. Again, similar to previous cases, there is a minor “incoherent zone” which begins right before the beginning of the fault at about 34th time instance (10 time units before the fault). The third group of disrupted zones is located between 2- to 9-year period band and this group may also be attributed to detection of the fault. This group late reacts to the fault. On the other hand, the arrows on Figure 6.5c within the fault zone are not straightly rightward directed as in Figure 6.3c and are not randomly directed as in Figure 6.4c. Since the magnitude of the fault in Eq. 6.6 is random and between zero and one, it can again be concluded that the magnitude of fault has significant effect on phase relationships. In other words, the severity of the changes in the angles of arrows is an indicator of the magnitude of the fault.

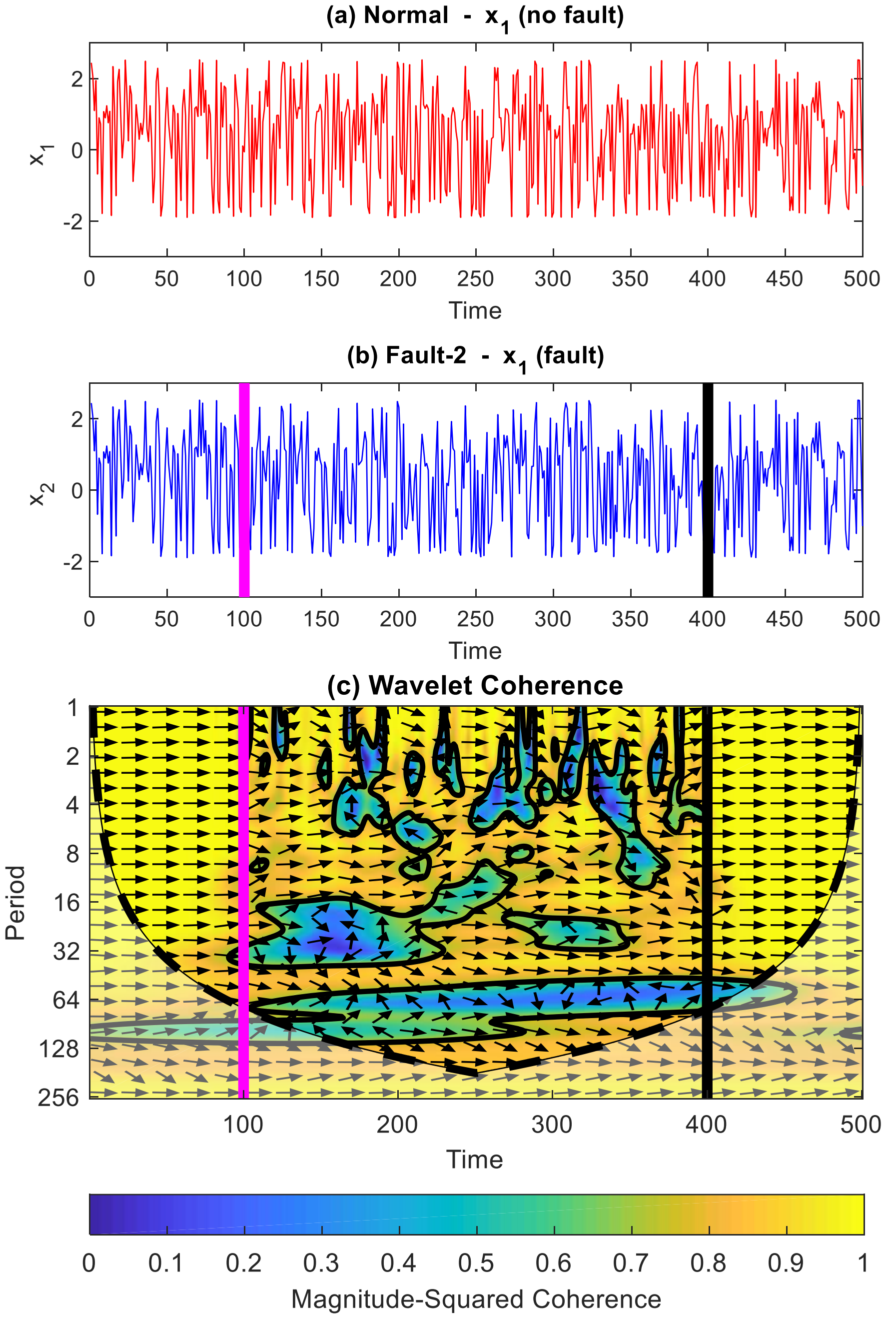

Figure 6.5. WCA of Series $x_1(t)$ (no fault) and $x_{1_{f_2}}(t)$ (fault-2).

In summary, these basic examples show that the WCA is a strong candidate to become a new process fault-detection tool. The analyses of this chapter show that the WCA (coherence levels) and the phase differences (arrow directions) are sensitive to the magnitude of the fault as well. On the other hand, the study done in this chapter is an offline analysis. There are edge effects associated with WCA and thus the significance of the WCA decays towards the edges where the COI appears. Therefore, the applicability of the WCA to online process fault detection, where the fault enters the WCA picture from its less significant edges, is still a question and must be analyzed further in more detail.

On the basis of learnings from the example of this chapter and from that of Chapter 3, the following table which summarizes the potential of the WCA for applications in FDD may be constructed.

Table 6.2. Summary of the Potential of the WCA for Applications in FDD (+: Definitely Positive, ?: Requires Further Investigation).

A Successful FDD Technique Should Possess	WCA Technique Possesses
Quick fault detection ability	+
Fault isolation ability to discriminate faults	?
Fault explanation ability	?
Simplicity to implement	+

7. CONCLUSIONS AND RECOMENDATIONS

Time series carry information in both time domain and frequency domain. There are successful tools which extract the information carried by time series. However, these tools have a critical deficiency; they can only work in one particular domain. On the other hand Wavelet Analysis (WA) effectively performs in both domains simultaneously that makes it possible to capture local spectral changes. In addition, most of the time series in engineering and economics are nonstationary and WA can cope with such nonstationary time series. Thanks to these positive aspects, WA has started to be widely used by academy in the last two decades. Likewise, this thesis has focused on presenting alternative chemical-industry related application fields of Continuous Wavelet Transform (CWT), Wavelet Power Spectrums (WPS), and Wavelet Coherence Analysis (WCA). In order to make a comprehensive study, CWT and WPS are used for univariate analyses whereas WCA is used for bivariate analyses.

Firstly, in Chapter 1, WA was introduced. It was verbally compared with the classical methods such as the Fourier Transform (FT). After that, alternative software programs with which one can perform and study WA were reviewed and a hybridization of the most widely used two of them was implemented and proposed for use in this thesis work. After this introduction, a relatively broad literature review on WA was given. In literature, WA is commonly used in several different territories. Initially, some articles related with economics, finance, and commodity prices have been reviewed. In those articles, researchers work with several different indicators such as oil price, stock price, inflation, and country currencies etc. These generally use WA for hedge accounting and risk management. In some other articles, WA are used to reveal interrelationship among certain variables in some specific fields such as medical, geophysics, meteorology, energy, etc.

In Chapter 2, mathematical background of WA was investigated in reasonable depth. The Morlet Wavelet was used throughout the thesis because of its wide usage in the literature and recognized power in localization in both time and frequency domains simultaneously (Tiwari et al., 2013). After that, derivations of CWT and WPS from Morlet Wavelet have been presented. Finally, formulization of WCA and calculation of phase differences between time series were explained. Furthermore, alternative software toolboxes for WA namely the AGToolbox, the ASToolbox and the MATLAB's default WCA function were comparatively studied. It was seen that perhaps the most important difference between these toolboxes was in their smoothing procedures. In the literature, there is not any single smoothing procedure agreed upon and used identically in all toolboxes. A modified version of the original AGToolbox, hybridized with some parts of the ASToolbox, was developed and used in this thesis since these two toolboxes are the most widely used ones in literature works.

In Chapter 3, performances of WPS and WCA were tested on simulated synthetic time series. The time series were created from a model which was originally used in (Aguiar-Conraria and Soares, 2011). So as to compare univariate performance of WPS, its results were compared with the results of the Power Spectral Density (PSD) which works only on frequency domain. WPS was not only overperformed PSD but also it detected sudden changes in the time series. Furthermore, Windowed and Lagged Correlation (WLC) was used to compare the result of WCA with the results of the traditional correlation approach. Although WLC eliminated the effect of phase difference to some extent, its results were too coarse for comparison with WCA. On the other hand, WCA was almost perfectly detected the coherency between the two series. Additionally, it showed remarkable performance for detecting phase differences between the two simulated time series.

In Chapter 4, the chemical industry related time series were analyzed in depth. Chemical Activity Barometer (CAB) is a composite index created by the American Chemical Council (ACC) which was built by using chemical-sectors related economic indicators. In regard of ACC, CAB is a leading indicator of the US economy, particularly the Industrial Production Index (IPI). In order to check whether CAB is a leading indicator, ACC uses three-month simple moving average (3MMA) and compares the results with the turning points of US economy, announced officially by the National Bureau of Economic Research (NBER). In this thesis work, WCA was applied to the monthly CAB and IPI data to check the claims of the ACC. The results have explicitly stated that the CAB and IPI are coherent at medium periods (3- to 12-year periods). However, due to the fact that US Business Cycles (BCs) are located at short periods (0.5- to 2-year periods), the focus was shifted to short-term periods. Short-term periods of Figure 4.3b and 4.7b revealed that the troughs claimed by the ACC and coherent zones at short-term periods coincide with each other. Detailed comparison of these coherent zones demonstrated that the troughs, most of the time, are preceded by the coherent zones on the WCA image of the CAB and IPI, especially for the troughs between 1945 and 2007. On the other hand, phase differences between the CAB and IPI congregated with phase differences between the troughs of the CAB and the troughs published by the NBER. These results were attributed to parallel moving tendencies of economic variables during epochs of recession. Furthermore, WCA recursively was applied to trending, detrended, and 3MMA of the same series. Consequently, resolution of the WCA image increased when detrended series were used instead of the original trending series and when the 3MMA series were used instead of both the original trending and detrended series. However, due to artificial lag introduced in the 3MMA process, the phase relationship got distorted and the arrows of the WCA no longer showed the actual direction.

In Chapter 5, experiences of Chapter 4 were applied to Chemical Engineering Plant Index (CEPCI) to check whether CEPCI is a leading indicator of the US economy. Unfortunately, monthly data of CEPCI was not available. Therefore, yearly data of the CEPCI were used. The motivation behind this chapter was to examine the binary relationships between the CAB and CEPCI pair and between the IPI and CEPCI pair with WCA in order to be able to sort these series with respect to their potential as being leading indicators of the US economy based on the phase relationships among them. To do so, firstly the original monthly data of the CAB and IPI were converted to yearly data and then the three yearly time series were detrended since the resolution of WCA image increases when detrended data are used. Additionally, in spite of the fact that BCs are located at short-term periods (0.5- to 2-year periods), only the medium- and long-term periods were studied since the data frequency decreased upon conversion from monthly to yearly series. Consequently, two important results have been obtained. The first one is that increasing the data collection period from months to years had drastic effects on low periods of the WCA image. The second is that the CEPCI was partially coherent with the CAB and IPI at medium term (3- to 12-year periods), however there was no solid evidence whether the

CEPCI leaded the CAB or the IPI. Therefore, it can not be said that the CEPCI is a leading indicator of the US economy by analyzing with the low-frequency yearly data.

In Chapter 6, the applicability of the WCA in Process Fault Detection (PFD) tasks was studied, to the best of our knowledge, for the first time in literature. In this experimental chapter, simple faults with different characteristics were used in order to examine whether WCA was a promising PFD tool or not. Two different synthetic time series (containing no fault) and four different faulty time series grouped into two faults were generated and used in the WCA of their binary pairs with unfaulty counterparts. Several interesting outcomes were obtained. The first observation was that the faults distorted coherent zones as well as phase-difference indicator arrows. The second observation was that there was direct proportion between the magnitude of the fault and the level of distortion of the coherent zones as well as the homogeneity of the direction of the phase arrows. However, while the coherent zones were more sensitive to the faults, arrows were affected after a certain threshold level of the fault magnitude. The third observation was that the WCA detected the faults no matter how abrupt or permanent were the faults.

There are two caveats for future studies. During the thesis, mostly the positive aspects of the WCA were put forward. Nevertheless, perhaps the most important limitation of the WCA is its aptness to only the binary time series. Therefore, it is impossible to perform WCA with multivariable or even with ternary time series. Any improvements in this aspect can make the WCA a much more attractive tool. However, this is not a straightforward task at all and requires deep theoretical development which is actually the job of the mathematicians.

Moreover, it was shown in Chapter 6 that WCA was a promising tool for PFD tasks. The series used were synthetic and the PFD analyses were offline. It is recommended to test the PFD performance of WCA with more realistic data, e.g., by using the Tennessee Eastman Plant benchmark problem. In addition, online image-processing tools may be barrowed from the computer science literature to test the applicability of WCA for online PFD tasks in real-time. However, anyone who will try WCA for PFD tasks, especially in real-time applications, should not forget that there is an obscure “edge effect” associated with any wavelet transform and thus with the WCA as well, due to cyclical nature of wavelets. Therefore, in online application of WCA, any new data point added to a streaming data series will fall into the end zone that suffers from the edge effects. Thus, one should check significance of detected fault right at the edge before reaching conclusions and taking further actions in real time.

As a last but important recommendation for future work it is suggested to investigate if the phase differences (arrow directions in the WCA image) and coherence levels (color coding of the WCA image), individually, can be used for the detection of two different fault types. For instance, the coherence levels may be more suitable in detecting classical faults such as mean, variance, and trend changes and the phase angles may be more suitable to detect slowly occurring / propagating phase-shift changes (e.g., obscure phase shifts due to slowly prevailing fouling phenomenon in heat exchangers)

REFERENCES

Abid, F., & Kaffel, B. (2018). Time–frequency wavelet analysis of the interrelationship between the global macro assets and the fear indexes. *Physica A: Statistical Mechanics and Its Applications*. https://doi.org/10.1016/j.physa.2017.08.057

ACC. (n.d.). Retrieved January 3, 2020, from https://www.americanchemistry.com/

Aguiar-Conraria, L., Azevedo, N., & Soares, M. J. (2008). Using wavelets to decompose the time-frequency effects of monetary policy. *Physica A: Statistical Mechanics and Its Applications*. https://doi.org/10.1016/j.physa.2008.01.063

Aguiar-Conraria, L. F., & Soares, M. J. (2007). Using cross-wavelets to decompose the time-frequency relation between oil and the macroeconomy. *NIPE Working Papers*.

Aguiar-Conraria, L., & Joana Soares, M. (2011). Business cycle synchronization and the Euro: A wavelet analysis. *Journal of Macroeconomics*. https://doi.org/10.1016/j.jmacro.2011.02.005

Aguiar-Conraria, L., Martins, M. M. F., & Soares, M. J. (2012). The yield curve and the macro-economy across time and frequencies. *Journal of Economic Dynamics and Control*. https://doi.org/10.1016/j.jedc.2012.05.008

Aguiar-Conraria, L., Martins, M. M. F., & Soares, M. J. (2013). Convergence of the Economic Sentiment Cycles in the Eurozone: A Time-Frequency Analysis. *Journal of Common Market Studies*. https://doi.org/10.1111/j.1468-5965.2012.02315.x

Aguiar-Conraria, L., Rodrigues, T. M., & Soares, M. J. (2014). *Oil Shocks and the Euro as an Optimum Currency Area*. https://doi.org/10.1007/978-3-319-07061-2_7

Aguiar-Conraria, L., & Soares, M. J. (2011). Oil and the macroeconomy: Using wavelets to analyze old issues. *Empirical Economics*. https://doi.org/10.1007/s00181-010-0371-x

Aguiar, L. F., & Soares, M. J. (2011). The Continuous Wavelet Transform: A Primer. *NIPE Working Papers*.

Akansu, A. N., & Haddad, R. A. (2001). Multiresolution Signal Decomposition: Transforms, Subbands, and Wavelets. In *Multiresolution Signal Decomposition*. https://doi.org/10.1016/B978-012047141-6/50007-0

Akoum, I., Graham, M., Kivihaho, J., Nikkinen, J., & Omran, M. (2012). Co-movement of oil and stock prices in the GCC region: A wavelet analysis. *Quarterly Review of Economics and Finance*. https://doi.org/10.1016/j.qref.2012.07.005

Aloui, C., & Hkiri, B. (2014). Co-movements of GCC emerging stock markets: New evidence from wavelet coherence analysis. *Economic Modelling*. https://doi.org/10.1016/j.econmod.2013.09.043

Aloui, C., Hkiri, B., Lau, C. K. M., & Yarovaya, L. (2016). Investors' sentiment and US Islamic and conventional indexes nexus: A time–frequency analysis. *Finance Research Letters*. https://doi.org/10.1016/j.frl.2016.06.002

Andries, A. M., Ihnatov, I., & Tiwari, A. K. (2014). Analyzing time-frequency relationship between interest rate, stock price and exchange rate through continuous wavelet. *Economic Modelling*. https://doi.org/10.1016/j.econmod.2014.05.013

Ashok, K., Guan, Z., & Yamagata, T. (2003). A look at the relationship between the ENSO and the Indian Ocean Dipole. *Journal of the Meteorological Society of Japan*. https://doi.org/10.2151/jmsj.81.41

Auth, C. (2013). *Continuous Wavelet Transform and Wavelet Coherence - Implementation and Applicatıon to the Diversification Analysis of Hedge Fund Returns*. https://www.nag.com/about/student_awards/christoph-auth-nag-student-award.pdf

Awerbuch, S., & Sauter, R. (2006). Exploiting the oil-GDP effect to support renewables deployment. *Energy Policy*. https://doi.org/10.1016/j.enpol.2005.04.020

Azman-Saini, W. N. W., Azali, M., Habibullah, M. S., & Matthews, K. G. (2002). Financial integration and the ASEAN-5 equity markets. *Applied Economics*. https://doi.org/10.1080/00036840210139364

Bai, L., Yan, S., Zheng, X., & Chen, B. M. (2015). Market turning points forecasting using wavelet analysis. *Physica A: Statistical Mechanics and Its Applications*. https://doi.org/10.1016/j.physa.2015.05.027

Barunik, J., Vacha, L., & Krištoufek, L. (2011). Comovement of Central European stock markets using wavelet coherence: Evidence from high-frequency data. *Working Papers IES*.

Benhmad, F. (2013). Bull or bear markets: A wavelet dynamic correlation perspective. *Economic Modelling*. https://doi.org/10.1016/j.econmod.2013.02.031

Bilgili, F. (2015). Business cycle co-movements between renewables consumption and industrial production: A continuous wavelet coherence approach. In *Renewable and Sustainable Energy Reviews*. https://doi.org/10.1016/j.rser.2015.07.116

Boldin, M. D. (1994). Dating Turning Points in the Business Cycle. In *The Journal of Business* (Vol. 67, pp. 97–131). The University of Chicago Press. https://doi.org/10.2307/2353282

Bry, G., & Boschan, C. (1971). *Cyclical Analysis of Time Series: Selected Procedures and Computer Programs*.

Burns, A. F., & Mitchell, W. C. (1946). Measuring Business Cycles. *Journal of the Royal Statistical Society*. https://doi.org/10.2307/2981375

Caldwell, D., & Ortego, J. (1975). A method for forecasting the CE plant cost index. *Chemical Engineering Magazine*, 83–85.

Chemical Activity Barometer vs. Industrial Production. (2019). American Chemical Council. https://www.americanchemistry.com/CAB-vs-Industrial-Production/

Chemical Engineering - Chemical Engineering essentials for the global chemical processing industries (CPI). (2020). https://www.chemengonline.com/

Chiang, L. H., Braatz, R. D., & Russell, E. (2001). *Fault detection and diagnosis in industrial systems*. Springer.

Cran, J. (1976). Cost indices. *Engineering and Process Economics*, *1*(1), 13–23. https://doi.org/10.1016/0377-841X(76)90042-5

Crowley, P. M. (2007). A guide to wavelets for economists. *Journal of Economic Surveys*. https://doi.org/10.1111/j.1467-6419.2006.00502.x

Cui, X., Bryant, D. M., & Reiss, A. L. (2012). NIRS-based hyperscanning reveals increased interpersonal coherence in superior frontal cortex during cooperation. *NeuroImage*. https://doi.org/10.1016/j.neuroimage.2011.09.003

Devedeux, D., Marque, C., Mansour, S., Germain, G., & Duchêne, J. (1993). Uterine electromyography: A critical review. *American Journal of Obstetrics and Gynecology*. https://doi.org/10.1016/0002-9378(93)90456-S

Ding, S. X. (2008). Model-based fault diagnosis techniques: Design schemes, algorithms, and tools. In *Model-based Fault Diagnosis Techniques: Design Schemes, Algorithms, and Tools*. https://doi.org/10.1007/978-3-540-76304-8

Dooley, C. (2012). No Title. *ACC's Economics and Statistics Publications*, 5.

Ferrer, R., Jammazi, R., Bolós, V. J., & Benítez, R. (2018). Interactions between financial stress and economic activity for the U.S.: A time- and frequency-varying analysis using wavelets. *Physica A: Statistical Mechanics and Its Applications*. https://doi.org/10.1016/j.physa.2017.10.044

Funashima, Y. (2017). Time-varying leads and lags across frequencies using a continuous wavelet transform approach. *Economic Modelling*. https://doi.org/10.1016/j.econmod.2016.08.024

Gabor, D. (1946). Theory of communication. Part 3: Frequency compression and expansion. *Journal of the Institution of Electrical Engineers - Part III: Radio and Communication Engineering*. https://doi.org/10.1049/ji-3-2.1946.0076

Gallegati, M. (2012). A wavelet-based approach to test for financial market contagion. *Computational Statistics and Data Analysis*. https://doi.org/10.1016/j.csda.2010.11.003

Garg, A., Xu, D., & Blaber, A. P. (2013). Statistical validation of wavelet transform coherence method to assess the transfer of calf muscle activation to blood pressure during quiet standing. *BioMedical Engineering Online*. https://doi.org/10.1186/1475-925X-12-132

Gençay, R., Selçuk, F., & Whitcher, B. (2002). WAVELET DENOISING. In *An Introduction to Wavelets and Other Filtering Methods in Finance and Economics*.

https://doi.org/10.1016/b978-012279670-8.50009-4

Graham, M., Kiviaho, J., & Nikkinen, J. (2013). Short-term and long-term dependencies of the S&P 500 index and commodity prices. *Quantitative Finance*. https://doi.org/10.1080/14697688.2013.768773

Graham, M., Kiviaho, J., Nikkinen, J., & Omran, M. (2013). Global and regional co-movement of the MENA stock markets. *Journal of Economics and Business*. https://doi.org/10.1016/j.jeconbus.2012.09.005

Grinsted, A., Moore, J. C., & Jevrejeva, S. (2004). Application of the cross wavelet transform and wavelet coherence to geophysical time series. *Nonlinear Processes in Geophysics*. https://doi.org/10.5194/npg-11-561-2004

Hanus, L., & Vacha, L. (2015). Business Cycle Synchronization within the European Union: A Wavelet Cohesion Approach. In *SSRN*. https://doi.org/10.2139/ssrn.2616055

Hassan, M., Terrien, J., Karlsson, B., & Marque, C. (2010). Application of wavelet coherence to the detection of uterine electrical activity synchronization in labor. *IRBM*. https://doi.org/10.1016/j.irbm.2009.12.004

Home | Oil & Gas Journal. (2020). https://www.ogj.com/

Huang, S., An, H., Gao, X., & Huang, X. (2016). Time-frequency featured co-movement between the stock and prices of crude oil and gold. *Physica A: Statistical Mechanics and Its Applications*. https://doi.org/10.1016/j.physa.2015.10.080

Hughes Hallett, A., & Richter, C. (2006). Is the convergence of business cycles a global or regional issue? The UK, US and Euroland. *International Journal of Finance and Economics*. https://doi.org/10.1002/ijfe.291

Jenkins, S. (2018). The CE Plant Cost Index: An Update. *Chemical Engineering Magazine*. https://www.chemengonline.com/ce-plant-cost-index-update/

Jiang, Y., Nie, H., & Monginsidi, J. Y. (2017). Co-movement of ASEAN stock markets: New evidence from wavelet and VMD-based copula tests. *Economic Modelling*. https://doi.org/10.1016/j.econmod.2017.04.012

Jones, C. M., & Kaul, G. (1996). Oil and the stock markets. *Journal of Finance*. https://doi.org/10.1111/j.1540-6261.1996.tb02691.x

Kristoufek, L. (2015). What are the main drivers of the bitcoin price? Evidence from wavelet coherence analysis. *PLoS ONE*. https://doi.org/10.1371/journal.pone.0123923

Labat, D. (2005). Recent advances in wavelet analyses: Part 1. A review of concepts. *Journal of Hydrology*. https://doi.org/10.1016/j.jhydrol.2005.04.003

Li, X. L., Chang, T., Miller, S. M., Balcilar, M., & Gupta, R. (2015). The co-movement and causality between the U.S. housing and stock markets in the time and frequency domains. *International Review of Economics and Finance*. https://doi.org/10.1016/j.iref.2015.02.028

Madaleno, M., & Pinho, C. (2014). Wavelet dynamics for oil-stock world interactions. *Energy Economics*. https://doi.org/10.1016/j.eneco.2014.06.024

Marczak, M., & Gómez, V. (2015). Cyclicality of real wages in the USA and Germany: New insights from wavelet analysis. *Economic Modelling*. https://doi.org/10.1016/j.econmod.2015.02.014

Marfatia, H. A. (2017). A fresh look at integration of risks in the international stock markets: A wavelet approach. *Review of Financial Economics*. https://doi.org/10.1016/j.rfe.2017.07.003

Mayes, D. G., & Crowley, P. M. (2009). How fused is the euro area core? *OECD Journal: Journal of Business Cycle Measurement and Analysis*. https://doi.org/10.1787/jbcma-v2008-art4-en

Mayes, D. G., Crowley, P. M. M., & Maraun, D. (2011). How Hard is the Euro Area Core? An Evaluation of Growth Cycles Using Wavelet Analysis. *SSRN Electronic Journal*. https://doi.org/10.2139/ssrn.1019955

Mazzi, G. L., & Scocco, M. (2002). *Business cycles analysis and related software applications*.

McCarthy, J., & Orlov, A. G. (2012). Time-frequency analysis of crude oil and S&P500 futures contracts. *Quantitative Finance*.

https://doi.org/10.1080/14697688.2012.686669

McDermott, C. J., & Scott, A. (2000). Concordance in Business Cycles. *IMF Working Papers*. https://doi.org/10.5089/9781451845563.001

Mensi, W., Hkiri, B., Al-Yahyaee, K. H., & Kang, S. H. (2018). Analyzing time–frequency co-movements across gold and oil prices with BRICS stock markets: A VaR based on wavelet approach. *International Review of Economics and Finance*. https://doi.org/10.1016/j.iref.2017.07.032

Mignard, D. (2014). Correlating the chemical engineering plant cost index with macro-economic indicators. *Chemical Engineering Research and Design*. https://doi.org/10.1016/j.cherd.2013.07.022

Misiti, M., Misiti, Y., Oppenheim, G., & Poggi, J. M. (2010). Wavelets and their Applications. In *Wavelets and their Applications*. https://doi.org/10.1002/9780470612491

Mudakkar, S. R., & Zaman, K. (2013). WITHDRAWN: A wavelet analysis of oil prices and stock market: evidence from Pakistan and India. *Energy Policy*. https://doi.org/10.1016/j.enpol.2013.07.141

Musulin, E. (2014). Spectral graph analysis for process monitoring. *Industrial and Engineering Chemistry Research*. https://doi.org/10.1021/ie403966v

Mutascu, M. (2018). A time-frequency analysis of trade openness and CO2 emissions in France. *Energy Policy*. https://doi.org/10.1016/j.enpol.2018.01.034

Ng, E. K. W., & Chan, J. C. L. (2012). Geophysical applications of partial wavelet coherence and multiple wavelet coherence. *Journal of Atmospheric and Oceanic Technology*. https://doi.org/10.1175/JTECH-D-12-00056.1

Pal, D., & Mitra, S. K. (2017). Time-frequency contained co-movement of crude oil and world food prices: A wavelet-based analysis. *Energy Economics*. https://doi.org/10.1016/j.eneco.2016.12.020

Pal, D., & Mitra, S. K. (2019). Oil price and automobile stock return co-movement: A wavelet coherence analysis. *Economic Modelling*.

https://doi.org/10.1016/j.econmod.2018.07.028

Papaioannou, G. P., Dikaiakos, C., Evangelidis, G., Papaioannou, P. G., & Georgiadis, D. S. (2015). Co-movement analysis of Italian and Greek electricity market wholesale prices by using a wavelet approach. *Energies*. https://doi.org/10.3390/en81011770

Percival, D. B., & Walden, A. T. (2000). *Wavelet methods for time series analysis*. Cambridge University Press.

Process Engineering. (2020). http://processengineering.co.uk/

Reboredo, J. C., Rivera-Castro, M. A., & Ugolini, A. (2017). Wavelet-based test of co-movement and causality between oil and renewable energy stock prices. *Energy Economics*. https://doi.org/10.1016/j.eneco.2016.10.015

Rua, A. (2010). Measuring comovement in the time-frequency space. *Journal of Macroeconomics*. https://doi.org/10.1016/j.jmacro.2009.12.005

Rua, A., & Nunes, L. C. (2009). International comovement of stock market returns: A wavelet analysis. *Journal of Empirical Finance*. https://doi.org/10.1016/j.jempfin.2009.02.002

Saâdaoui, F., Naifar, N., & Aldohaiman, M. S. (2017). Predictability and co-movement relationships between conventional and Islamic stock market indexes: A multiscale exploration using wavelets. *Physica A: Statistical Mechanics and Its Applications*. https://doi.org/10.1016/j.physa.2017.04.074

Soares, M. J., & Aguiar-Conraria, L. (2011). *Wavelets, Economics and Politics*. https://sites.google.com/site/aguiarconraria/joanasoares-wavelets

Sousa, R., Aguiar-Conraria, L., & Soares, M. J. (2014). Carbon Financial Markets: a time-frequency analysis of CO2 price drivers. *NIPE Working Papers*.

Sun, Q., & Xu, W. (2018). Wavelet analysis of the co-movement and lead–lag effect among multi-markets. *Physica A: Statistical Mechanics and Its Applications*. https://doi.org/10.1016/j.physa.2018.08.102

Swift, T. K. (2015). *PRACTITIONER'S SECTION: Chemical Industry Activity as a leading indicator of the business cycle*. Journal of Business Chemistry.

https://www.businesschemistry.org/article/?article=204

Tiwari, A. K. (2013). Oil prices and the macroeconomy reconsideration for Germany: Using continuous wavelet. *Economic Modelling*. https://doi.org/10.1016/j.econmod.2012.11.003

Tiwari, A. K., Bhanja, N., Dar, A. B., & Olayeni, O. R. (2013). Analyzing Time–Frequency Based Co-movement in Inflation: Evidence from G-7 Countries. *Computational Economics*. https://doi.org/10.1007/s10614-013-9408-5

Tiwari, A. K., Mutascu, M. I., & Albulescu, C. T. (2016). Continuous wavelet transform and rolling correlation of European stock markets. *International Review of Economics and Finance*. https://doi.org/10.1016/j.iref.2015.12.002

Torrence, C., & Compo, G. P. (1998). A Practical Guide to Wavelet Analysis. *Bulletin of the American Meteorological Society*. https://doi.org/10.1175/1520-0477(1998)079<0061:APGTWA>2.0.CO;2

Torrence, C., & Webster, P. J. (1999). Interdecadal changes in the ENSO-monsoon system. *Journal of Climate*. https://doi.org/10.1175/1520-0442(1999)012<2679:icitem>2.0.co;2

Uddin, G. S., Bekiros, S., & Ahmed, A. (2018). The nexus between geopolitical uncertainty and crude oil markets: An entropy-based wavelet analysis. *Physica A: Statistical Mechanics and Its Applications*. https://doi.org/10.1016/j.physa.2017.12.025

Vacha, L., & Barunik, J. (2012). Co-movement of energy commodities revisited: Evidence from wavelet coherence analysis. *Energy Economics*. https://doi.org/10.1016/j.eneco.2011.10.007

Vacha, L., Janda, K., Kristoufek, L., & Zilberman, D. (2013). Time-frequency dynamics of biofuel-fuel-food system. *Energy Economics*. https://doi.org/10.1016/j.eneco.2013.06.015

Vatavuk, W. M. (2002). Updating the CE plant cost index. In *Chemical Engineering*.

Venkatasubramanian, V., Rengaswamy, R., Yin, K., & Kavuri, S. N. (2003). A review of process fault detection and diagnosis part I: Quantitative model-based methods. *Computers and Chemical Engineering*. https://doi.org/10.1016/S0098-1354(02)00160-6

Yang, L., Cai, X. J., & Hamori, S. (2017). Does the crude oil price influence the exchange rates of oil-importing and oil-exporting countries differently？A wavelet coherence analysis. *International Review of Economics and Finance*. https://doi.org/10.1016/j.iref.2017.03.015

Yang, L., Cai, X. J., Zhang, H., & Hamori, S. (2016). Interdependence of foreign exchange markets: A wavelet coherence analysis. *Economic Modelling*. https://doi.org/10.1016/j.econmod.2016.01.022

APPENDIX A: MATLAB CODE USED

```
echo off; clc; clear all; close all; format short g; warning off;
rng('default'); % Comment this to get different random series on each run

% Example2_Cross_PhaseDifference.m of ASToolbox
delt=12;
t = 0 : 1/delt : 50; % Note that dt = 1/12 !!!
lt=length(t);
r=1;
x=sin(2*pi*t/3)+3*sin(2*pi*t/6)+randn(1,lt)*r;
tin=0:1/delt:25;
tfin=25+1/delt:1/delt:50;
yin=4*sin(2*pi*((tin+5/delt)/3))-...
    3*sin(2*pi*((tin-10/delt)/6))+randn(1,length(tin))*r;
yfin=4*sin(2*pi*((tfin-5/delt)/3))-...
     3*sin(2*pi*((tfin+10/delt)/6))+randn(1,length(tfin))*r;
y=[yin, yfin];

Lt = length(t);

DATA(:,1)=x;
DATA(:,2)=y;

st = delt; % for years

names = {'Series x(t)','Series y(t)'};

% DATA=detrend(DATA);
DATA=([mapminmax(DATA')]'+1)/2; % map between 0 & +1

dt = unique(round(diff(t),6)); % Sampling Interval

tunit = {'years'}; % For axis labelling 'months'/'seconds'/...

% DJ : Number of Octaves per Scale. Spacing between discrete scales.
%      A smaller # will give better scale resolution, but be slower to plot.
DJ = 1/32;

LPer = 0.15; % Lower period for WCA
UPer = 32; % Lower period for WCA


%--- Period-band selections for phase-difference & time-lag computations
LPhaseDif = [2.5 3.5 5]/1; % Lower Phase Difference Band
UPhaseDif = [3.5 5.0 7]/1; % Upper Phase Difference Band
%-END- Period-band selections for phase-difference & time-lag computations

d1 = DATA(:,1);
d2 = DATA(:,2);

figure(111222111)
subtightplot(3,1,1,[0.15,0],[0.005,0.045],[0.05,0.015])
```

```
plot(t,x,'r-','LineWidth',1.0);
title(['(a)  Series ',names{1}],'FontName',' ','FontSize',10);
xlabel(['Time (',strvcat(tunit),')',],'FontName',' ','FontSize',10);
ylabel(['Values'],'FontName',' ','FontSize',10);
grid on

subtightplot(3,1,2,[0.15,0],[0.035,0.015],[0.06,0.015])
plot(t,y,'b-','LineWidth',1.0);
title(['(b)  Series ',names{2}],'FontName',' ','FontSize',10);
xlabel(['Time (',strvcat(tunit),')',],'FontName',' ','FontSize',10);
ylabel(['Values'],'FontName',' ','FontSize',10);
grid on

subtightplot(3,1,3,[0.15,0],[0.085,0.015],[0.06,0.015])
plot(t,x,'r-','LineWidth',1.0);
hold on
plot(t,y,'b-','LineWidth',1.0);
title(['(c)  Series ',names{1}, ' and ',names{2}],'FontName',' ','FontSize',10);
xlabel(['Time (',strvcat(tunit),')',],'FontName',' ','FontSize',10);
ylabel(['Values'],'FontName',' ','FontSize',10);
legend(names,'Location','B')
hold off
grid on

%--- AGToolbox
hFig2=figure(10); set(hFig2,'Position',[800, 40, 800, 800],'Name','AGToolbox Example');

%--- Plot of Series
subtightplot(4,2,[1 2],[0.06,0.],[0.0,0.025],[0.05,0.015])
plot(t,d1,'r-','LineWidth',1.0);
hold on
plot(t,d2,'b-','LineWidth',1.0);
title(['(a)  Series ',names{1}, ' and ',names{2}],'FontName',' ','FontSize',10);
xlabel(['Time (',strvcat(tunit),')',],'FontName',' ','FontSize',10);
ylabel('Normalized Series Values','FontName',' ','FontSize',10);
legend(names,'Location','Best')
hold off
grid on
%-END- Plot of Series

%--- Plot of Coherency and COI
subtightplot(4,2,[3 5 7],[0.06,0.],[0.025,0.025],[0.05,-0.05])

%-------------------------------------------------------------------------
[WCoh,phaseDif,powerX,powerY,coiX,coiY,period] = wtcUA([t' d1], [t' d2],
       'DJ',DJ, 'MinScale',0.12/1, 'MaxScale',UPer/1, 'Mother','MORLET',
       'MakeFigure',1, 'MonteCarloCount',10, 'pictEnh',1,
       'ArrowDisplayThreshold',0.01, 'ArrowDensity',[30 30],
       'ArrowSize',1.5, 'ArrowHeadSize',1.5);
coi=min(coiX,coiY); hold on;
plot(t,log2(coi),'w','LineWidth',3,'LineStyle','--');
%-------------------------------------------------------------------------

xlabel(['Time (',strvcat(tunit),')',],'FontName',' ','FontSize',10);
ylabel(['Period (',strvcat(tunit),')',],'FontName',' ','FontSize',10);
title('(b) Wavelet Coherence');
```

```
c=colorbar('southoutside');
c.Label.String = 'Magnitude-Squared Coherence';
c.Label.FontSize = 10;
c.FontSize = 10;
c.Ticks = [0.0: 0.1 : 1.0];
colormap(parula)

%--- Plot Phase-Differences & Instantaneous Time-Lags
labels = {'c','d','e'};
for i=1:length(LPhaseDif)
clear irow meanPer timeLag
subtightplot(4,2,4+2*(i-1),[0.06,0.],[0.05,0.025],[0.25,0.015])

%--- Mean Phase Difference
[irow,~]=find((period >= LPhaseDif(i)) & (period <= UPhaseDif(i)));
PM(i,:) = mean(phaseDif(irow,:));

[mn,rowix]=min(abs(period-UPhaseDif(i)));
PM(i,:) = phaseDif(rowix,:);
%-END- Mean Phase Difference

%--- Instantaneous Time-Lag
meanPer=mean(period(irow)); timeLag(i,:)=(PM(i,:)*meanPer)/(2*pi);
%-END- Instantaneous Time-Lag

erbars=std(phaseDif(irow,:));  Standard Deviation
shadedErrorBar(t',PM(i,:)',erbars,'lineprops','r','patchSaturation',0.1); hold on;
legend('Mean Phase Difference','Location','northwest' )
ylim([-pi +pi])
set(gca,'YTick',-pi:pi/2:pi)
set(gca,'YTickLabel',{'-\pi','-\pi/2','0','+\pi/2','+\pi'})
hrline=refline(0,0); hrline.Color='k'; hrline.LineWidth=2;
ylabel('Phase Difference','FontName',' ','FontSize',10);
title(['(',labels{i},') ',num2str(LPhaseDif(i)),'~',num2str(UPhaseDif(i)),' period
band'],'FontName',' ','FontSize',10);
set(get(get(hrline,'Annotation'),'LegendInformation'),'IconDisplayStyle','off');
box on
if i==length(LPhaseDif)
   xlabel(['Time (',strvcat(tunit),')',],'FontName',' ','FontSize',10);

end
end

tightfigUA();
movegui(hFig2,'northeast');
%-END- Plot Phase-Differences & Instantaneous Time-Lags

%--- Plot Mean Coherence & Mean Phase-Difference Spectra Across All Periods
hFig15=figure(15); set(hFig15,'Position',[400, 100, 680, 500],'Name','AGToolbox
Example');
subtightplot(2,2,1,[0.15,0.09],[0.08,0.04],[0.08,0.015])
shadedErrorBar(t,mean(WCoh,1),std(WCoh,0,1),'lineprops',{'r','LineWidth',2},'patchSatura
tion',0.15); hold on;
xlabel(['Time (',strvcat(tunit),')',],'FontName',' ','FontSize',9);
ylabel('Coherence Spectrum','FontName',' ','FontSize',9);
title('a) Mean Coherence Spectrum Across Periods','FontName',' ','FontSize',9);
```

```
grid on
box on

subtightplot(2,2,3,[0.15,0.09],[0.08,0.00],[0.08,0.015])
shadedErrorBar(t,mean(phaseDif,1),std(phaseDif,0,1),'lineprops',{'r','LineWidth',2},'pat
chSaturation',0.15); hold on;
ylim([-pi +pi]);
set(gca,'YTick',-pi:pi/2:pi)
set(gca,'YTickLabel',{'-\pi','-\pi/2','0','+\pi/2','+\pi'})
hrline=refline(0,0); hrline.Color='k'; hrline.LineWidth=2;
xlabel(['Time (',strvcat(tunit),')',],'FontName',' ','FontSize',9);
ylabel('Phase-Difference Spectrum','FontName',' ','FontSize',9);
title('b) Mean Phase-Difference Spectrum Across Periods','FontName',' ','FontSize',9);
grid on
box on

subtightplot(2,2,2,[0.15,0.09],[0.08,0.04],[0.08,0.015])

[uu,~]=find(period<=30);
shadedErrorBar(period(uu),mean(WCoh(uu,:),2),std(WCoh(uu,:),0,2),'lineprops',{'b','LineW
idth',2},'patchSaturation',0.2); hold on;
xlabel(['Period (',strvcat(tunit),')',],'FontName',' ','FontSize',9);
ylabel('Coherence Spectrum','FontName',' ','FontSize',9);
title('c) Mean Coherence Spectrum Across Time','FontName',' ','FontSize',9);
grid on
box on

subtightplot(2,2,4,[0.15,0.09],[0.08,0.00],[0.08,0.015])
shadedErrorBar(period,mean(phaseDif,2),std(phaseDif,0,2),'lineprops',{'b','LineWidth',2}
,'patchSaturation',0.2); hold on;
ylim([-pi +pi]);
set(gca,'YTick',-pi:pi/2:pi)
set(gca,'YTickLabel',{'-\pi','-\pi/2','0','+\pi/2','+\pi'})
hrline=refline(0,0); hrline.Color='k'; hrline.LineWidth=2;
xlabel(['Period (',strvcat(tunit),')',],'FontName',' ','FontSize',9);
ylabel('Phase-Difference Spectrum','FontName',' ','FontSize',9);
title('d) Mean Phase-Difference Spectrum Across Time','FontName',' ','FontSize',9);
xlim([0 30])
grid on
box on
tightfigUA();
%--- Plot Mean Coherence & Mean Phase-Difference Spectra Across All Periods

%--- PLOTs for individual series (univariate)
hFig1=figure(20); set(hFig1,'Position',[800, 100, 800, 700],'Name',' ');
for i=1:2
    if i==1; d=d1; power=powerX; coi=coiX;
    else;    d=d2; power=powerY; coi=coiY;  end;
    clear yticks

%--- Plot of Series
subtightplot(3,2,i,[0.15,0.09],[0.05,0.03],[0.08,0.015])

if i==1; plot(t,d,'r-','LineWidth',1.0); else; plot(t,d,'b-','LineWidth',1.0); end;
title(['Series ',strvcat(names(i))],'FontName',' ','FontSize',10);
xlabel(['Time (',strvcat(tunit),')',],'FontName',' ','FontSize',10);
```

```
ylabel('Normalized Series Values','FontName',' ','FontSize',10);
yticks([0 : 0.2 : 1]);
%-END- Plot of Series

%--- Plot WPS
pictEnh = 0.2; % Picture enhancer
grid on

subtightplot(3,2,2+i,[-0.05,0.09],[0.05,0.03],[0.08,0.015])

imagesc(t,log2(period),power.^pictEnh);
yticks = 2.^(fix(log2(min(period))) : 1 : fix(log2(max(period))));
title(['Wavelet Power Spectrum of ',strvcat(names(i))],'FontName',' ','FontSize',10);
xlabel(['Time (',strvcat(tunit),')',],'FontName',' ','FontSize',10);
ylabel(['Period (',strvcat(tunit),')',],'FontName',' ','FontSize',10);
set(gca,'YLim',ylim,'YDir','reverse','YTick',log2(yticks), ...
        'YTickLabel',yticks,'YGrid','on');
colormap('jet');
hold on
%-END- Plot WPS

plot(t,log2(coi),'w','LineWidth',3,'LineStyle','--');

%--- Compute and Plot Fourier Power Spectrum
subtightplot(3,2,4+i,[0.17,0.09],[0.06,0.01],[0.08,0.015])

minPeriod = 1;
maxPeriod = 20;

spP=FourierSpectrum(d, 40, 0, 2, dt,minPeriod,maxPeriod); % From ASToolbox
xticks = 2.^(fix(log2(minPeriod)):fix(log2(maxPeriod)));
set(gca,'XTick',xticks,'XTickLabel',xticks,'FontSize',10);
grid on;
xlabel(['Period (',strvcat(tunit),')',],'FontName',' ','FontSize',10);
ylabel('PSD','FontName',' ','FontSize',10);
title(['Power Sepctral Density of ',strvcat(names(i))],'FontName',' ','FontSize',10);
grid on

end
tightfigUA();
movegui(hFig1,'northwest');
%-END- PLOTs for individual series (univariate)

%--- Image of Phase Angles
hFig4=figure(35);

ConLev = 3; % Adjust this w.r.t. WCA arrows

imagesc(t,log2(period),phaseDif,[-pi +pi]); hold on; grid on;
contour(t,log2(period),phaseDif, ConLev, 'color','k','LineWidth',1.5,'ShowText','off')

xlabel(['Time (',strvcat(tunit),')',],'FontName',' ','FontSize',10);
ylabel(['Period (',strvcat(tunit),')',],'FontName',' ','FontSize',10);
Yticks = 2.^(fix(log2(min(period))):fix(log2(max(period))));
set(gca,'YLim',log2([min(period),max(period)]),'YDir','reverse', ...
        'layer','top','YTick',log2(Yticks(:)),'YTickLabel',num2str(Yticks'));
```

```
title('Distribution of Phase Angles')
axis square
c=colorbar('eastoutside');
c.Label.String = 'Phase Angle';
c.FontSize = 10;
c.Ticks = [-pi:pi/2:pi];
c.TickLabels={'-\pi','-\pi/2','0','+\pi/2','+\pi'};
colormap(jet(4))
grid on
tightfigUA(1.25);
%-END- Image of Phase Angles

%-END- AGToolbox

%--- Correlation Analysis
figure (105)
subtightplot(2,1,1,[-0.2,0.09],[0.08,0.04],[0.08,0.05])
MAXLAG=60;
WINDOW=72;
NOVERLAP=WINDOW-1;
[C,L,T]=corrgram(d1,d2,MAXLAG,WINDOW,NOVERLAP); grid on; hold on;
ConLev=8;
c=colorbar;
c.Label.String = 'Correlation Coefficient';
c.Label.FontSize = 10;
contour(T,L,C, ConLev, 'color','k','LineWidth',1.5,'ShowText','off')
hrline=refline(0,0); hrline.Color='k'; hrline.LineWidth=2;
xlabel(['Time (',strvcat(tunit),')',],'FontName',' ','FontSize',10);
title(['a) Windowed and Lagged Correlation, Window Length =
',num2str(round(WINDOW*dt,1)),' ',strvcat(tunit)],'FontName',' ','FontSize',10);
ylabel(['Lag (',strvcat(tunit),')',],'FontName',' ','FontSize',10);
xlim([0 length(t)])
set(gca,'XTick',0:96:length(t))
set(gca,'XTickLabel',ceil(0:96*dt:length(t)*dt))

set(gca,'YTick',-MAXLAG:12:MAXLAG)
set(gca,'YTickLabel',round(-MAXLAG*dt:12*dt:MAXLAG*dt))

subtightplot(2,1,2,[0.5,0.09],[0.08,0.04],[0.08,0.1665])
R_move=movcorr(d1,d2,WINDOW,'Endpoints','shrink');
plot(t,R_move); grid on;
title(['b) Windowed Correlation at Lag = 0, Window Length =
',num2str(round(WINDOW*dt,1)),' ',strvcat(tunit)],'FontName',' ','FontSize',10);
xlabel(['Time (',strvcat(tunit),')',],'FontName',' ','FontSize',10);
ylabel('Correlation Coefficient','FontName',' ','FontSize',10);
xlim([0 t(end)])
hold off;
tightfigUA(1.75);


WINDOWs=fix([0.5 1 2 4 6 8 12 16 20]/dt);
MAXLAG=80;
hFig110=figure(110); set(hFig110,'Position',[400, 40, 700, 600],'Name','Windowed &
Lagged Correlation');
for i=1:length(WINDOWs)
subtightplot(3,3,i,[0.09,0.065],[0.07,0.03],[0.055,0.02])
```

```
WINDOW=WINDOWs(i); NOVERLAP=WINDOW-1;
[C,L,T]=corrgram(d1,d2,MAXLAG,WINDOW,NOVERLAP); grid on; hold on;
colorbar('off')
ConLev=3;
contour(T,L,C, ConLev, 'color','k','LineWidth',1.5,'ShowText','off')
xlabel(['Time (',strvcat(tunit),')',],'FontName',' ','FontSize',10);
ylim([-MAXLAG +MAXLAG])
title(['Period ',num2str(round(WINDOW*dt,1))],'FontName',' ','FontSize',10);
grid on;
hrline=refline(0,0); hrline.Color='k'; hrline.LineWidth=2;
xticklabels(round((xticks./max(xticks))*t(end),1))
end
hold off;
tightfigUA();


% clear Lwin RMovCor
k0=2;
for k=k0:fix(Lt/2)-k0
    n=k-k0+1; LWin(n)=k; R=movcorr(d1,d2,k,'Endpoints','shrink');
    RMovCor(n,:)=R;
end
figure(115)
imagesc(t,t(LWin),RMovCor); grid on; hold on;
ConLev=3;
contour(t,t(LWin),RMovCor, ConLev, 'color','k','LineWidth',1.5,'ShowText','off')
c=colorbar;
c.Label.String = 'Correlation Coefficient';
c.Label.FontSize = 10;
xlabel(['Time (',strvcat(tunit),')',],'FontName',' ','FontSize',10);
ylabel(['Centered Window Length (Period (',strvcat(tunit),'))'],'FontName','
','FontSize',10)
title('Moving Centered Window Correlation')
hold off;
tightfigUA(1.75);
%-END- Correlation Analysis
```